

## **INFORMATION TO USERS**

This manuscript has been reproduced from the microfilm master. UMI films the text directly from the original or copy submitted. Thus, some thesis and dissertation copies are in typewriter face, while others may be from any type of computer printer.

**The quality of this reproduction is dependent upon the quality of the copy submitted.** Broken or indistinct print, colored or poor quality illustrations and photographs, print bleedthrough, substandard margins, and improper alignment can adversely affect reproduction.

In the unlikely event that the author did not send UMI a complete manuscript and there are missing pages, these will be noted. Also, if unauthorized copyright material had to be removed, a note will indicate the deletion.

Oversize materials (e.g., maps, drawings, charts) are reproduced by sectioning the original, beginning at the upper left-hand corner and continuing from left to right in equal sections with small overlaps. Each original is also photographed in one exposure and is included in reduced form at the back of the book.

Photographs included in the original manuscript have been reproduced xerographically in this copy. Higher quality 6" x 9" black and white photographic prints are available for any photographs or illustrations appearing in this copy for an additional charge. Contact UMI directly to order.

# **UMI**

A Bell & Howell Information Company  
300 North Zeeb Road, Ann Arbor MI 48106-1346 USA  
313/761-4700 800/521-0600



RICE UNIVERSITY

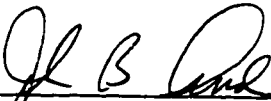
LATE QUATERNARY EVOLUTION OF THE CENTRAL TEXAS  
SHELF: SEQUENCE STRATIGRAPHIC IMPLICATIONS

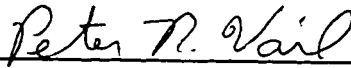
by

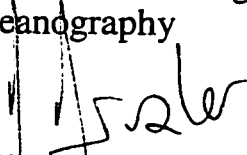
BRENDA JEAN ECKLES

A THESIS SUBMITTED  
IN PARTIAL FULFILLMENT OF THE  
REQUIREMENTS FOR THE DEGREE  
MASTER OF ARTS

APPROVED, THESIS COMMITTEE:

  
\_\_\_\_\_  
John B. Anderson, Director  
Professor and Chairman  
Geology and Geophysics

  
\_\_\_\_\_  
Peter R. Vail  
W. Maurice Ewing Professor of  
Oceanography

  
\_\_\_\_\_  
André W. Droxler  
Associate Professor  
Geology and Geophysics

Houston, Texas  
September, 1996

**UMI Number: 1384360**

---

**UMI Microform 1384360**  
**Copyright 1997, by UMI Company. All rights reserved.**

**This microform edition is protected against unauthorized  
copying under Title 17, United States Code.**

---

**UMI**  
**300 North Zeeb Road**  
**Ann Arbor, MI 48103**

## **ABSTRACT**

### **Late Quaternary Evolution of the Central Texas Shelf: Sequence Stratigraphic Implications**

by

Brenda Jean Eckles

This study documents the evolution of the interdeltaic central Texas continental shelf over the last 350,000 years. The dataset consists of high-resolution seismic data, platform boring descriptions, oxygen isotope analyses, and radiocarbon dates. A strong correlation exists between seismic facies and lithofacies enabling seven stages of evolution to be mapped. The distribution of these facies is primarily controlled by fourth-order glacio-eustatic cycles.

Seismic stratigraphy, oxygen isotope analyses, and radiocarbon dating were integrated to develop an independent sea-level curve for the area. Longshore and surface currents transport large volumes of sand into the area which is deposited as widespread, thick (>10 meters) barrier-bar highstand sand bodies on the inner shelf. Sediments are deposited and preserved in a repetitive manner during each glacio-eustatic cycle. This

implies a predictable pattern of deposition, therefore, allowing for the development of depositional models that can be applied to ancient deposits in the exploration for hydrocarbons.

## **ACKNOWLEDGMENTS**

This study is one part of a series of integrated projects being performed by a team of graduate students under the supervision of Dr. John B. Anderson. I am thankful for having the opportunity to participate in this exciting study, and even more grateful for the wonderful group of people that I have worked with. As an advisor, Dr. Anderson offers constant support and his vast knowledge base for us to learn from. As a team leader, he provides motivation, stimulates creativity, and is an endless energy source for the group. This team of past and present graduate students includes Ken Abdulah, Nicki Atkinson, Laura Banfield, Phil Bart, Jana DaSilva, Tony Rodriguez, Stephanie Shipp, and Jen Snow. Their neverending support, countless discussions, questions, and inspirational ideas has proven invaluable.

I wish to thank Dr. André Droxler and Dr. Pete Vail, my other committee members, for their interest and guidance and for always taking the time to answer my questions or look over my data with me. I have also benefited from interaction with other professors in the department, including Dr. Jinny Sisson, who was a member of my academic advisory committee and assisted with my study by flying me over the modern coastal deposits of the central Texas shelf. I am also grateful to Dr. Rusty Riese,

whom I have taken two classes from. I enjoyed these immensely and walked away from them with far more knowledge than the syllabus indicated I would.

I also wish to thank numerous other students in the department who have been extremely helpful throughout my time at Rice, especially Andy Cunningham for his suggestions, support, and always being there to bounce ideas off of, and Vitor Abreu for his time and willingness to share his knowledge of biostratigraphy and stable isotopes.

My data acquisition during August of 1995 would not have gone so smoothly if not for Mark Herring, captain of the R/V Lone Star, and Dave Mucciarone's instruction on the use of all the acquisition hardware and software.

This study was funded by a consortium of petroleum companies, including AGIP, Amoco, BP Exploration, Conoco, Exxon, Marathon, Mobil, Pan Canadian, Shell, and Union Pacific Resources. I would like to offer special thanks to Mike Helton, Laura Jennings, and the entire Sequence Stratigraphy group at Amoco for their help and allowing me access to a workstation and Landmark Seisworks 2D software license, which I used for the interpretation of the seismic dataset. Bruce Ahrendsen and various other people at Fugro-McClelland have been extremely helpful in allowing me access to their database of platform boring descriptions and



samples. The borehole description dataset has been an integral part of this study.

Initial editing of this thesis was performed by Laura Banfield and Jen Snow. I would like to thank them for all their help, support, and mostly their friendship.

Finally, I wish to thank my fiancé, Chris White, and my parents, Bill and Connie Eckles. Their neverending encouragement and support has always kept me going. All three knew I would finish before I ever saw the light at the end of the tunnel.

## TABLE OF CONTENTS

ABSTRACT .....	ii
ACKNOWLEDGMENTS .....	iv
TABLE OF CONTENTS.....	vii
LIST OF FIGURES.....	x
LIST OF TABLES .....	xiii
LIST OF PLATES .....	xiii
INTRODUCTION.....	1
GEOLOGIC SETTING .....	4
History of the Gulf of Mexico .....	4
The Quaternary Setting.....	11
Subsidence.....	13
Growth Faulting .....	13
Wind and Current Influence.....	15
Glacio-eustatic Sea-level .....	18
PREVIOUS WORK.....	21
DATASET AND METHODS .....	31
Seismic Acquisition .....	31
Seismic Processing .....	31
Seismic Interpretation.....	33

Lithostratigraphy .....	33
Oxygen Isotope Analyses .....	34
Radiocarbon Dating.....	37
<b>DATA AND RESULTS.....</b>	<b>38</b>
Seismic Stratigraphic Surfaces.....	38
Seismic Facies.....	40
Seismic Facies Unit A (SFU A).....	41
Seismic Facies Unit B (SFU B) .....	41
Seismic Facies Unit C (SFU C) .....	44
Seismic Facies Unit D (SFU D).....	48
Oxygen Isotope Stratigraphy .....	51
Radiocarbon Dating.....	55
Chronostratigraphy .....	57
<b>INTEGRATED INTERPRETATION .....</b>	<b>58</b>
Stage 9 Highstand Deposits.....	59
Stage 8 to 7 Transgressive Deposits.....	61
Stage 7 Highstand Deposits.....	63
Stage 6 to 5 Transgressive Deposits.....	64
Stage 5 Highstand Deposits.....	67
Stage 3 Highstand Deposits.....	69
Stage 2 to 1 Transgressive Deposits.....	70

DEPOSITIONAL MODELS .....	72
DISCUSSION .....	76
CONCLUSIONS .....	82
REFERENCES .....	85
APPENDIX 1: Platform Boring B-92 data .....	90
APPENDIX 2: Grain size analyses results.....	96
APPENDIX 3: Condensed platform boring descriptions.....	103

## LIST OF FIGURES

Figure 1. General study area map .....	2
Figure 2. Cenozoic drainage basins (after Winker, 1981) .....	8
Figure 3. Cenozoic depocenters (after Salvador, 1991) .....	9
Figure 4. Detailed bathymetric map of study area.....	12
Figure 5. Structural trends (after Bradshaw and Watkins, 1994) .....	14
Figure 6. Evolution of shale ridges (after Berryhill et al., 1986).....	16
Figure 7. Wind and current patterns (after Lohse, 1955).....	17
Figure 8. Compilation of Late Quaternary sea-level curves .....	19
Figure 9. The SPECMAP curve, converted to depth by G. Haddad.....	20
Figure 10. Wilcox Group interdeltic deposits (after Fisher and McGowen, 1967) .....	22
Figure 11. Yegua formation depositional systems (after Meckle and Galloway, 1996) .....	24
Figure 12. Frio formation depositional systems (after Galloway, 1982).....	25
Figure 13. Ingleside beach-ridge trend (after Winker, 1979) .....	27
Figure 14. Interpreted transgressive/regressive deposits (after Berryhill et al., 1986).....	28

Figure 15. Late Wisconsinan streamplain deposits (after Berryhill et al., 1986).....	30
Figure 16. Seismic grid and platform boring dataset map.....	32
Figure 17. Sample platform boring description .....	35
Figure 18a. Seismic line 40 demonstrates minor incision by SB8 on the inner shelf .....	39
Figure 18b. Seismic line 13 demonstrates high relief of SB2 on the middle shelf.....	39
Figure 19. Strike and dip seismic example of SFU A .....	42
Figure 20. Platform boring description illustrating lithofacies associated with SFU A .....	43
Figure 21. Strike and dip seismic example of SFU B.....	45
Figure 22. Platform boring description illustrating lithofacies associated with SFU B .....	46
Figure 23. Strike and dip seismic example of SFU C.....	47
Figure 24. Platform boring description illustrating lithofacies associated with SFU C .....	49
Figure 25. Strike and dip seismic example of SFU D .....	50
Figure 26. Location map and seismic of reefs observed in the study area .....	52
Figure 27. Oxygen isotope record for platform boring B-92 .....	53

Figure 28. Integrated chronostratigraphy of oxygen isotope record, radiocarbon dates, and seismic surfaces correlated to the SPECMAP curve .....	54
Figure 29. Stage 9 highstand areal distribution and isopach map .....	60
Figure 30. Stage 8 to 7 transgressive deposits isopach map .....	62
Figure 31. Stage 7 highstand areal distribution and isopach map .....	65
Figure 32. Stage 6 to 5 transgressive deposits areal distribution and isopach map.....	66
Figure 33. Stage 5 highstand areal distribution and isopach map .....	68
Figure 34. Stage 3 highstand areal distribution and isopach map .....	71
Figure 35. Stage 2 to 1 isopach map.....	73
Figure 36a. Block diagram of early highstand deposition .....	75
Figure 36b. Block diagram of late highstand deposition .....	75
Figure 36c. Block diagram of highstand deposits exposed and mildly eroded during maximum sea-level fall .....	75
Figure 37a. Block diagram of early transgressive deposits.....	77
Figure 37b. Block diagram of late transgressive deposits.....	77
Figure 38. Block diagram demonstrating cyclic deposition .....	78

## **LIST OF TABLES**

Table 1. Results from AMS radiometric dating performed on samples from platform boring B-92.....	56
---	----

## **LIST OF PLATES**

(Plates are located in map pocket)

- Plate 1. Montage of seismic line 11 and integrated chronostratigraphy.
- Plate 2. Interpreted dip profile: seismic line 9.
- Plate 3. Interpreted dip profile: seismic line 13.
- Plate 4. Interpreted dip profile: seismic line 5.
- Plate 5. Interpreted strike profile: seismic line 40.



## INTRODUCTION

This project is a high-resolution sequence stratigraphic investigation of the continental shelf located offshore Texas between Matagorda Island and Baffin Bay (Fig. 1). It is an interdeltic, ramp-shaped portion of the shelf situated between the Rio Grande and Colorado/Brazos fluvial-deltaic systems.

The main objective of this study was to determine the response of an interdeltic prograding margin to the global eustatic changes of the last 350,000 years. A second objective was to identify and map the distribution of sand bodies through several glacial eustatic cycles in order to develop a model for sand prediction in interdeltic regions. These objectives have been achieved through an integration of seismic stratigraphy, lithostratigraphy, oxygen isotope stratigraphy, and chronostratigraphy.

Due to the absence of major fluvial input coupled with relatively high subsidence rates ( $\sim 1$  mm/yr), the central Texas shelf is considered a prime location for attempting to deconvolve the autocyclic and glacial eustatic influences on seismic stratigraphy. Having been termed "The Texas Mud Blanket" by Shideler (1981), deposition in the study area was thought to consist mostly of hemipelagic sediments delivered to the central Texas shelf primarily from the Mississippi River. Platform boring

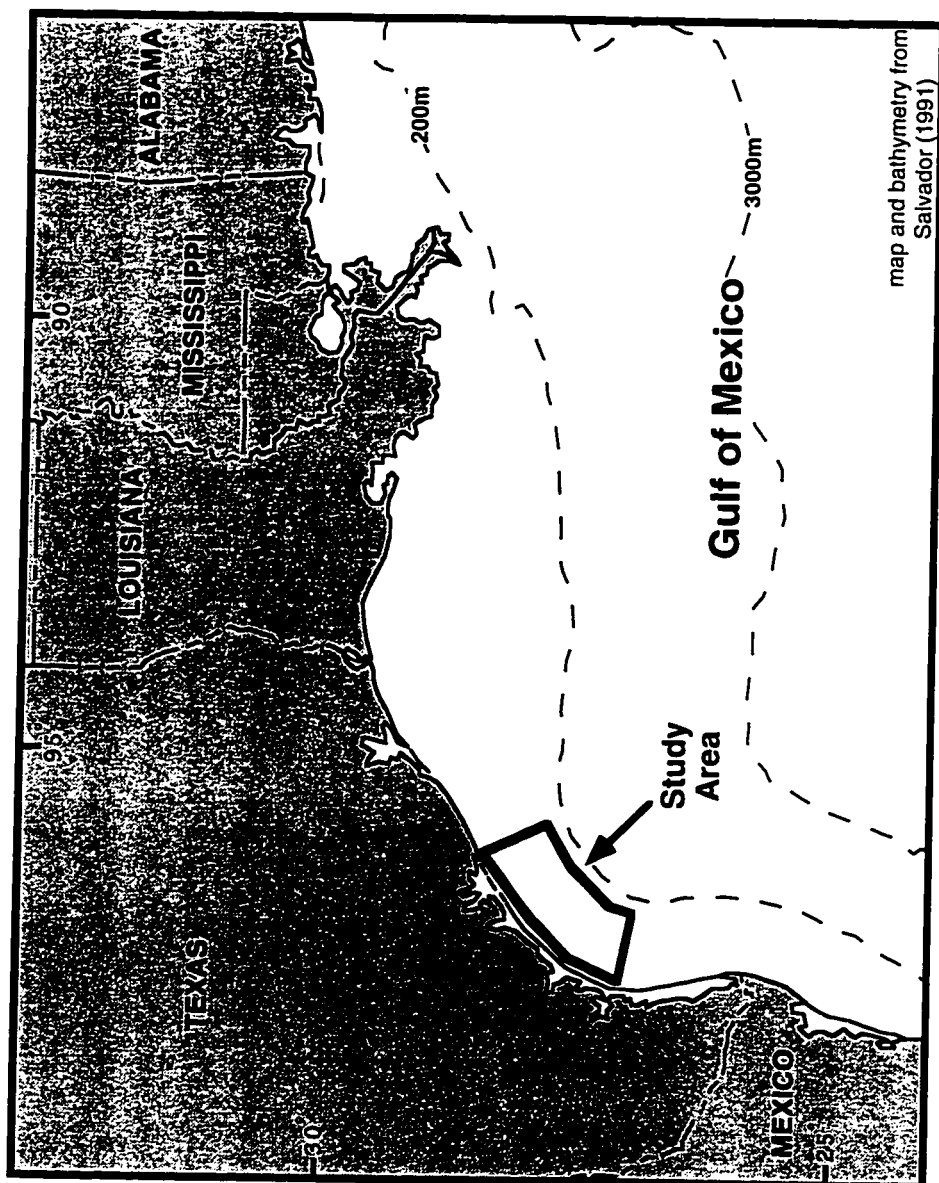


Figure 1. General location of study area.

descriptions show this portion of the shelf to be far more sandy than the modern highstand mud drape suggests. Sand bodies over 10 meters (32 ft) thick are sourced by longshore currents from the Rio Grande and Colorado fluvial-deltaic systems.

High frequency sea-level fluctuations during the Quaternary have resulted in a relatively condensed stratigraphic section in which several glacial eustatic cycles are imaged using high-resolution tools. Integrating near-outcrop scale seismic data with lithologic information from boring descriptions results in a spatial understanding of depositional environments. Adding radiometric dating and chronostratigraphy allows placement of these depositional systems into the proper geologic time frame.

A series of seven paleogeographic maps showing the distribution and thicknesses of depositional systems at various time intervals has been compiled. These maps show a strong repetition of depositional processes over each fourth order (100,000 year) glacial eustatic cycle. This repetition enabled the development of depositional models which may be applicable to the prediction of facies distribution in more ancient strata of the central Texas shelf and similar settings elsewhere.

## **GEOLOGIC SETTING**

### **History of the Gulf of Mexico**

The beginning stages of the Gulf of Mexico basin are not well understood. Magnetic anomalies, typically used to define sea-floor spreading, are weak and unorganized, which may be due to the great depth of burial or the high crustal temperatures present in the basin (Sawyer et al., 1991). Gravity surveys are of little use due to the widespread salt bodies. Seismic data does not provide much insight into the early evolution of the Gulf because the acoustic energy rapidly attenuates in the thick Cenozoic clastic sediments. The large impedance contrast between the Cenozoic clastics and Cretaceous carbonates also creates a barrier to acoustic energy, and the presence of salt makes seismic imaging difficult (Sawyer et al., 1991). Due to the fact that direct evidence of the early history of the Gulf of Mexico basin is missing, various theories have developed. An integration of a few main ideas is presented.

The Gulf of Mexico basin was initiated in the Late Triassic to Early Jurassic as a result of crustal attenuation and sea-floor spreading associated with the breakup of the supercontinent Pangea. During the breakup, terrestrial syn-rift deposition occurred throughout the United States and

Mexico regions, predominantly in the form of redbeds (Worrall and Snelson, 1989; Salvador, 1991).

Waters from the Pacific Ocean initially entered the proto-Gulf of Mexico through central Mexico during the Middle Jurassic (Salvador, 1991). The basin was a large shallow body of hypersaline water with limited ocean communication in an arid to semiarid climate, thus encouraging evaporation and salt deposition. The resultant salt deposits range from 1500-2000 meters in thickness (Worrall and Snelson, 1989).

In the latest Late Jurassic, emplacement of the oceanic crust ended. As the basin began to cool, contract, and subside, a widespread marine transgression commenced and continued through the earliest Early Cretaceous. Florida and the Yucatan remained as lowlands above sea level, preventing communication with the Atlantic Ocean (Salvador, 1991). The rapidly subsiding oceanic crust in the center of the basin was covered by several kilometers of water flowing in from the Pacific Ocean. The continental shelf and slope were formed over transitional crust and possessed a broad shallow ramp-like geometry (Sawyer et al., 1991). These shallow shelves allowed for the deposition of carbonates everywhere, except for in the northeast, where terrigenous clastics began to enter the basin (Salvador, 1991; Worrall and Snelson, 1989).

The Late Jurassic transgression reached its peak in the earliest Cretaceous when seawater finally covered the Florida platform, allowing the Gulf of Mexico to extend from the Pacific to the Atlantic and up through the Cretaceous Interior Seaway. By this time, the basic stratigraphic, structural, and geographic framework of today's Gulf of Mexico basin was established (Worrall and Snelson, 1989; Salvador, 1991; Sawyer et al., 1991). During the Early Cretaceous, siliciclastic sedimentation was limited to the northern part of the basin, while steep carbonate platforms dominated the eastern and southern regions, and gentler carbonate shelves existed in the west (Worrall and Snelson, 1989).

A huge fall of sea level occurred in the Mid- to Late Cretaceous, creating the mid-Cenomanian unconformity. This exposed the shallow shelves, therefore terminating carbonate deposition and severing communication with the Western Interior Seaway. A major transgression followed the lowstand during the Turonian, reestablishing connection with the Western Interior Seaway. Carbonate development was again initiated in the west, south, and east; while terrigenous clastics were sourced from the north.

The Late Cretaceous Laramide orogeny permanently cut off the Gulf of Mexico from the Cretaceous Interior Seaway and the Pacific Ocean. A huge increase in siliciclastic input along the western and northwestern

margins of the basin resulted, restricting carbonate deposition to the Yucatan area.

The Cenozoic was a period of immense siliciclastic influx to the northern and western portions of the basin, resulting in the deposition of prograding clastic wedges that exhibit numerous transgressive/regressive cycles. Each successive episode saw the shorelines, shelves, and shelf margins migrate progressively basinward (Salvador, 1991).

During the Paleocene to early Eocene, rivers draining into the Houston and Mississippi embayments supplied most of the sediment in the north-northwest Gulf of Mexico (Fig. 2). This marks the beginning of development of the Cenozoic section, which is up to 10 kilometers thick offshore Texas. These clastics were mainly deposited in fluvial and deltaic environments off Mississippi, Louisiana, Arkansas, and northeast Texas (Salvador, 1991). Deposition off central Texas was in the form of barrier-bar and strand-plain systems with landward lagoons (Fisher and McGowen, 1967). Longshore currents transported the sediments from the delta lobes in the northeast (Fisher and McGowen, 1967; Salvador, 1991).

The Middle Eocene through the Oligocene saw a gradual shift in the depocenter from the northern Gulf of Mexico margin to the Rio Grande area of South Texas (Fig. 3). During this time, cyclic sedimentation produced alternating packages of thick deltaic or strand-plain sands and

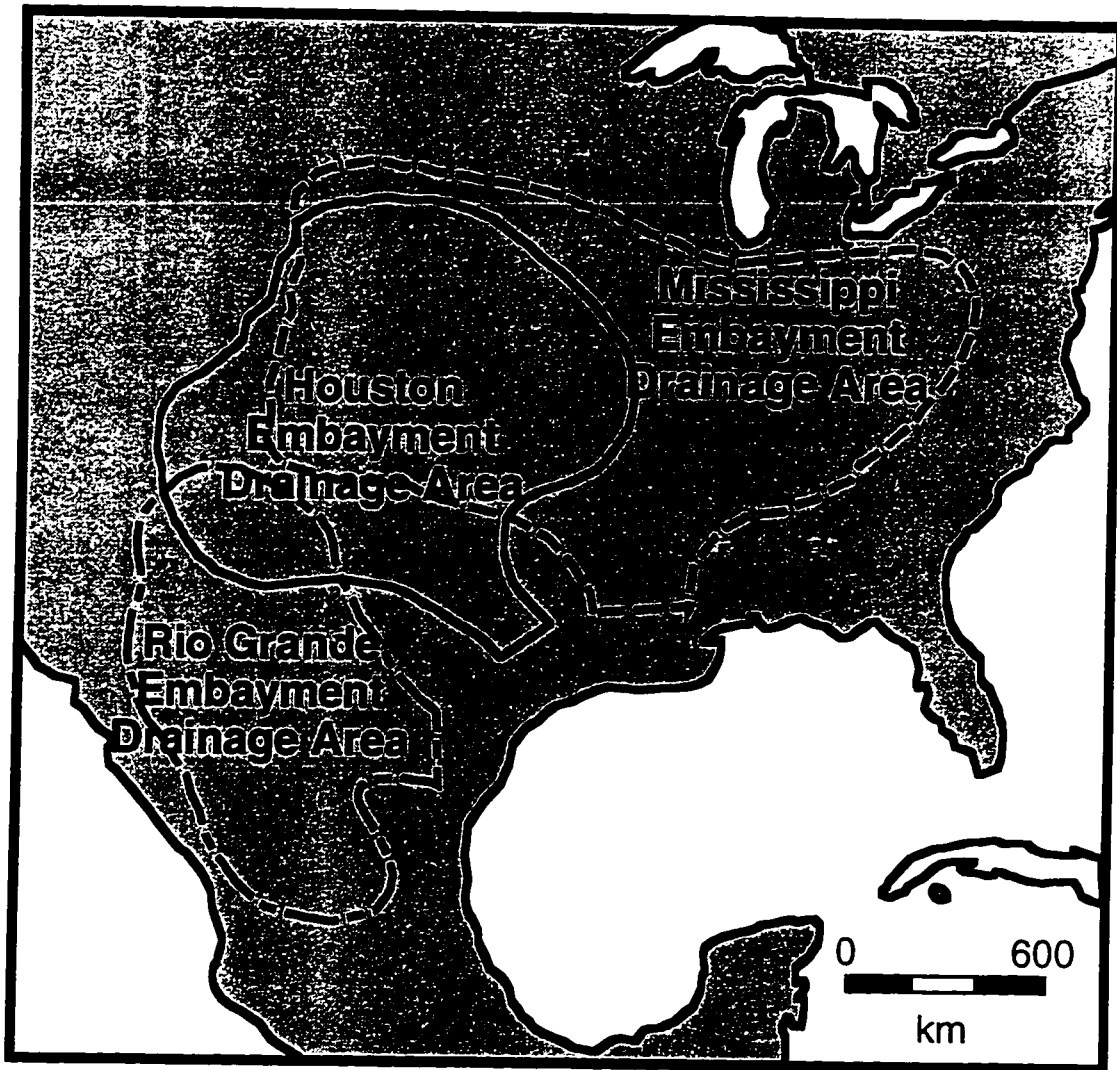


Figure 2. Cenozoic drainage basins (after Winker, 1981).



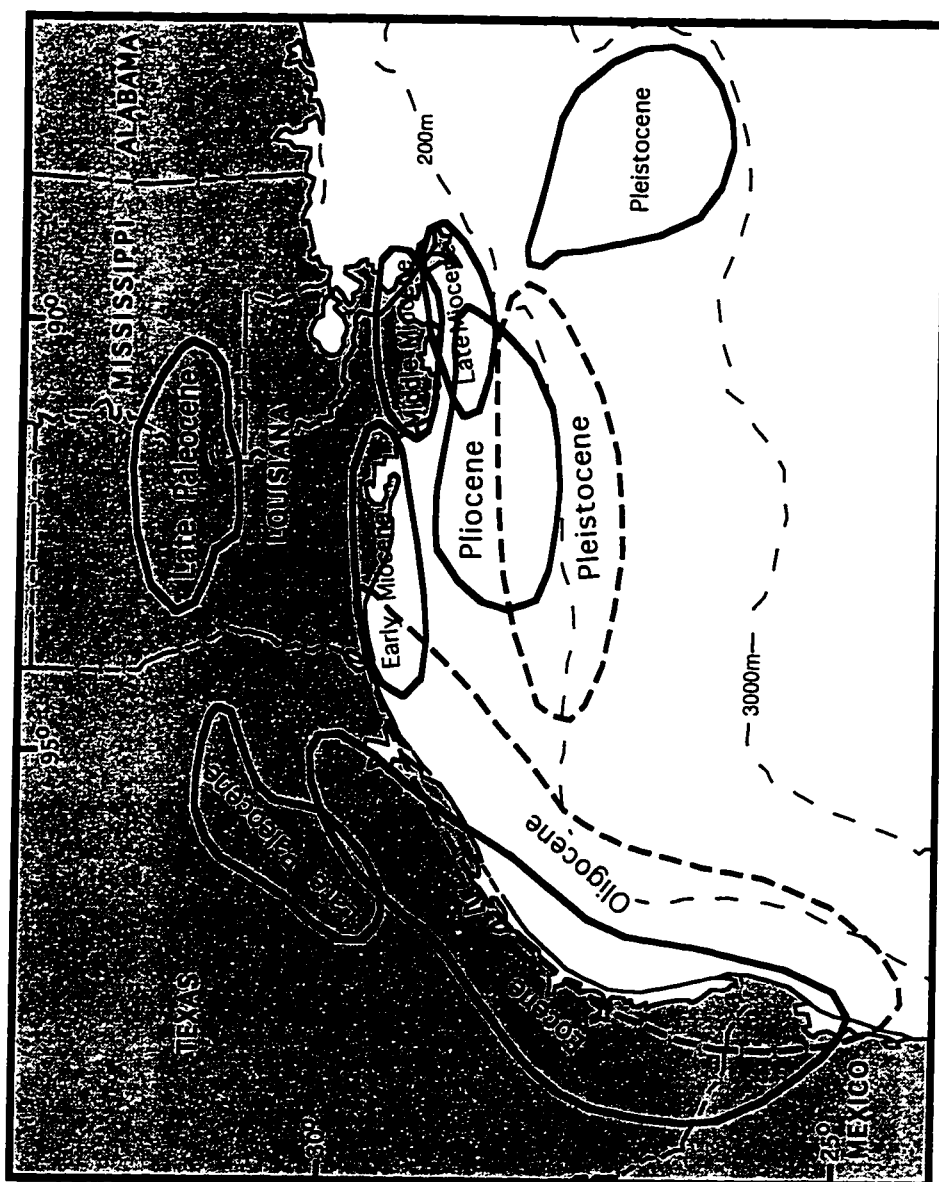


Figure 3. Cenozoic depocenters in the northwest Gulf of Mexico (after Salvador, 1991).

thin transgressive shaley sequences (Boyd and Dyer, 1964; Galloway et al., 1982; Salvador, 1991). Central Texas was situated between the two large fluvial-deltaic systems of the Houston and Rio Grande embayments, and again developed a wave-dominated strand-plain and barrier-bar system with updip lagoons and downdip shales. Growth faults developed on the basinward side of these deposits. Influx of terrigenous sediments into the northwestern Gulf of Mexico basin increased to a maximum during the Late Oligocene, resulting in the largest progradational clastic wedge of the Cenozoic. Due to this huge sediment load, the Jurassic Louann Salt was mobilized, causing reactivation of preexisting salt structures and the formation of many new ones (Salvador, 1991).

In the latest Oligocene to Miocene, the depocenter of the northern Gulf of Mexico returned to the Mississippi embayment (Fig. 3) following a widespread transgression. The highstand once again produced thick offlapping wedges during the Miocene, causing an 80 kilometer basinward advancement of the shelf and remobilization of salt structures, which in turn induced numerous growth faults. These same depositional processes continued into the Pliocene, when the main depocenter was located to the southwest of the present Mississippi River delta.

Although cyclic sedimentation patterns due to glacial-eustasy are present in the Tertiary section of the northwestern Gulf of Mexico, they

are much more dominant in the Pleistocene section. This is due to higher frequency glacial eustasy caused by northern hemisphere glaciation. This glacial eustatic influence on sedimentation overshadowed tectonics and sediment supply as regulating factors in Quaternary stratigraphic development. High sedimentation rates persisted, allowing the continued mobilization of salt due to sediment loading.

The late Quaternary (last 350,000 years) stratigraphic record of the central Texas continental shelf is examined in this thesis. This study describes the recent stratigraphy and seeks to investigate the roles of sediment supply, tectonics, and eustasy on deposition. Throughout the Cenozoic, sedimentation on the central Texas shelf has been sourced by the longshore transport of siliciclastic sediments from the Rio Grande, Colorado, Brazos, and Mississippi fluvial/deltaic systems. The various stratigraphic patterns observed in the section have been controlled by sediment supply, depocenter locations, and fluctuations in global sea level.

### **The Quaternary Setting**

The study area for this project covers approximately 12,000 square kilometers of the Texas continental shelf from Matagorda Island to 27°N, just south of Baffin Bay. It extends from a water depth of 20 meters out to the 150 meter bathymetric contour near the shelf edge (Figure 4).

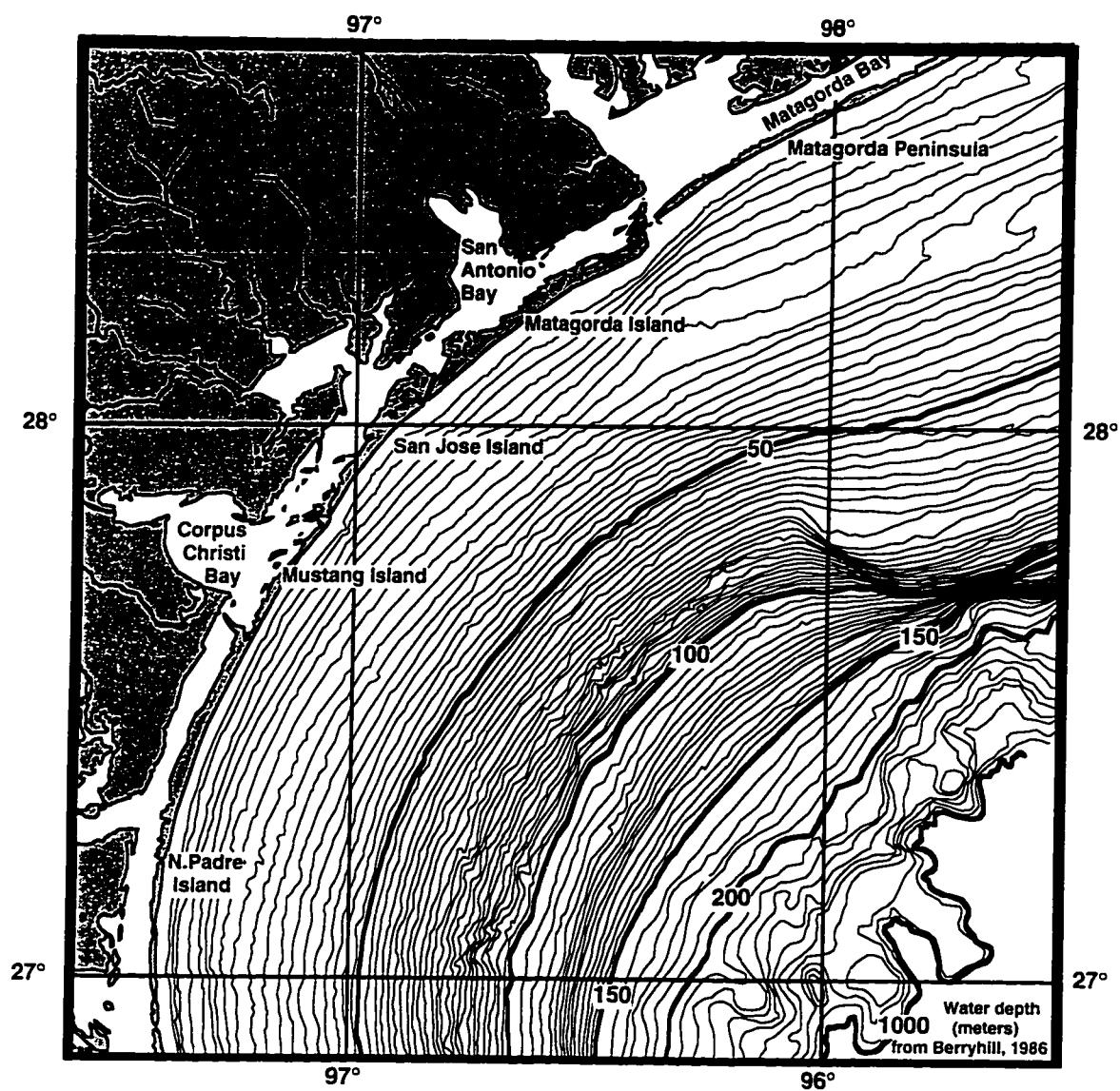


Figure 4. Detailed bathymetric map of study area.

Temporally, the data spans the last 350,000 years, or the three most recent glacial cycles. Several elements influence deposition of sedimentary packages on the central Texas shelf, including subsidence, growth faulting due to shale tectonics, wind and current patterns, and changes in global sea level.

### *Subsidence*

Estimates of subsidence due to flexure loading and sediment compaction on the central Texas shelf over the last 120,000 years vary from about 0.1 mm/yr. on the inner shelf to 1.2 mm/yr. on the outer shelf (Winker, 1979). Assuming the same shelf gradient has persisted throughout the time frame of this study, the above estimates agree well with calculations from this dataset, which demonstrate between 0.25 to 1.0 mm/yr. subsidence. Sediment compaction is thought to contribute very little to the overall accommodation space (Siringan, 1993), therefore, the primary mechanism for subsidence is assumed to be the flexure of the underlying lithosphere in response to sediment load (Walcott, 1972).

### *Growth Faulting*

Shale tectonics have led to several growth fault systems on the Texas shelf and slope (Fig. 5). Heavily faulted anticlines in the near surface are

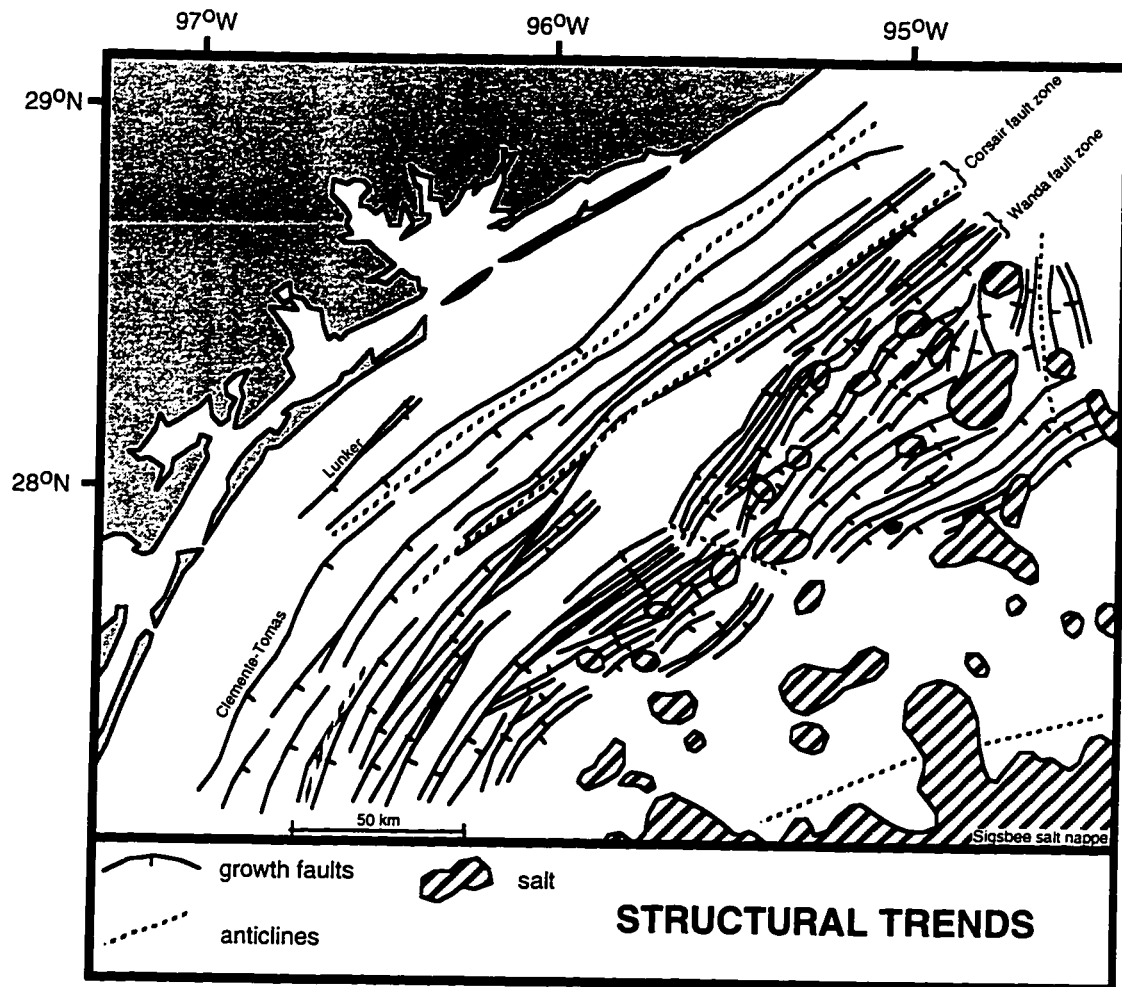


Figure 5. Structural trends offshore central Texas, including growth faults, salt structures, and salt- and shale-cored anticlines (from Bradshaw and Watkins, 1994).

manifestations of overpressured shale ridges at depth (Bradshaw and Watkins, 1994). During progradation, the overpressured Tertiary shales behave as a viscous fluid and migrate away from the sediment load (usually landward) and into an uplift (Fig. 6). This differential loading and corresponding shale flowage results in the initiation of down-to-the-basin growth faults. All of the faults offset Pleistocene sediments and some reach the Quaternary and even the seafloor, indicating that the faulting process continues today.

#### Wind and Current Influence

The present wind and current patterns affecting the western margin of the Gulf of Mexico are considered to have remained essentially unchanged throughout the Quaternary. During most of the year, the predominant winds are east-southeasterly, approaching the northeast Texas coast at oblique angles, thus setting up south-westward longshore currents and transport (Fig. 7) towards the central Texas shelf. Similar winds strike the south Texas coast, creating a northward movement of water and sediments, again towards the central Texas shelf (Lohse, 1956; Curray, 1960, Rezak et al., 1985). These converging longshore currents not only carry enough sediments to the western Texas coast to create beach and barrier-bar sand bodies, but some of this material even becomes available

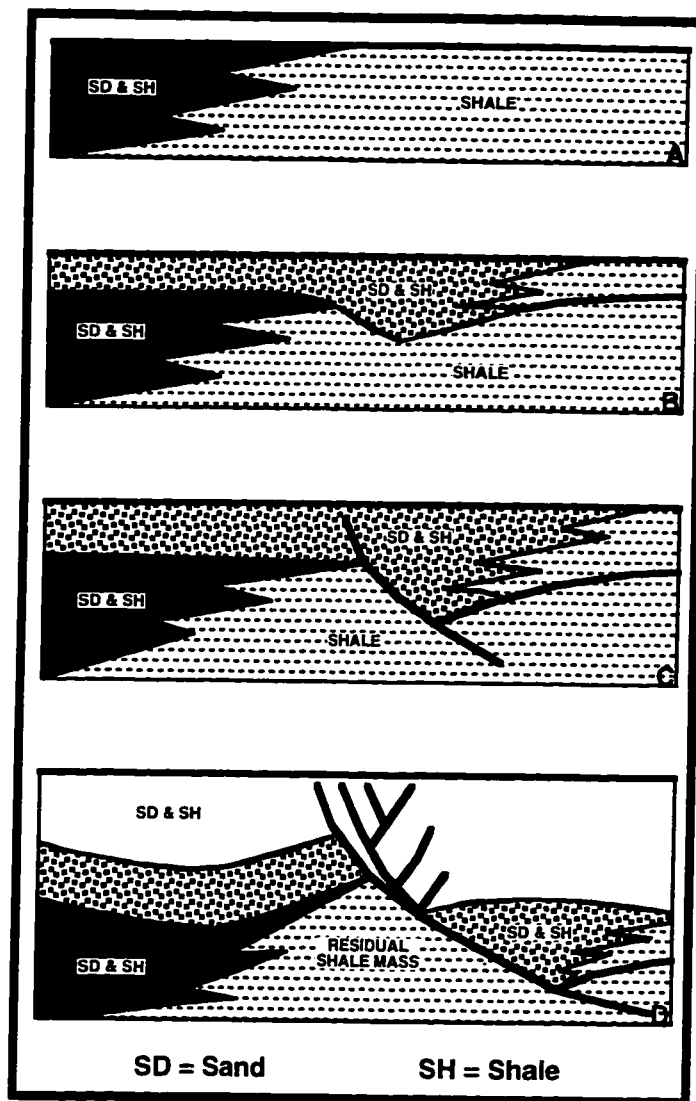


Figure 6. Conceptual diagram showing progression of shale rise and faulting as a result of sediment loading (from Berryhill et al., 1986).



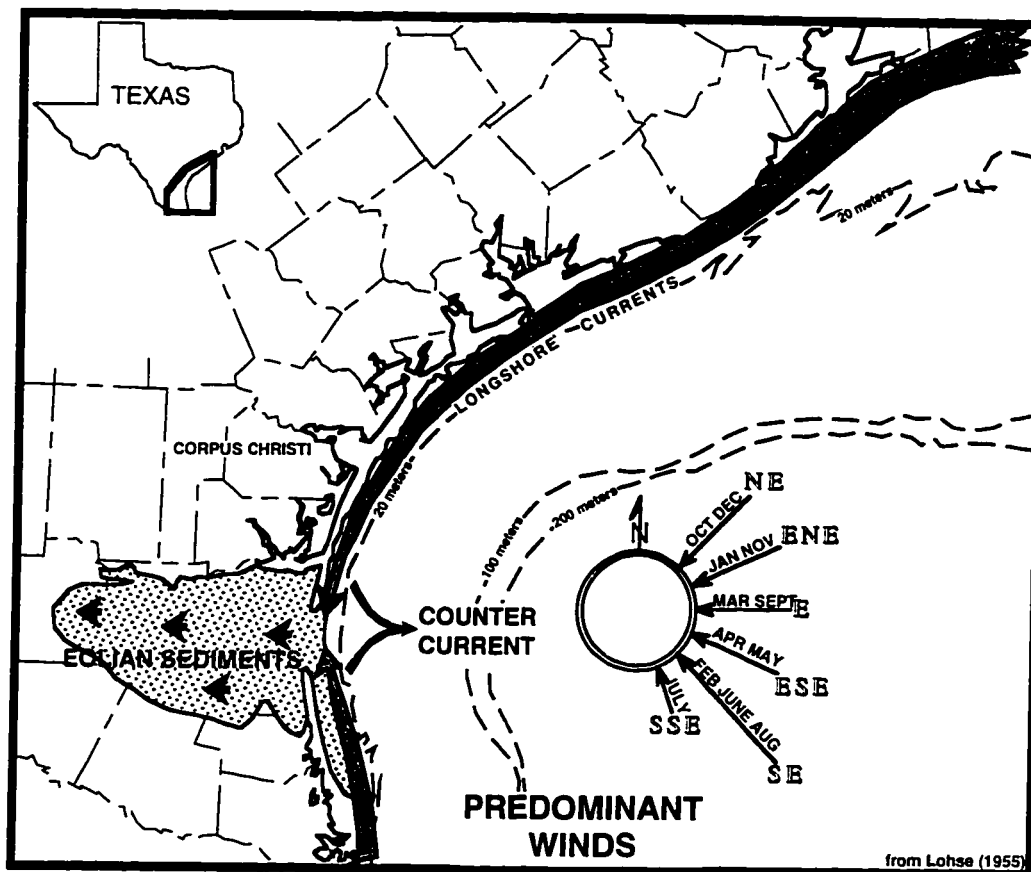


Figure 7. Predominant winds and resulting current patterns (from Lohse, 1955).

for eolian sorting and transport, thereby creating the vast sandsheet that is filling Laguna Madre today (Lohse, 1956).

### *Glacio-eustatic Sea-level*

Pleistocene glacial events have been found to play an important role in determining the stratigraphy of the Quaternary sediments in the Gulf of Mexico as evidenced by Fisk (1944), LeBlanc and Hodgson (1959), Winker (1979), Berryhill et al. (1986), Thomas and Anderson (1991), Abdullah and Anderson (1991), Siringan (1993), Sarzalejo (1993), Sydow and Roberts (1994), Anderson et al. (1994), Abdullah (1994), and many others. Attempts to obtain an accurate sea-level record for the Quaternary have encountered much difficulty due to various complicating factors such as local subsidence, radiometric dating errors, and incorrect paleo-water depth estimates for microfauna. Figure 8 shows a compilation of several of these curves compared to the standard Late Quaternary oxygen isotope record. The oxygen isotope SPECMAP curve (Imbrie et al., 1984) has been converted to depth by G. Haddad (Fig. 9), and has proven to be a good proxy for changes in global sea-level. Therefore, it is used in this study as an independent indicator of sea-level. The results of this study demonstrate that the fourth order (100,000 year) fluctuations observed on

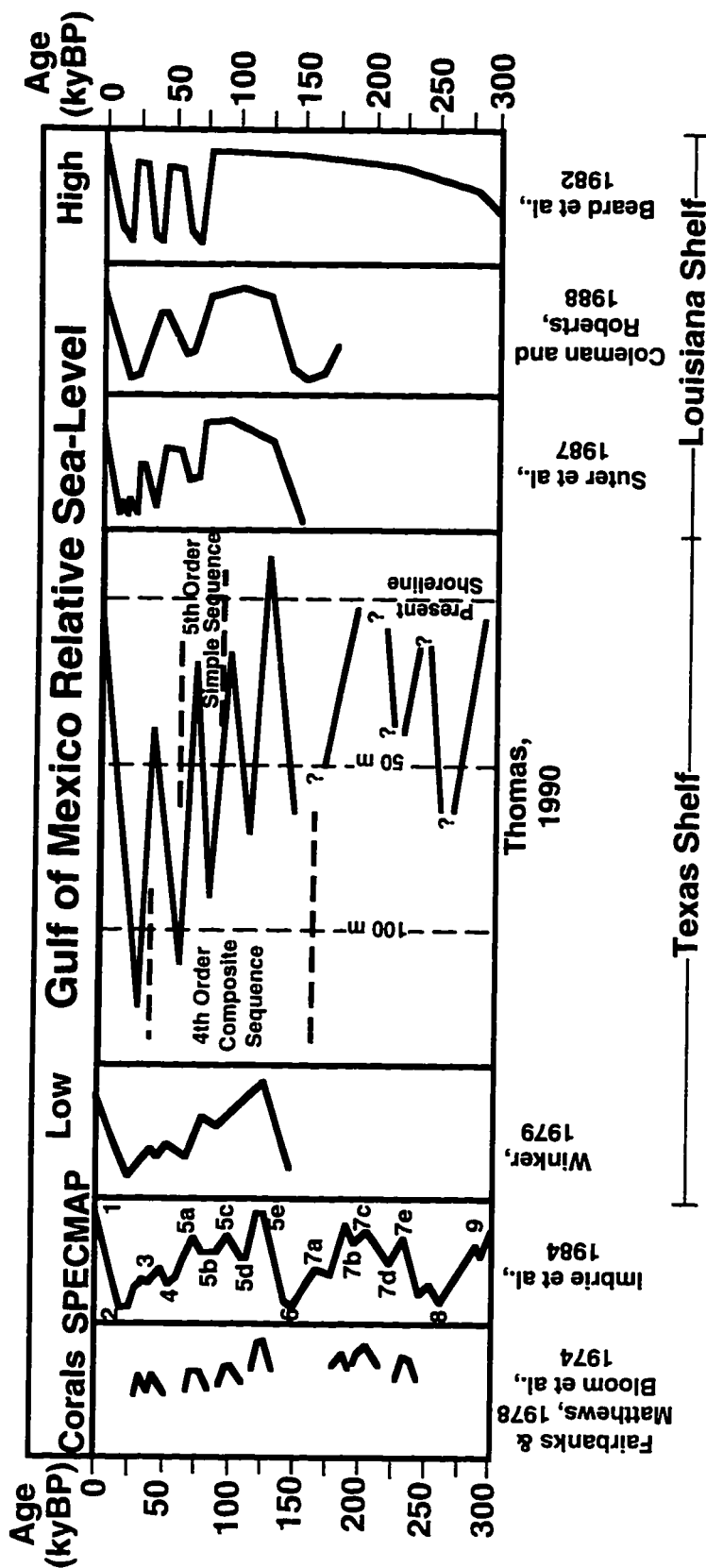


Figure 8. Compilation of Late Quaternary sea-level curves as compared to the SPECMAP curve.

# **Glacio-Eustatic Sea Level** **From SPECMAP (Imbrie et al., 1984)** **(converted to depth by Geoff Haddad)**

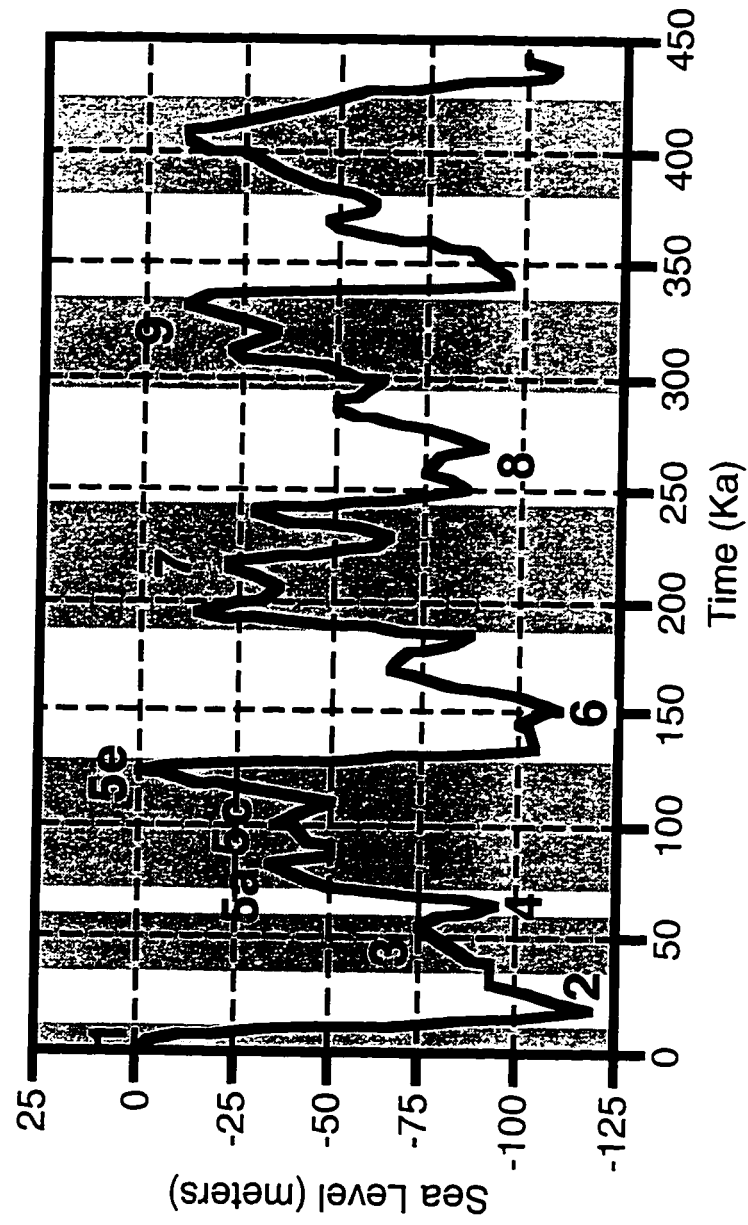


Figure 9. Oxygen isotope SPECMAP curve (Imbrie et al., 1984)  
 converted to depth by G. Haddad.

the SPECMAP curve control the distribution of facies on the central Texas shelf.

## **PREVIOUS WORK**

Central Texas Tertiary interdeltaic deposits outcrop onshore and are prolific oil and gas sources and reservoirs. Much work has been performed on these deposits using outcrop studies and subsurface well data in an attempt to understand their relationship to the occurrence of oil and gas.

The Upper Paleocene-Lower Eocene Wilcox group contains several environments analogous to those found on the present-day central Texas coast and shelf (Fisher and McGowen, 1967). Longshore currents transported sands southwestward from the Rockdale (Guadalupe-Colorado-Brazos-Trinity) delta system and deposited them along the coast, forming the San Marcos Strandplain-Bay System (Fig. 10). The strandplain deposits are well-sorted, fine-grained sheet and tabular sand bodies situated parallel to the paleoshoreline with thicknesses up to 16 meters (50 ft). Moving southwestward along strike, the strandplain system narrows into the Cotulla Barrier-Bar and Indio Bay-Lagoon Systems (Fig. 10). The elongate, strike-parallel bodies composing the barrier-bar system contain very well-

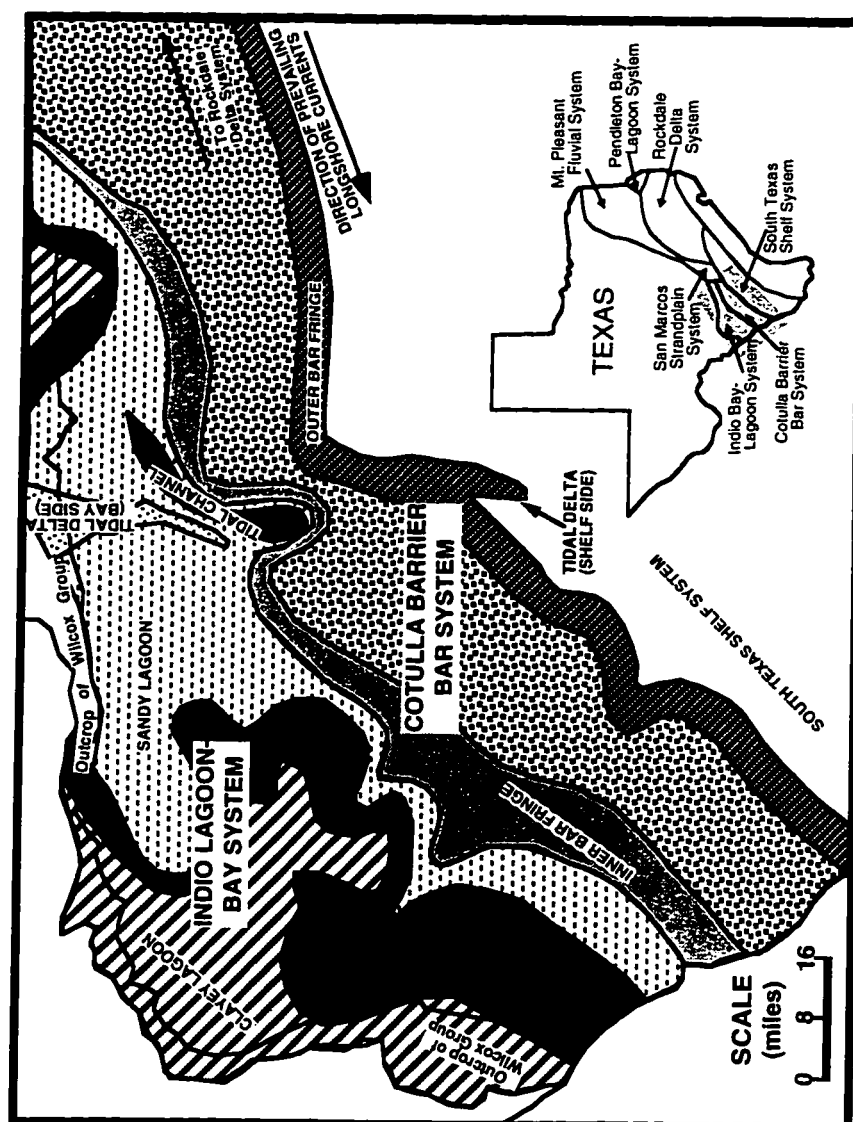


Figure 10. Map of Wilcox depositional systems (modified from Fisher and McGowan, 1967).

sorted, fine-grained sands that range up to 30 meters (100 ft) thick. The landward lagoon system is characterized by thin-bedded, laminated and burrowed gypsiferous or calcareous muds. Seaward of the barrier-bars lies the South Texas Shelf System (Fig. 10), composed predominately of gray or olive mud deposited on an extensive, shallow-water continental shelf (Fisher and McGowen, 1967).

The middle Eocene Yegua Formation was also deposited on a muddy, shallow, low-angle shelf (Meckle and Galloway, 1996). A wave-dominated regime situated between two fluvial-dominated systems again resulted in the deposition of elongate strike-oriented sand deposits, which are interpreted as barrier-bars or strandplain systems (Fig. 11). Landward of these systems, a sand-starved lagoon was formed, while basinward a muddy shelf existed. Unlike the Wilcox barrier-bar sands, which were sourced from the northeast, the Yegua sands appear to have originated mainly from the southwest. This indicates either an increase in sediment supply to the Rio Grande fluvial-deltaic system or a slight change in the wind pattern and resulting surface currents to transport the sediments from the southwest.

The Oligocene Frio Formation also exhibits a barrier/strandplain system, but its landward equivalent was a coastal lake/streamplain environment rather than a lagoon system (Fig. 12). The Choke

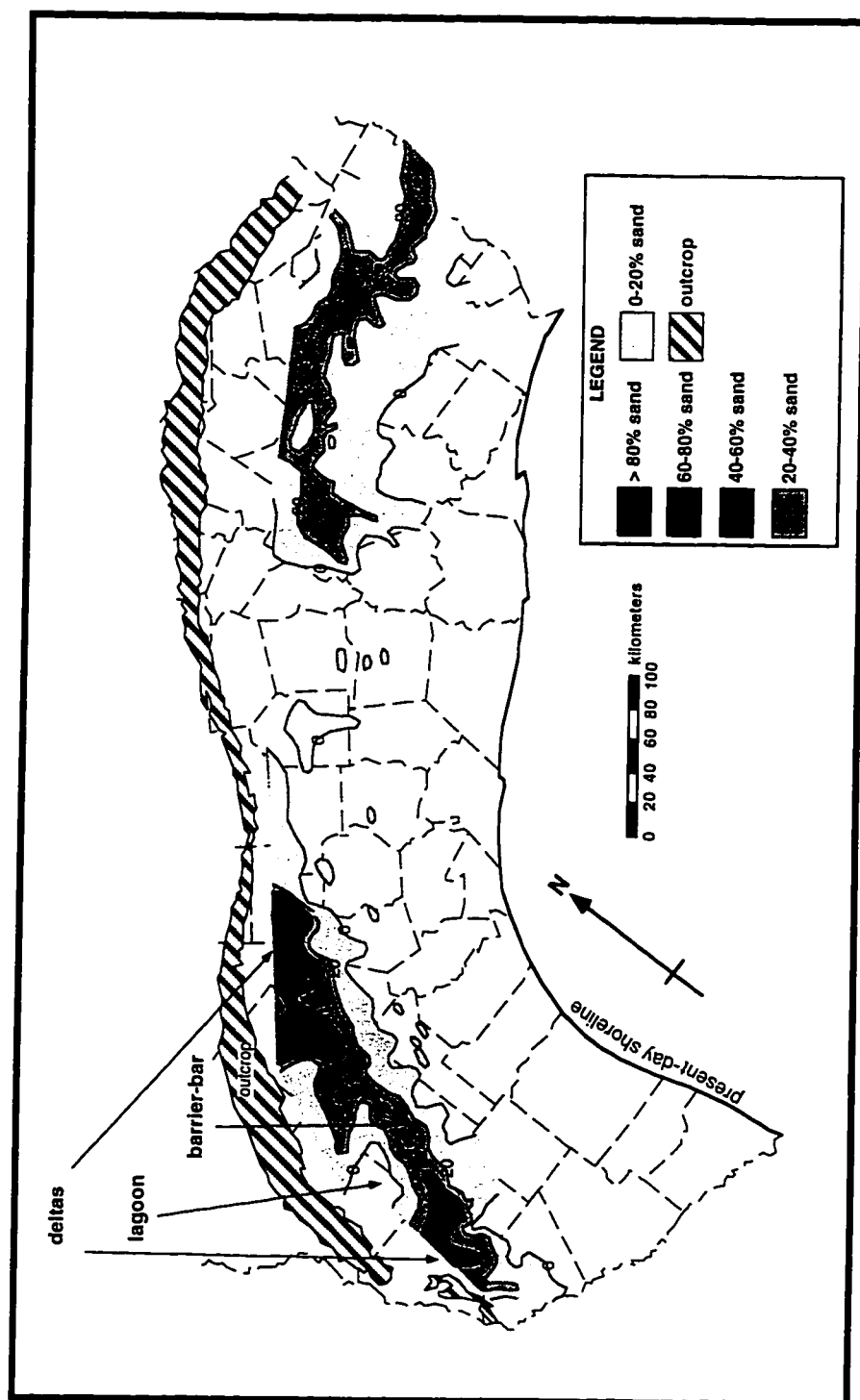


Figure 11. Depositional systems of the Yegua formation (modified from Meckle and Galloway, 1996).



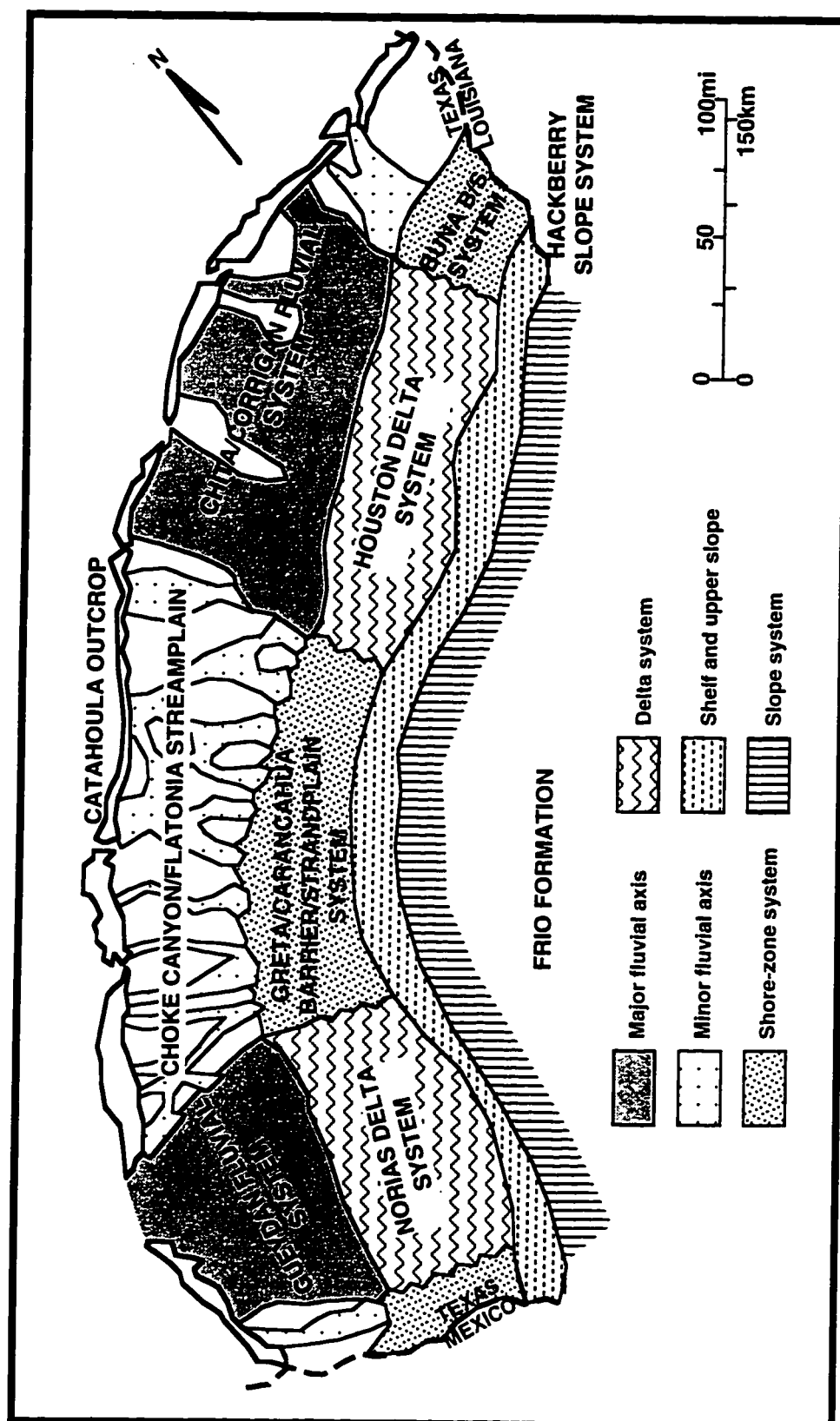


Figure 12. Depositional systems of the Frio Formation (modified from Galloway et al., 1982).

Canyon/Flatonía streamplain is a broad, muddy apron containing many thin, narrow, dip-oriented, channel-fill and meanderbelt sandstone bodies, which are encased in coastal lake mudstone sequences (Galloway et al., 1982). The Greta/Carancahua barrier/strandplain system lies on the basinward edge of these deposits. The bars consist of well-sorted, fine-grained sands, which appear massively aggradational in cross-section varying in width from 40 to 65 kilometers. Seaward, these sands abruptly pinch out into gray and green shales (Boyd and Dyer, 1964). Dual province sand mineralogy (Bebout et al., 1978) and the relatively uniform development of sands between the two delta systems indicates that converging longshore currents from both the southwest and the northeast sourced the barrier and strandplain sands (Galloway et al, 1982).

The central Texas coast barrier-bar/strandplain system has persisted into the Quaternary as evidenced by remnants of the Late Pleistocene Ingleside Beach-Ridge trend observed onshore extending from Matagorda Bay to Baffin Bay (Fig. 13). Outcrop and subsurface data show these to be thick sands that interfinger with lagoonal clay updip (Winker, 1979).

Berryhill et al. (1986) used high-resolution seismic data to study the late Quaternary continental shelf in the Gulf of Mexico. They identified several transgressive/regressive sequences on the seismic sections (Fig. 14), but had little lithologic or chronostratigraphic control to aid their

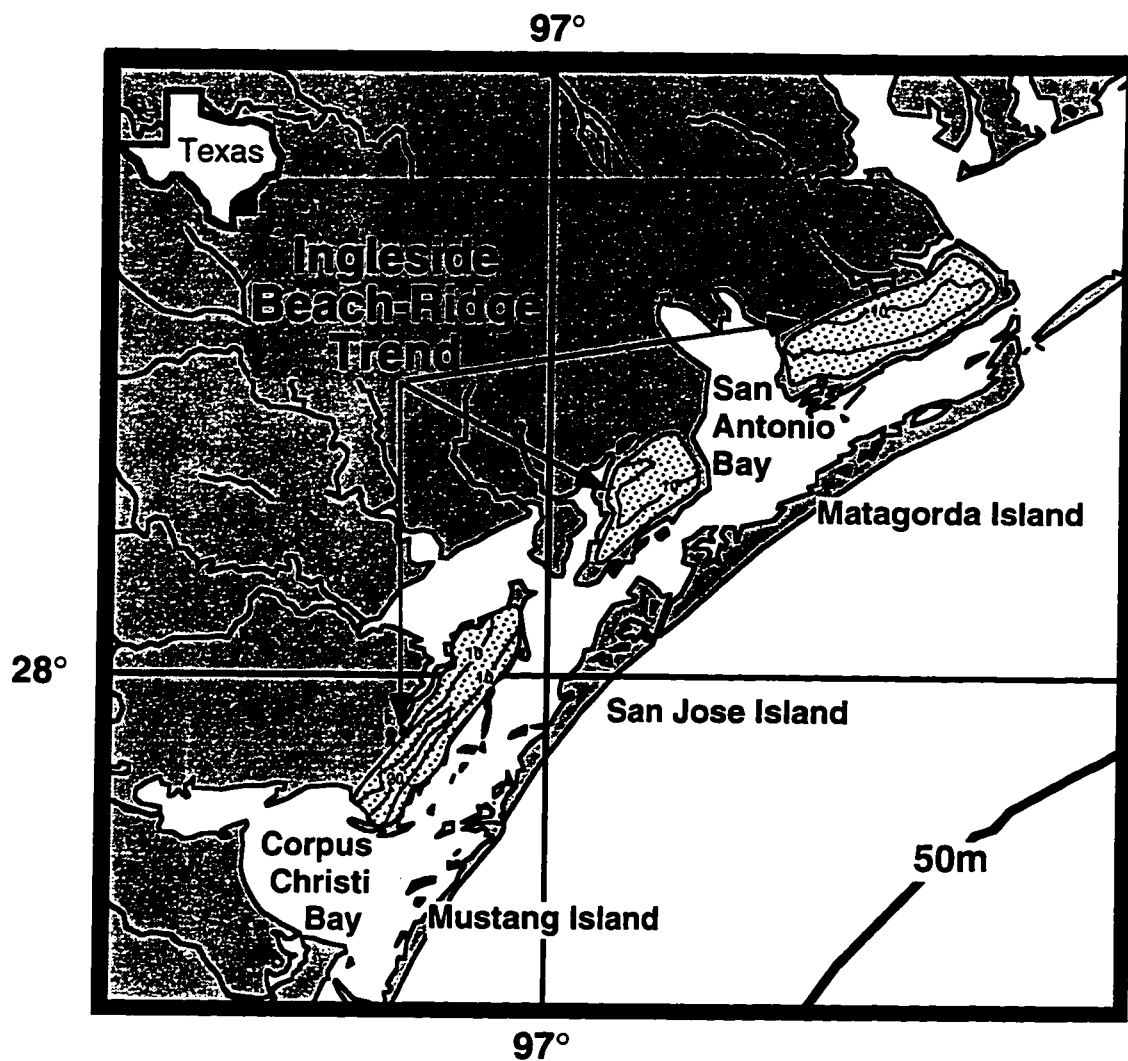


Figure 13. Map of Ingleside beach-ridge trend (modified from Winker, 1979).

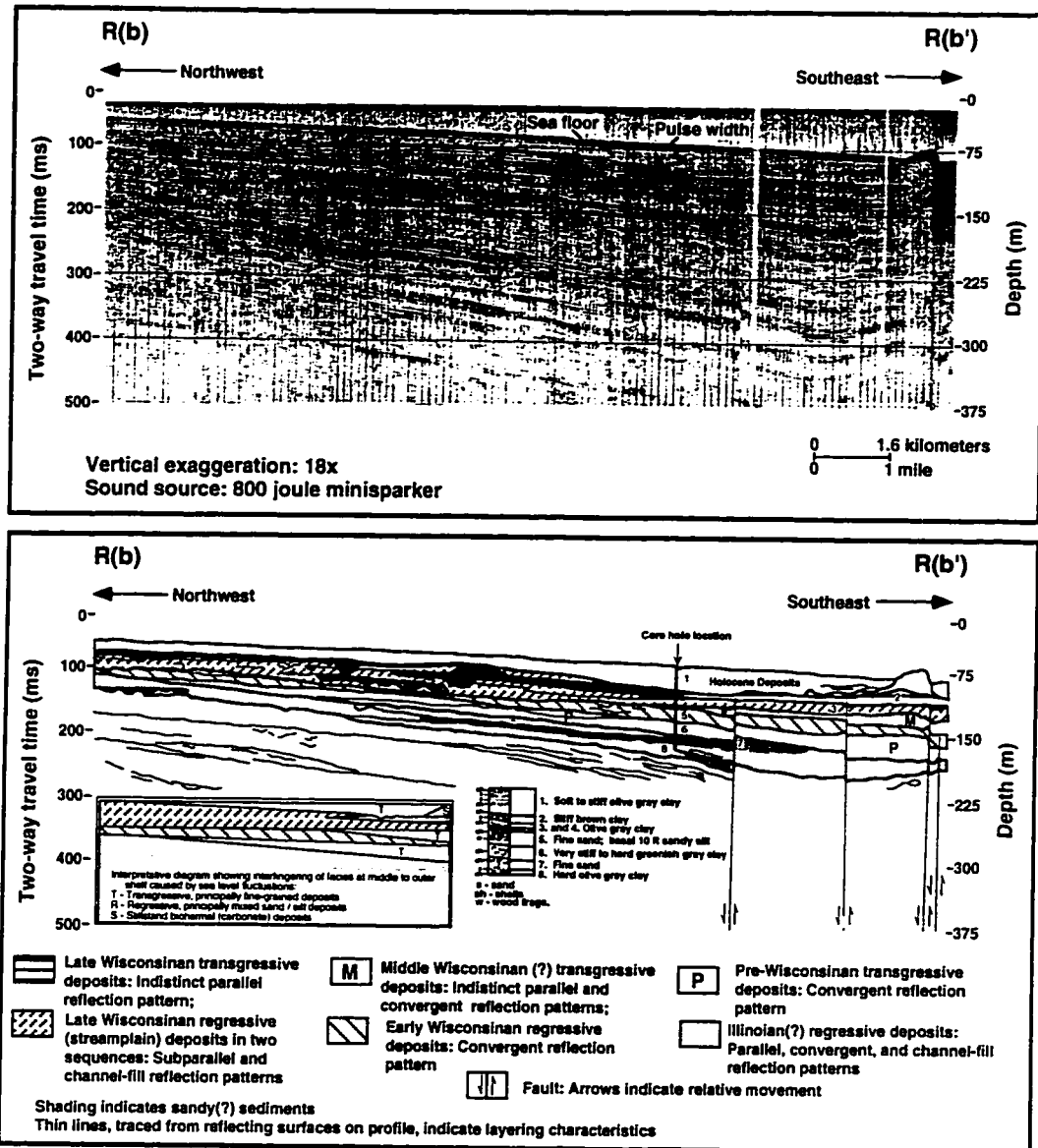


Figure 14. High-resolution seismic data and interpretation of alternating transgressive/regressive deposits (from Berryhill et al., 1986).

interpretations. A map of the Late Wisconsinan (most recent lowstand) suggests that, as in the Tertiary Frio Formation, the central Texas shelf consisted of a streamplain system of coalesced fluvial deposits extending to about the mid-shelf, with a barrier coastline seaward of this streamplain (Fig. 15). Situated above these coastal deposits is a series of strike-aligned drowned corallgal reefs (Rezak et al., 1985; Berryhill et al., 1986). The reefs vary in relief from 1 to 22 meters and are composed of dead coral and coralline material. Radiocarbon dating of reef material has yielded ages ranging from 18,000 to 10,580 yr BP (Bright and Rezak, 1976; Berryhill et al., 1976).

The wave-dominated, interdeltaic setting of the central Texas shelf appears to have existed for at least 65 million years and continues today. This dataset demonstrates the same type of environments during the Late Quaternary, but through the integration of seismic imaging, lithologic control, and chronostratigraphy, this study yields a better overall understanding of the interdeltaic environment, its corresponding facies, and their sequence stratigraphic relationships.

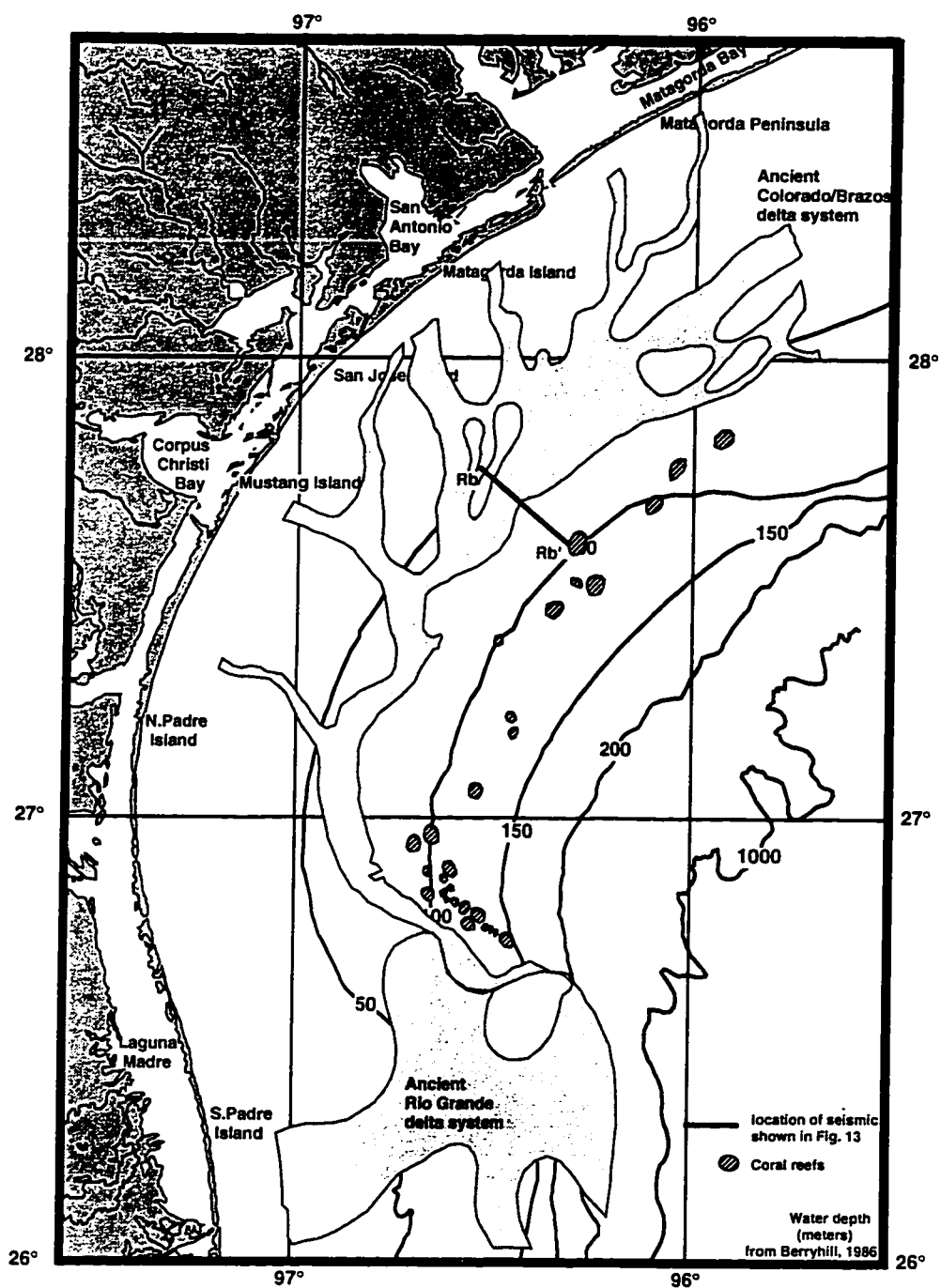


Figure 15. Map of Late Wisconsin deposits illustrating streamplain system dominating the shelf during the lowstand (after Berryhill et al., 1986).

## **DATASET AND METHODS**

### **Seismic Acquisition**

A total of 1200 kilometers of 2-dimensional, single-channel, high-resolution seismic data were collected (Fig. 16) using Rice University's research vessel, the *R/V Lone Star*. The seismic records were shot with a 15 cubic inch SSI water gun, which generates frequencies of 40-2000 Hz, and recorded using an Elics, PC based, Delph 2 acquisition system. The water gun was fired at 3 second intervals with 480 msec of data recorded at a sampling rate of 1/4 msec. A total of 12 lines were collected. Nine dip lines, spaced 10-15 km apart, and 3 regional strike lines located in shallow (35 meters), intermediate (70 meters), and shelf edge (150 meters) water depths. A Trimble Differential GPS with an accuracy of approximately +/- 15 m was used for positioning.

### **Seismic Processing**

Basic digital processing of the seismic dataset was performed on a workstation using ProMax software. Because the data were single channel and sampled low-dip strata, not much processing was needed. This limited processing includes mutes, filters, and an Automatic Gain Control (AGC). A top mute was employed to remove water column noise. The frequency

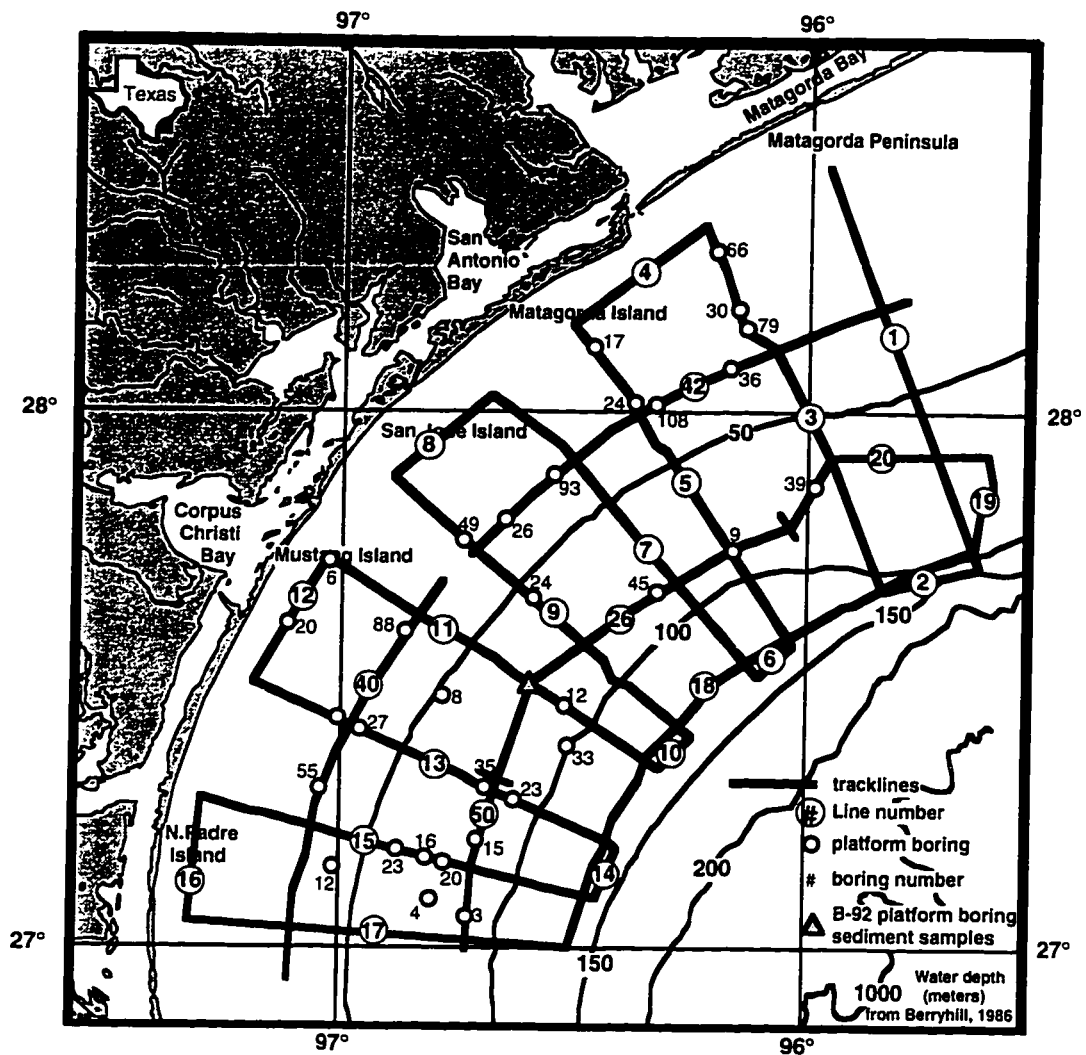


Figure 16. Seismic and platform boring dataset location map.



content of the data indicated that the usable signal was primarily between 120 and 800 Hz, therefore, an Ormsby bandpass filter of 90-180-720-1440 was applied. Finally, a mean AGC with a 10 msec operator length was used for better visual interpretation.

### **Seismic Interpretation**

The processed seismic data were loaded onto a Sun workstation equipped with Landmark's Seisworks 2D software for interpretation. The basic tenants of seismic stratigraphy (Vail et al., 1977) were implemented during the interpretation process. First, major surfaces were identified and correlated throughout the dataset. Reflection terminations against the surfaces aided in the interpretation of the surface type (i.e. sequence boundary, flooding surface, or ravinement surface). Next, higher order surfaces and internal reflection patterns were analyzed to further the understanding of the stratigraphy and depositional environments.

### **Lithostratigraphy**

Platform boring descriptions (ranging from 20-150 meters long) from 33 locations (Fig. 16) and core samples from one boring location (150 meters long) comprise the lithologic control for this study. The extent to which lithofacies can be integrated with the seismic data to better

facies interpretation is limited by the detail of the platform boring descriptions. The descriptions are broken up into gross lithologies, sediment colors, and variations in stiffness with no indication of internal sedimentary structures (Fig. 17; Appendix 3), therefore, limiting depositional environment interpretation.

The lithologic data are tied to the seismic data using an average velocity of 1525 m/sec. Although true velocities may vary from this value, similar conversions have been used in other studies (1525 m/sec by Abdulah, 1995; 1500 m/sec by Sydow and Roberts, 1994), and a strong correlation is observed between lithologic boundaries and changes in seismic character. One source of error that may exist in the ties between the seismic data and lithologic descriptions is in projecting the core positions laterally onto the seismic lines. Most of the seismic data were acquired within 100 meters of key platform borings, but a few borehole locations are several kilometers from the nearest seismic line, thus requiring lateral projection.

### **Oxygen Isotope Analyses**

The SPECMAP curve (Imbrie et al., 1984) is used in this project to provide independent evidence of glacial and interglacial stages (Fig. 9). Using the extrapolation that  $\delta^{18}\text{O}$  can also represent changes in ice volume

## Matagorda Island Block 639 B-36

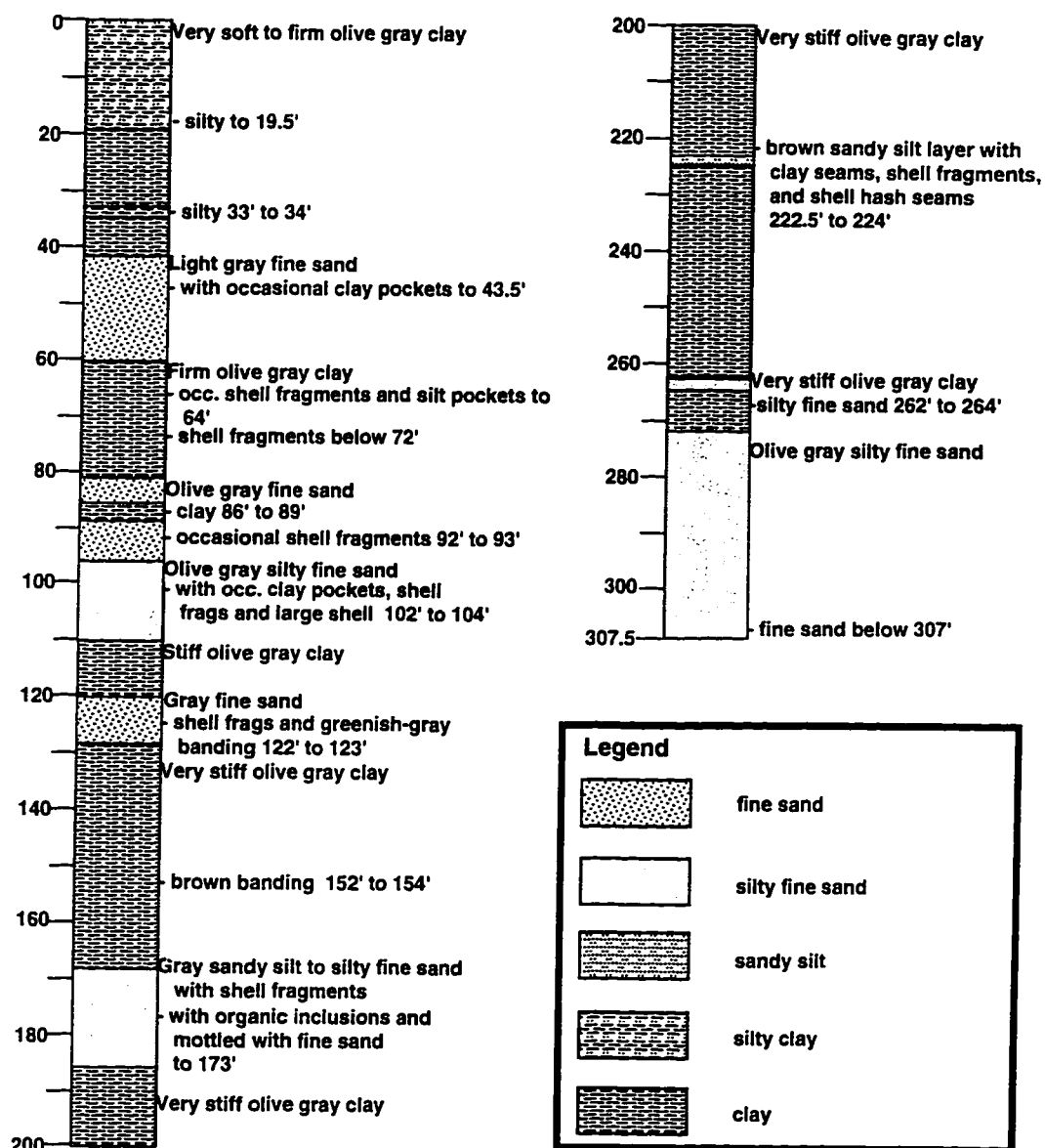


Figure 17. Example of a typical platform boring description.

(Shackleton and Opdyke, 1973), the curve was converted to depth by G. Haddad, using a 10 meter sea-level change for every 0.1 per mil change in  $\delta^{18}\text{O}$  (Shackleton and Opdyke, 1973). This yields a curve which serves as a proxy to glacio-eustatic sea level.

Oxygen isotope analyses were performed on samples from the B-92 platform boring (Fig. 16) using the planktic foraminifera *Globigerinoides ruber*. Initially sampled by Fugro-McClelland, samples were available at approximately one-foot intervals for the upper 100 feet of the boring and then at approximately ten-foot intervals for the lower 300 feet. Each sample was soaked in Calgon solution in a 45°C oven for 1-2 days to disaggregate the clays. Next the samples were washed through a 63  $\mu\text{m}$  sieve and allowed to dry in a 45°C oven. Once dry, the samples were sieved into three fractions: 63 to 250  $\mu\text{m}$ , 250 to 355  $\mu\text{m}$ , and >355  $\mu\text{m}$ . *Globigerinoides ruber* occurring within the 250 to 355  $\mu\text{m}$  fraction were selected for analysis. The total number picked for each sample is listed in Appendix 1. The foraminifera were then cleaned by filling the sample vials halfway with deionized water and dipping them into an ultrasonic cleaner for approximately one second intervals. Isotopic measurements were performed on a mass spectrometer at the University of Maine under the supervision of Dr. Jim Wright and results were adjusted to PDB.

## Radiocarbon Dating

Accelerator Mass Spectrometry (AMS) radiocarbon dating ( $^{14}\text{C}$ ) of planktonic foraminifera provides accurate dates for samples less than 45,000 years in age (Faure, 1986). This method was applied to two samples from the B-92 platform boring, one at a depth of 19 meters (61 ft) and the other at 25.8 meters (82.5 ft). The planktonic foraminifera selected were from the 250 to 355  $\mu\text{m}$  fraction. Since the AMS technique required at least 5 mg of sample, therefore, other planktonic foraminifera had to be picked in addition to *Globigerinoides ruber*, and included *Globorotalia menardii*, *Globigerinoides trilobus*, and *Neogloboquadrina dutertrei*. Sample preparation was much the same as for oxygen isotope analysis, except that no Calgon solution was used and special care was taken to always use deionized water rather than tap water which may alter the carbon content. The deeper sample was sent to Beta Analytic Inc. for analysis and the shallower one was sent to Woods Hole Oceanographic Institute.

## DATA AND RESULTS

### Seismic Stratigraphic Surfaces

Seismic stratigraphy suggests that key bounding surfaces enable the separation of genetically related strata (Vail et al., 1977). These surfaces are categorized by the manner in which seismic reflections above and below the surface are terminated. Two primary types of seismic stratigraphic surfaces prevail throughout this dataset.

Erosional surfaces associated with maximum sea-level fall appear as high-amplitude, continuous reflectors. These surfaces erosionally truncate reflectors below, and reflectors above onlap them (Plates 1-5). These are the sequence boundaries of Vail et al. (1977). On the inner shelf, a few minor fluvial incisions mark the sequence boundaries, most notable on strike lines (Fig. 18a). On the middle shelf, these surfaces are often associated with significant relief that is also seen on dip lines (Fig. 18b), and they tend to be smooth on the outer shelf. Four regional sequence boundaries have been identified in this dataset. From oldest to youngest, they are labeled SB8, SB6, SB4, and SB2 as shown on Plates 1 and 2.

Downlap surfaces associated with maximum sea-level rise are imaged as moderate to high amplitude, continuous reflectors. The reflectors below these surfaces demonstrate toplap and concordance, and those above

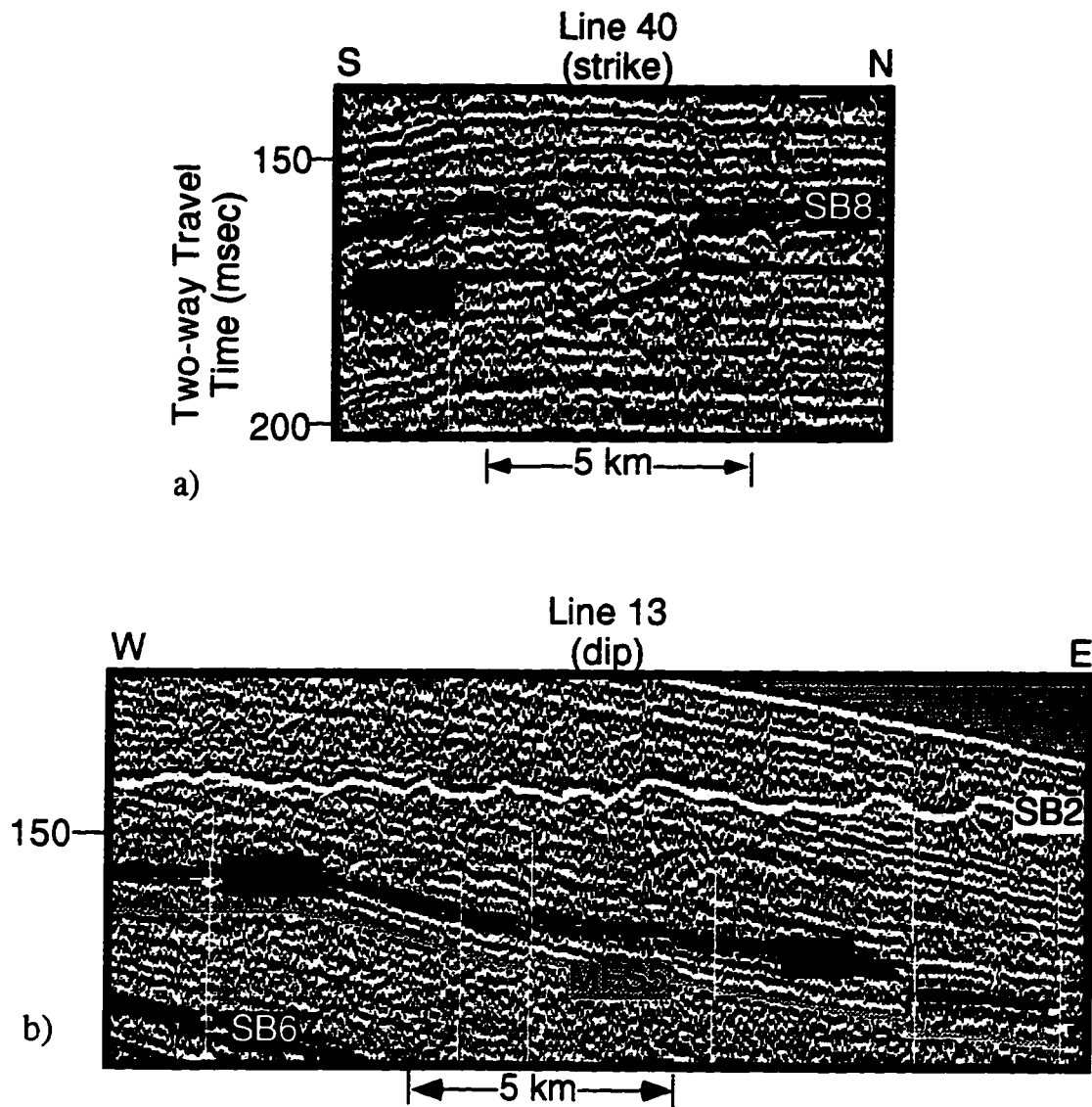


Figure 18. a) Seismic example of an incision associated with a sequence boundary, SB8, in strike view. b) Seismic line 13 illustrating significant relief associated with a sequence boundary, SB2, in dip view. (See location map, Figure 16.)

downlap onto them (Plates 1-5). These are the maximum flooding surfaces of Vail et al. (1977). These flooding surfaces are generally smooth reflectors in both strike and dip view, with little relief throughout the area. Four regional maximum flooding surfaces have been identified in this dataset. From oldest to youngest, they are designated MFS9, MFS7, MFS5, and MFS3, which is amalgamated with the SB4 sequence boundary (Plates 1 and 2).

These sequence boundaries and maximum flooding surfaces form the major boundaries between alternating transgressive and regressive deposits. Sequence boundaries form the base of these transgressive deposits, while flooding surfaces are their upper boundary. Conversely, regressive deposits begin after the flooding surface and are terminated by a sequence boundary.

## **Seismic Facies**

Variations of seismic reflection character within genetically related stratigraphic packages allow for classification of seismic facies. Characteristics of these facies, examined from both strike and dip views, assist in determining the depositional environment of the stratigraphic unit. These characteristics include external geometry, internal reflection pattern,



reflection continuity, and amplitude. Four types of seismic facies are observed in this seismic dataset.

#### *Seismic Facies Unit A (SFU A)*

From both strike and dip perspectives, SFU A contains very continuous, sub-parallel reflectors of low to moderate amplitude within an overall wedge geometry (Fig. 19; Plates 1 and 2) that extends across the entire shelf. The base of SFU A onlaps a sequence boundary, and the top of the unit is concordant with the above flooding surface, placing it in the transgressive systems tract (Van Wagoner et al., 1988). Platform boring B-45 (Fig. 20) shows the typical lithology within SFU A. The greenish-gray or olive clay containing scattered shell fragments generally indicates marine deposition. SFU A occurs repeatedly through time, with three examples observed in this dataset (Plates 1-5). The facies are interpreted to be transgressive shelf clays, similar to the modern Holocene Texas mud blanket. Deposition of SFU A is from settling of hemipelagic muds carried into the area by converging longshore and surface currents.

#### *Seismic Facies Unit B (SFU B)*

SFU B occurs on the inner to middle shelf regions of the study area. In dip view, it is characterized by discontinuous, low-amplitude, chaotic seismic reflection patterns that occasionally exhibit faint high-angle

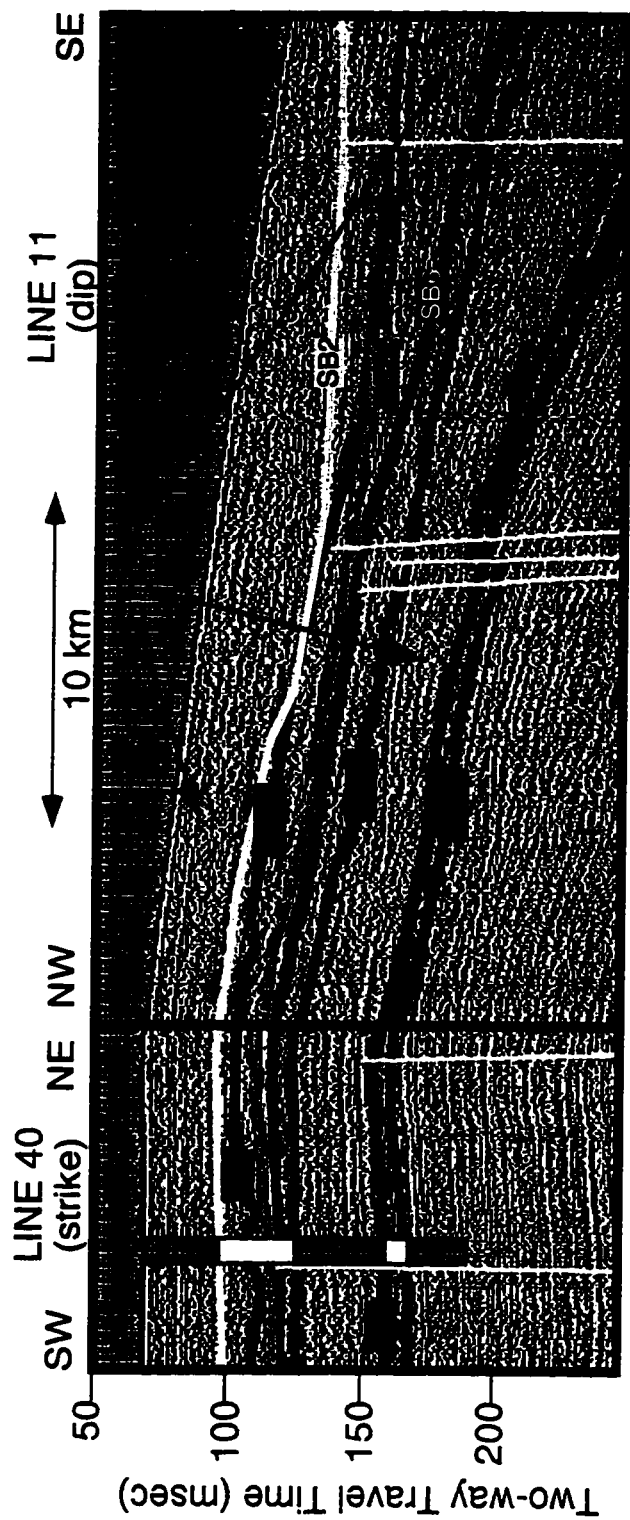


Figure 19. Strike and dip seismic example of SFU A, transgressive muds. Platform boring

B-88 demonstrates the correlation between seismic character and lithofacies. Yellow represents sand or silt and gray represents clay.

### Mustang Island Block A-113 B-45

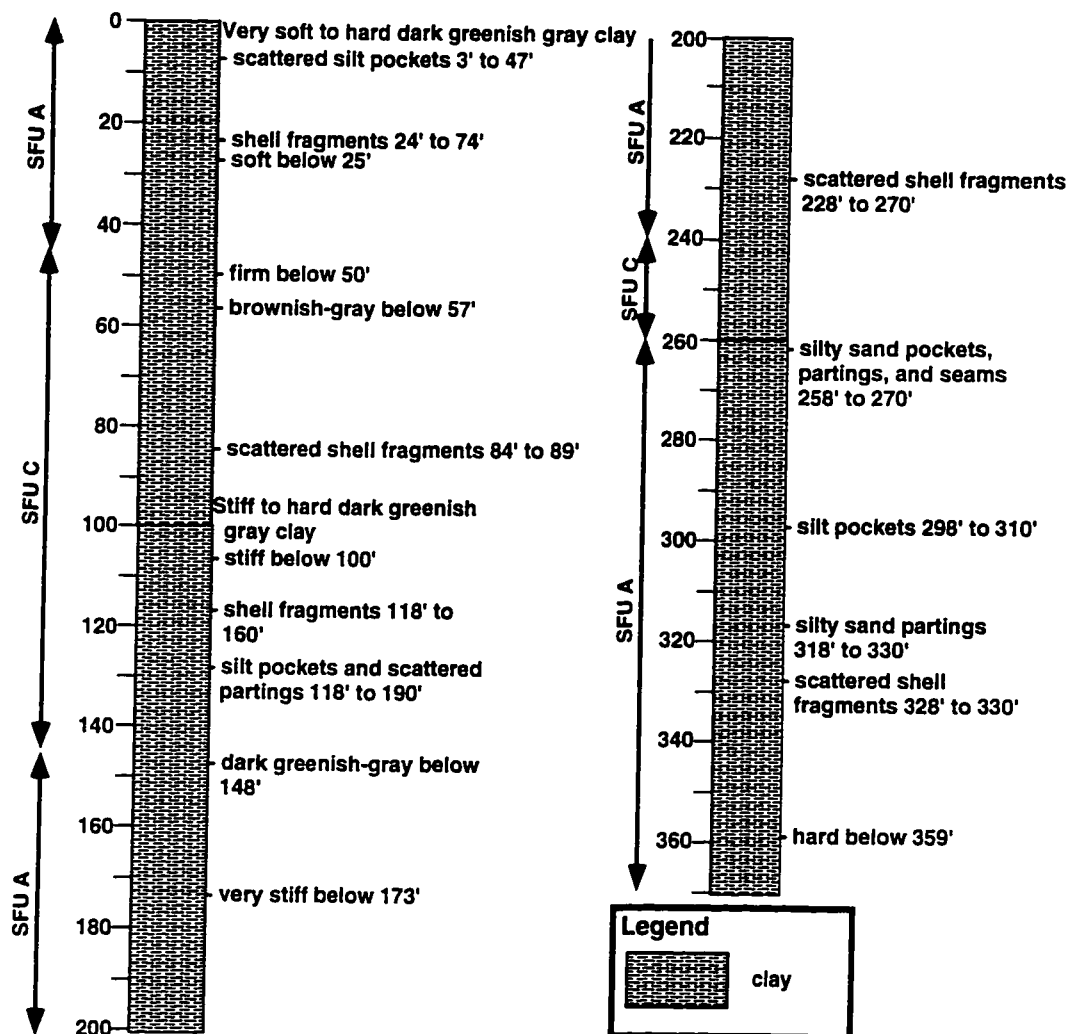


Figure 20. Platform boring description B-45 illustrating lithofacies associated with SFU A: greenish-gray clay with occasional shell fragments. See dataset map (Figure 16) for borehole location.

shingled clinoforms within a bank-shaped geometry (Fig. 21; Plates 1 and 2). Along strike, this facies appears chaotic to transparent (Fig. 21). High-angle basinward pinchouts define the downdip limit of this facies. SFU B downlaps onto a basal flooding surface and is capped or partially eroded by a sequence boundary, placing this facies into a highstand systems tract (Van Wagoner et al., 1988). Lithofacies associated with SFU B are comprised of a light gray fine to silty fine sand, often containing scattered shell fragments (Figure 22). Grain size analyses from platform boring B-92 demonstrate a slight coarsening upwards sequence (Appendix B). An example of SFU B occurs in each of the four time intervals studied in this area (Plates 1-5). These facies have been interpreted to be highstand barrier-bar sands prograding into shallow water. Longshore currents erode these sands from the Colorado and Rio Grande deltas and transport them into the area (Fig. 7).

#### *Seismic Facies Unit C (SFU C)*

SFU C is restricted to the middle to outer shelf areas of this dataset and is the downdip time-equivalent package to SFU B. Within a wedge-shaped external geometry, SFU C consists of generally continuous, low to moderate amplitude, tangential oblique prograding clinoform reflections that at times appear almost transparent (Fig. 23; Plates 1 and 2). These

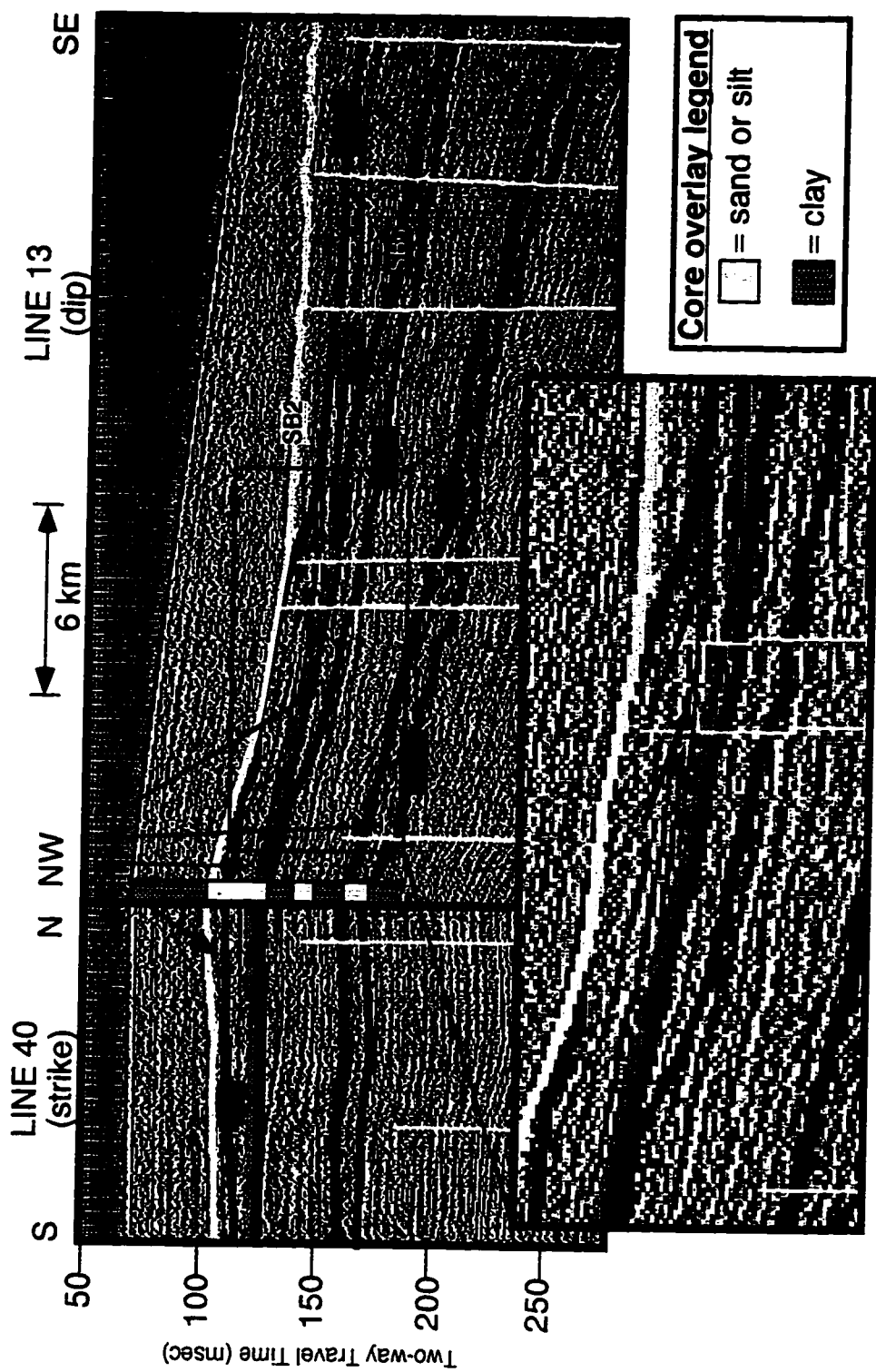


Figure 21. Strike and dip seismic example of SFU B, barrier-bar sands. Platform boring B-27 demonstrates the correlation between seismic character and lithofacies.

### Mustang Island Block 847 B-27

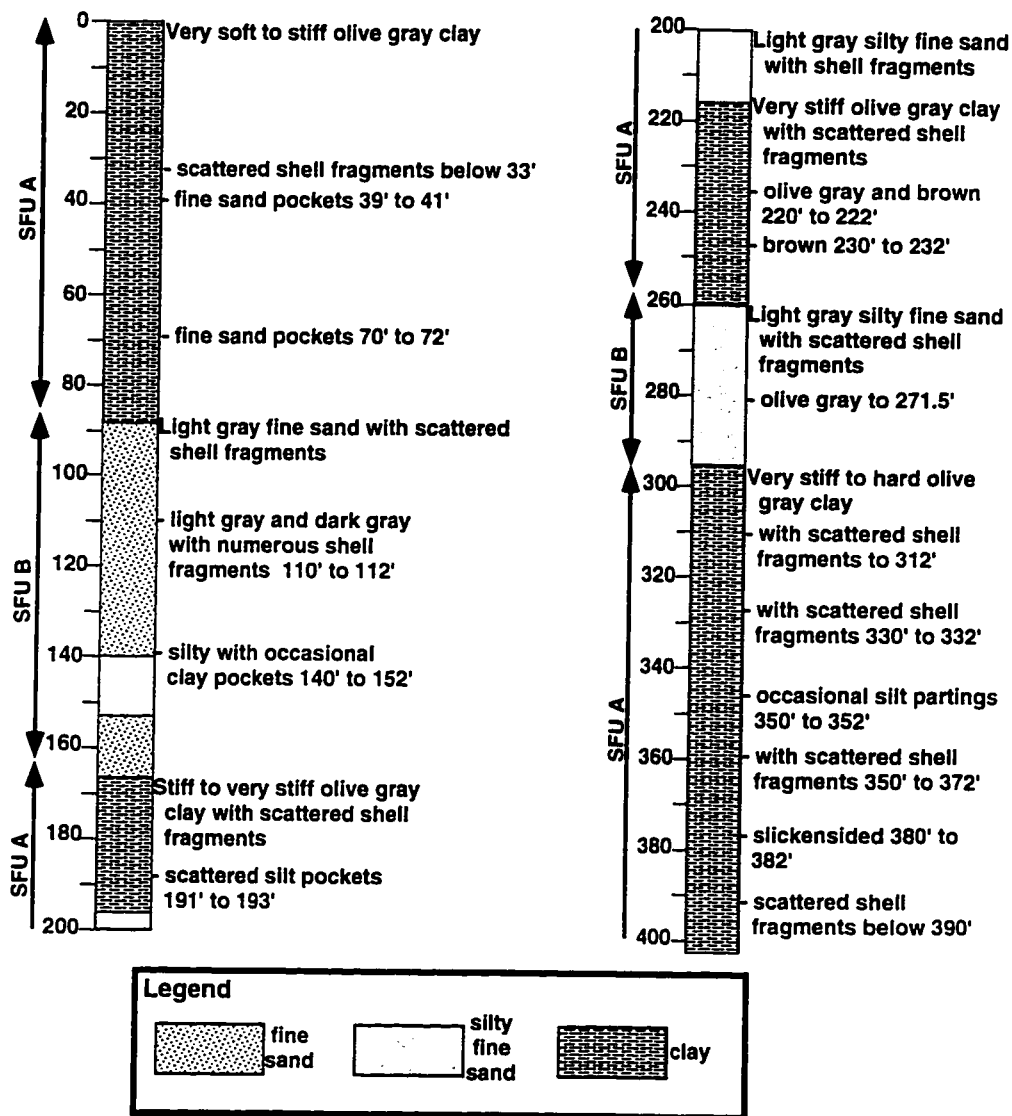


Figure 22. Platform boring description B-27 illustrating lithofacies associated with SFU B: light gray fine to silty fine sand with scattered shell fragments. A condensed lithlog of this platform boring is shown on Figure 21 and Plate 3. See dataset map (Figure 16) for borehole location.

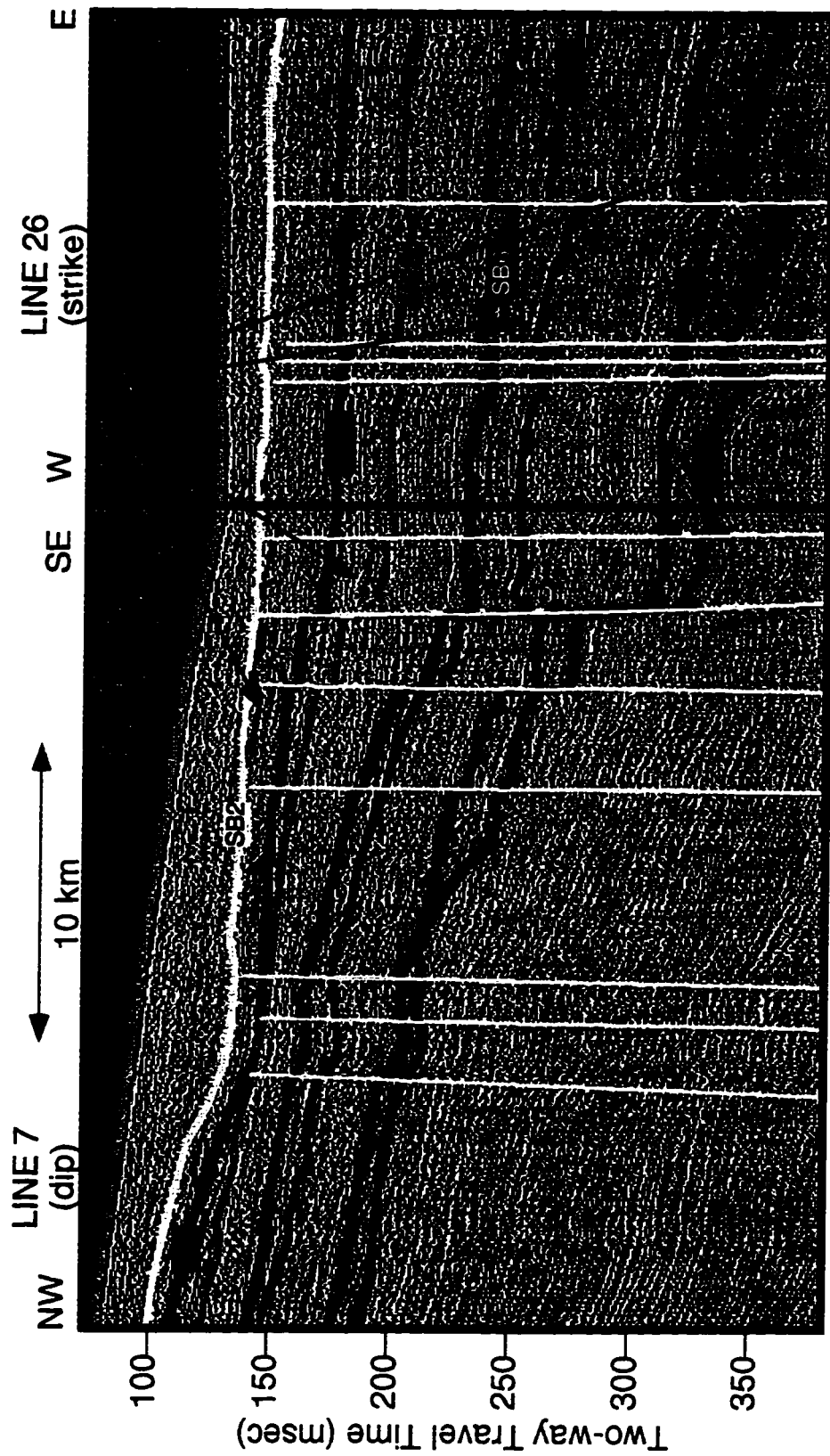


Figure 23. Dip and strike seismic example of SFU C, highstand shelf muds.

characteristics are the same in both the strike and dip directions (Fig. 23). The package thins and pinches out updip to meet the downdip pinchout of SFU B. SFU C exhibits basal downlap onto a flooding surface and a sequence boundary erosionally truncates it at the top, placing it into the highstand systems tract (Van Wagoner et al., 1988). Brown to olive clays with occasional brown mottling and calcareous nodules compose most of SFU C as seen in platform boring B-35 (Fig. 24). Four time intervals exhibit an occurrence of SFU C (Plates 1 and 2), which is interpreted to be a highstand muddy shelf unit which is syndepositional with SFU B. Converging longshore and surface currents transport these muds into the area from Mississippi, Colorado, and Rio Grande river sources, similar to the modern "Texas Mud Blanket" (Shideler, 1981).

#### Seismic Facies Unit D (SFU D)

Low amplitude, discontinuous, chaotic to transparent seismic reflectors within pinnacles of small areal extent characterize SFU D from both strike and dip perspectives (Fig. 25; Plates 1 and 2). These pinnacles range from 4 to 35 meters in height and can be up to 3 km in diameter. Data beneath SFU D is often completely obliterated, and when underlying reflections can be seen, velocity pull-ups exist. Due to limited core data and sparse occurrence of the facies, no platform borings from this study



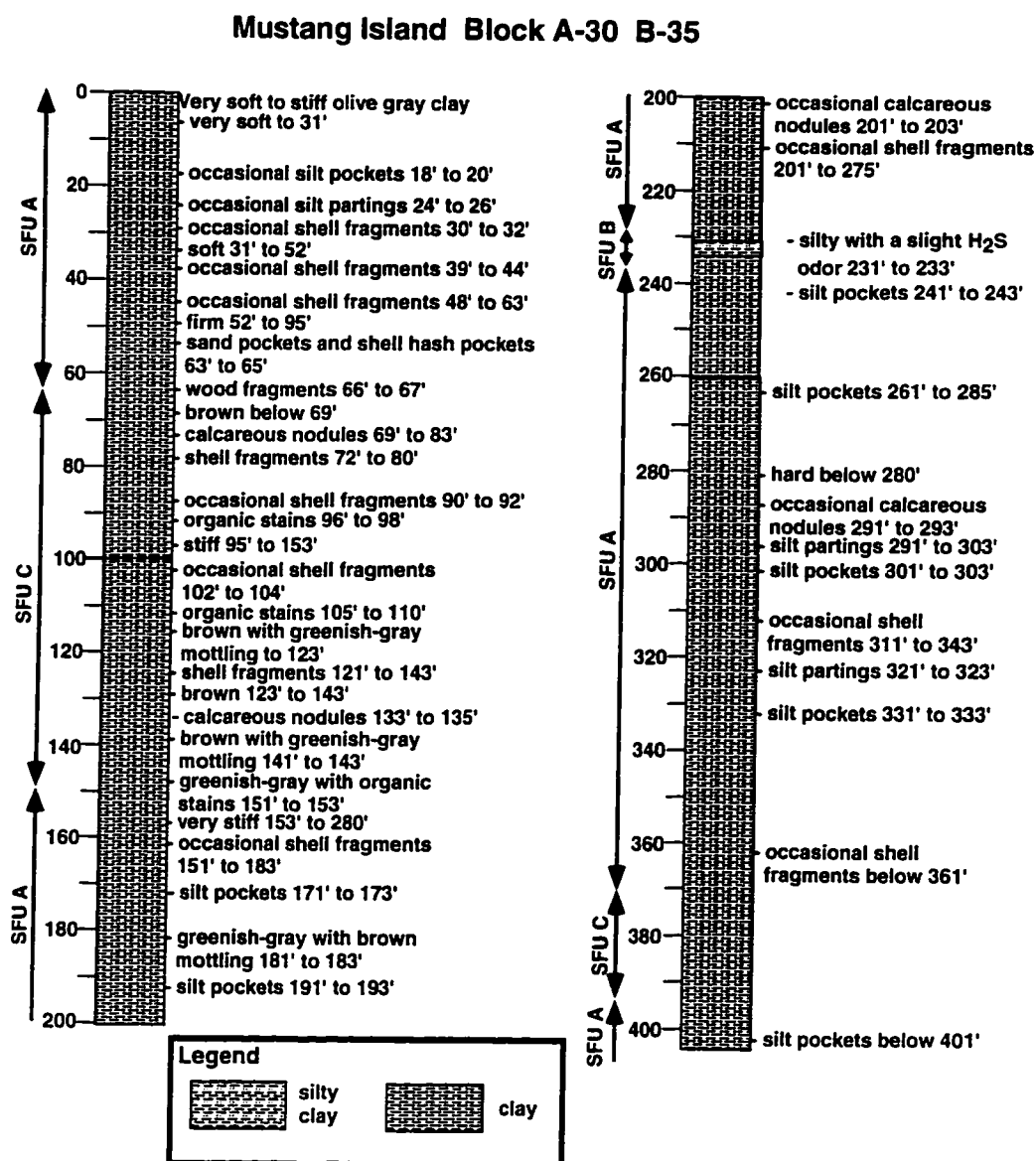


Figure 24. Platform boring description B-35 illustrating lithofacies associated with SFU C: brown or mottled clay, often with calcareous nodules. See dataset map (Figure 16) for borehole location.

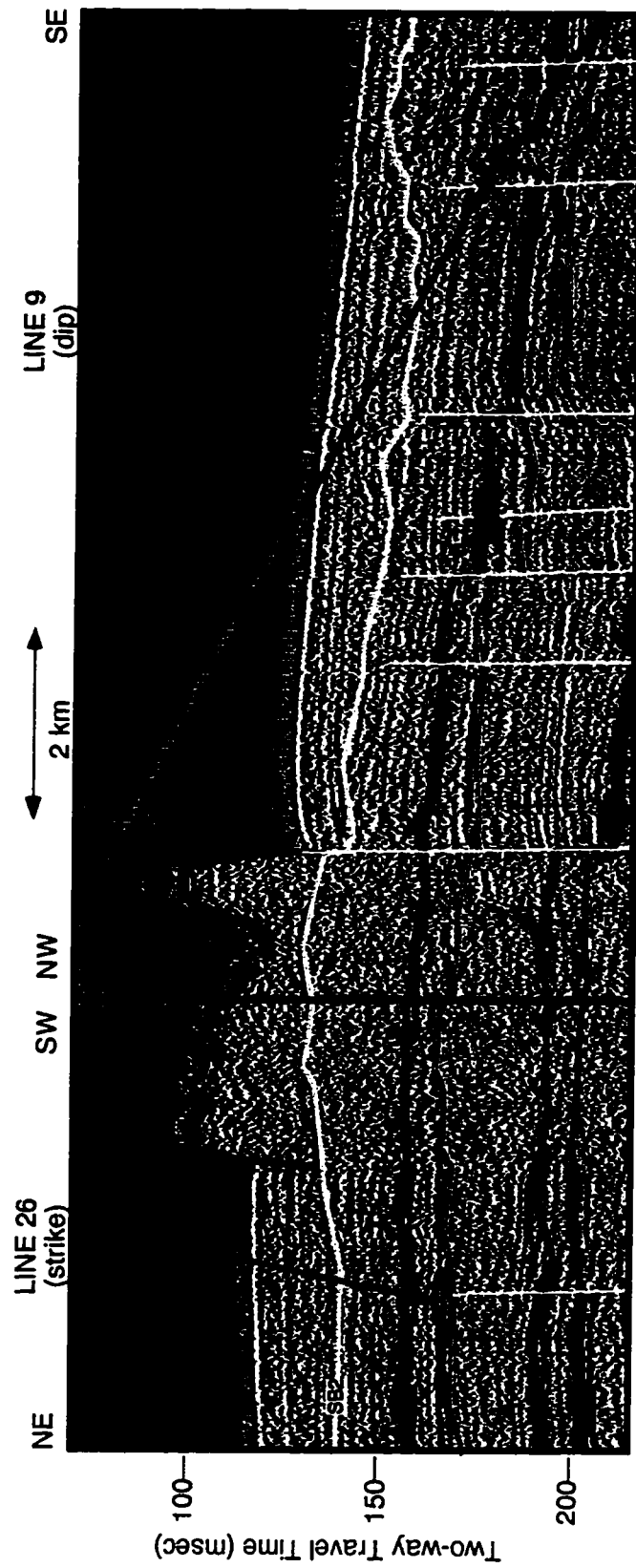


Figure 25. Strike and dip seismic example of SFU D, carbonate reefs. The large, shallow reef is Hospital Rock (Rezrak et al., 1985; Berryhill et al., 1986).

sample the lithology of SFU D, but previous works (Bright and Rezak, 1976; Rezak et al., 1985) describe it to contain dead coral and coralline algae nodules. Five occurrences of SFU D from two different time intervals are identified in this dataset (Fig. 26). The two deeper reefs lie above a flooding surface and the three stratigraphically higher reefs appear to be situated on a sequence boundary. All are located between 60 and 75 meters of present-day water depth on the middle to outer shelf. The upthrown block of a major growth fault resulted in a topographic high, controlling the location of reef development (Fig. 26).

### **Oxygen Isotope Stratigraphy**

Oxygen isotope analyses provide an independent sea level curve for the study area. Figure 27 shows the oxygen isotope record for platform boring B-92 (location map, Fig. 16) generated from the planktic foraminifera *Globigerinoides ruber*. The high frequency fluctuations observed in the raw data have been smoothed to represent the fourth (100,000 year) and fifth (20,000 year) glacio-eustatic cycles.

The correlation of the seismic stratigraphic surfaces to the oxygen isotope curve, is shown on Figure 28 and Plate 1. Sequence boundaries observed in the seismic data correspond to the less negative oxygen isotope values, but since lowstand deposits are not observed in the study area, the

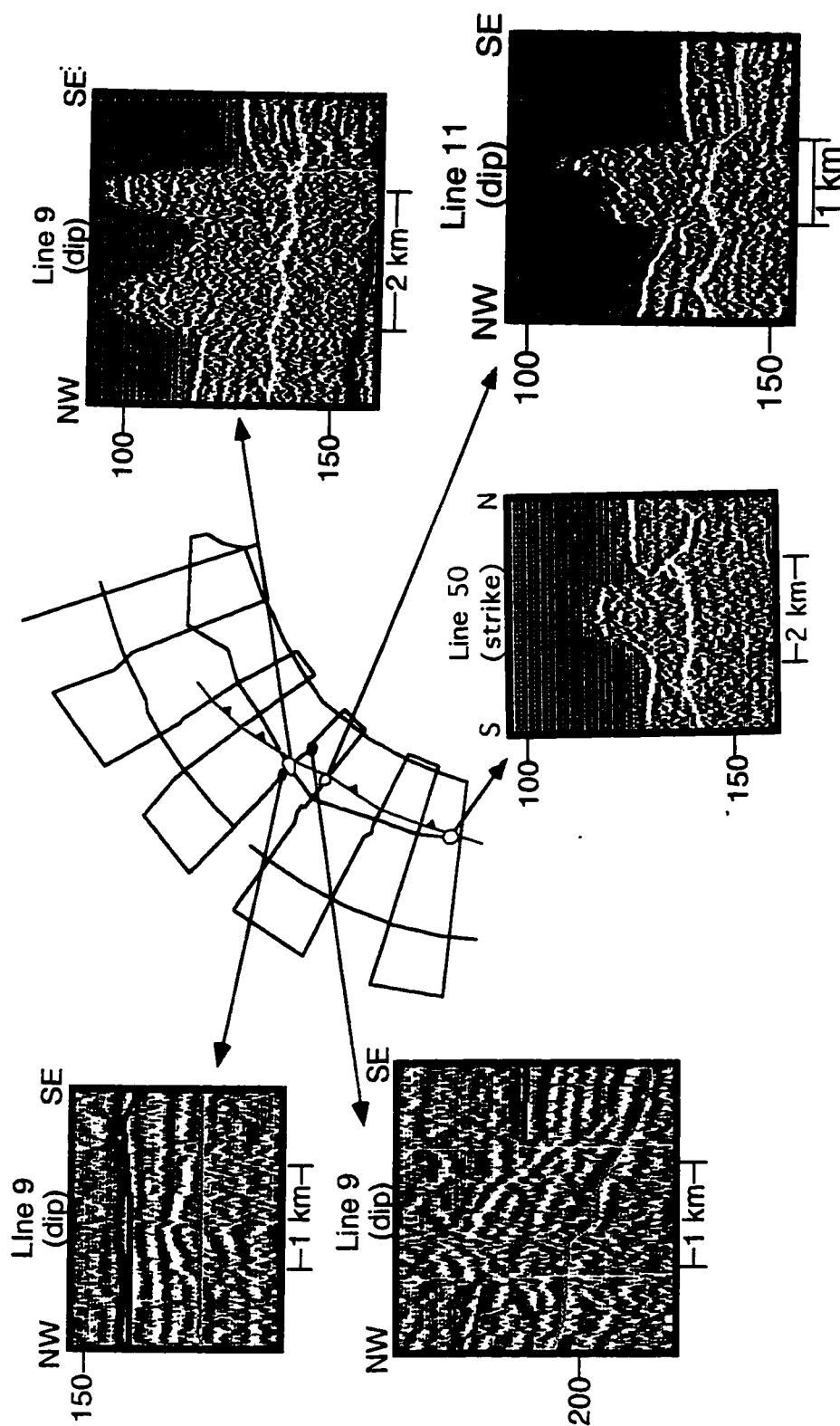


Figure 26. Seismic displays and locations of reefs observed in the study area.

Most of the reefs are situated one the edge of the upthrown block of a large growth fault.

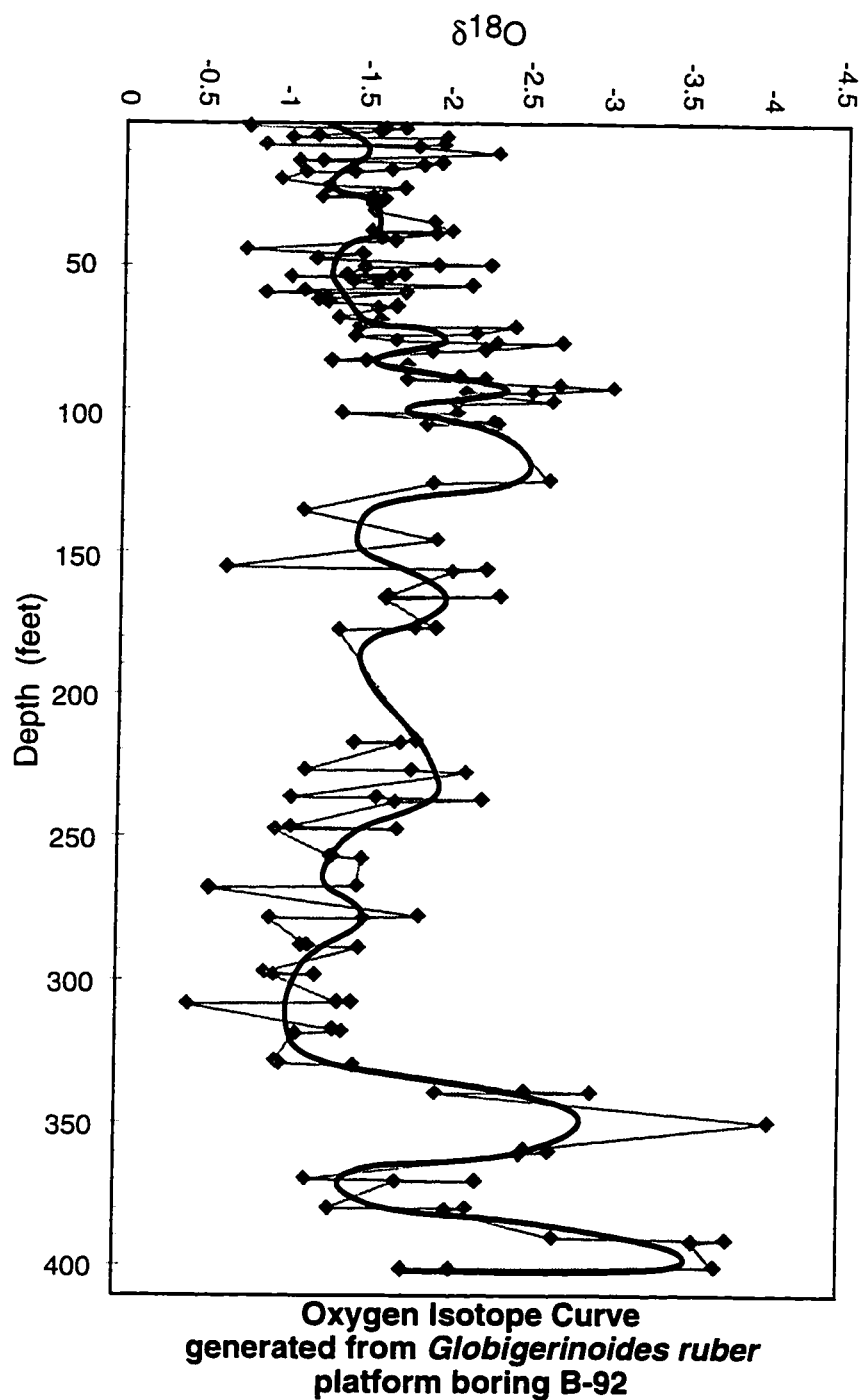


Figure 27. Oxygen isotope record from platform boring B-92 (see location map, Figure 16). Gray curve represents data adjusted to PDB and black curve illustrates a smoothing of that data.

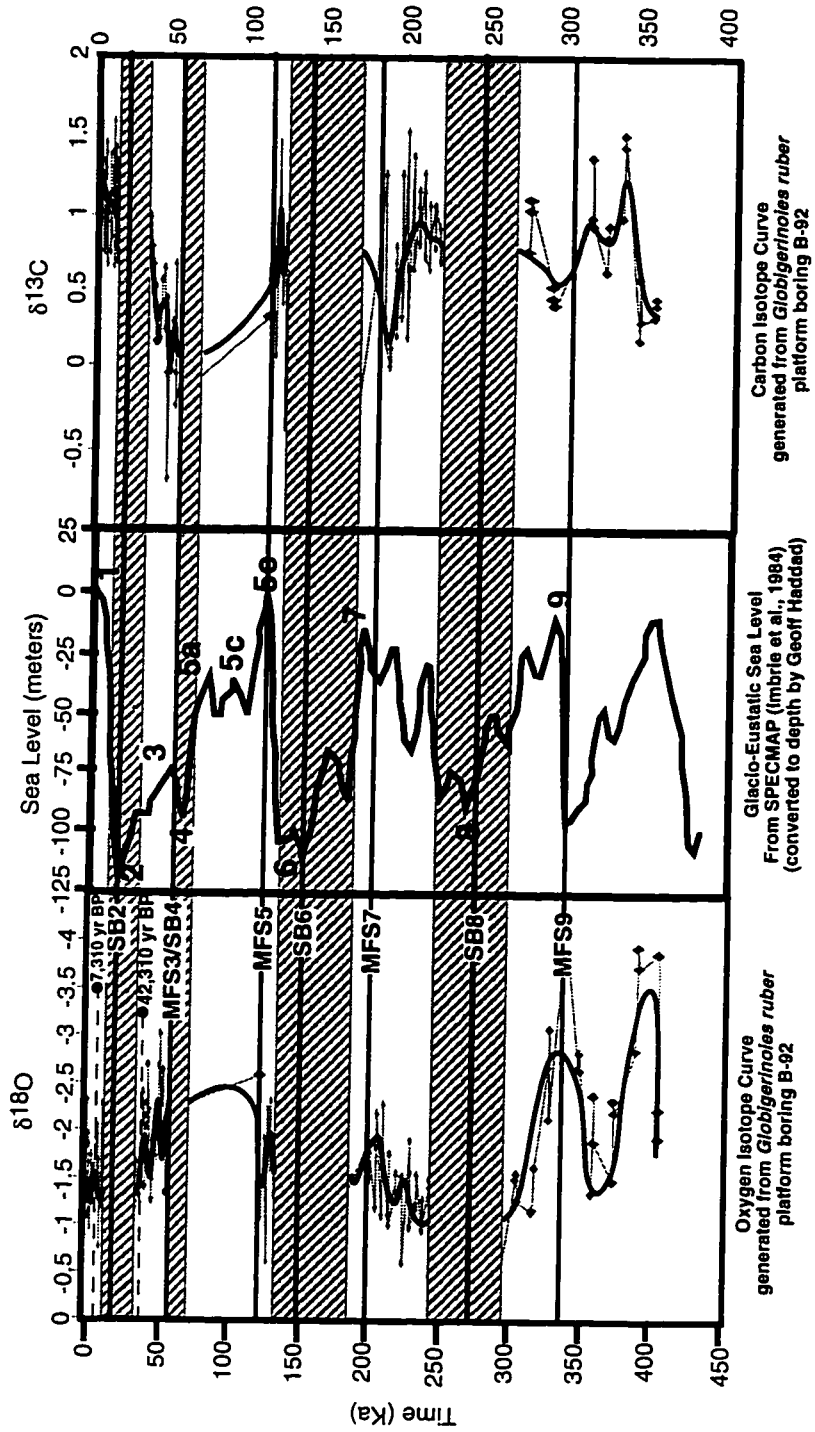


Figure 28. Compilation and comparison of seismic stratigraphic surfaces, oxygen isotope curve, carbon isotope curve, and the depth-converted SPECMAP curve.

positive oxygen isotope values generally associated with sequence boundaries do not occur. The flooding surfaces observed on the seismic data correspond well to negative peaks on the oxygen isotope curve and the carbon isotope curve. (Carbon isotope values were reported with the oxygen isotope values, but have not been interpreted for this study.) This correlation indicates that the major depositional units observed in the seismic cyclostratigraphy are primarily controlled by fluctuations in global sea-level.

As stated in the Methods section, the SPECMAP curve (Imbrie et al., 1984) serves as a proxy to glacio-eustatic sea-level. By comparing the B-92 oxygen isotope curve and seismic stratigraphic surfaces to the SPECMAP curve, a chronostratigraphic framework for the study area can be developed.

### **Radiocarbon Dating**

AMS radiocarbon dating performed on two samples from the B-92 platform boring (Table 1; Fig. 28) provides direct chronostratigraphic control for the upper part of the B-92 oxygen isotope curve. One date is just deeper than and the other just shallower than the SB2 surface (shallowest sequence boundary), confining its age and placing it into oxygen isotope Stage 2. The age of 42,310 yr BP for the deeper (25.8

## **Radiocarbon Dates from Platform Boring B-92**

Sample #	Depth (meters)	Measured C14 Age
53	19 (61 ft)	7310 +/- yr BP
72	25.8 (82.5 ft)	42870 +/- 930 yr BP

Table 1. Results of AMS radiometric dating performed on planktonic foraminifera from platform boring B-92 (see location map, Figure 16).



meters) sample can be questioned though, because it conflicts with biostratigraphic evidence. Some of the planktic foraminifera (approximately 10% by weight) selected for radiocarbon dating were *Globorotalia menardii*, which disappeared from the Gulf of Mexico approximately 90,000 yr BP and did not reappear until around 11,000 yr BP. Despite this conflict of evidence, the date is considered to be good because a stratigraphically equivalent sample from a platform boring approximately 100 km to the south has been dated using only the planktonic foraminifera *Globigerinoides ruber* and has yielded a date within 2000 years of this one (Banfield, pers. comm.). The *Globorotalia menardii* may have been reworked, in which case the correct date would actually be slightly younger than 42,310 yr BP, still placing the SB2 surface into oxygen isotope Stage 2. This age control strengthens the tie between the B-92 oxygen isotope curve and the SPECMAP curve, resulting in tighter chronostratigraphic control.

### **Chronostratigraphy**

Correlation between the B-92 oxygen isotope curve (Fig. 27), radiocarbon dates (Table 1), and SPECMAP curve (Fig. 9) results in tentative chronologic control at that location (Fig. 28). Seismic stratigraphic surfaces and facies units tied into this location and previous

work on the East Texas Shelf (Abdulah, 1995) provide the means to extrapolate this chronology throughout the entire study area. The integration of all three types of data establishes a chronostratigraphic framework that can be used as a basis for understanding the evolution of the study area.

## **INTEGRATED INTERPRETATION**

A chronostratigraphic framework, developed by integrating the oxygen isotopic data, radiocarbon dates, and seismic stratigraphic interpretations, is used to reconstruct the evolution of the study area. Seven stages of evolution are observed during the past 350,000 years. Isopach maps of the seismic facies units (previously interpreted in Data and Results) demonstrate the distribution of depositional systems during each of the seven time intervals. These intervals are correlated to the depth-converted SPECMAP curve (Fig. 9), to examine the control of global sea-level fluctuations on depositional processes.

## **Stage 9 Highstand Deposition**

The oldest unit mapped in the study area downlaps onto the Stage 9 maximum flooding surface, MFS9, and is bounded above by the Stage 8 sequence boundary, SB8 (Plates 1-5). Oxygen isotopic analyses indicate that this unit may have been deposited during oxygen isotope Stage 9, suggesting a time interval of deposition of approximately 340,000 to 300,000 yr BP (Fig. 28). The Stage 9 unit is composed of SFU B and SFU C. SFU B is interpreted as highstand aggrading and prograding barrier-bar sands and SFU C as a coeval muddy shelf.

Figure 29 shows the distribution of SFU B and SFU C during the Stage 9 sea-level highstand. As demonstrated by the isopach in Figure 29, the maximum thickness of the sand body is greater than 10 meters (32 ft), while the muddy shelf deposits range up to 30 meters (100 ft) thick. The Stage 9 highstand deposits are oriented parallel to the present-day coastline (Fig. 29). The barrier-bar sands in SFU B narrow and pinch out to the northeast, suggesting that either the Rio Grande delta was the major sand source or that a Stage 9 highstand Colorado delta was preventing bar deposition in the north.

As shown in Figure 29, there are regions of the middle shelf where the two facies overlap. The overlap occurs where the youngest barrier-bar sand has prograded and downlapped onto the oldest portion of the coeval

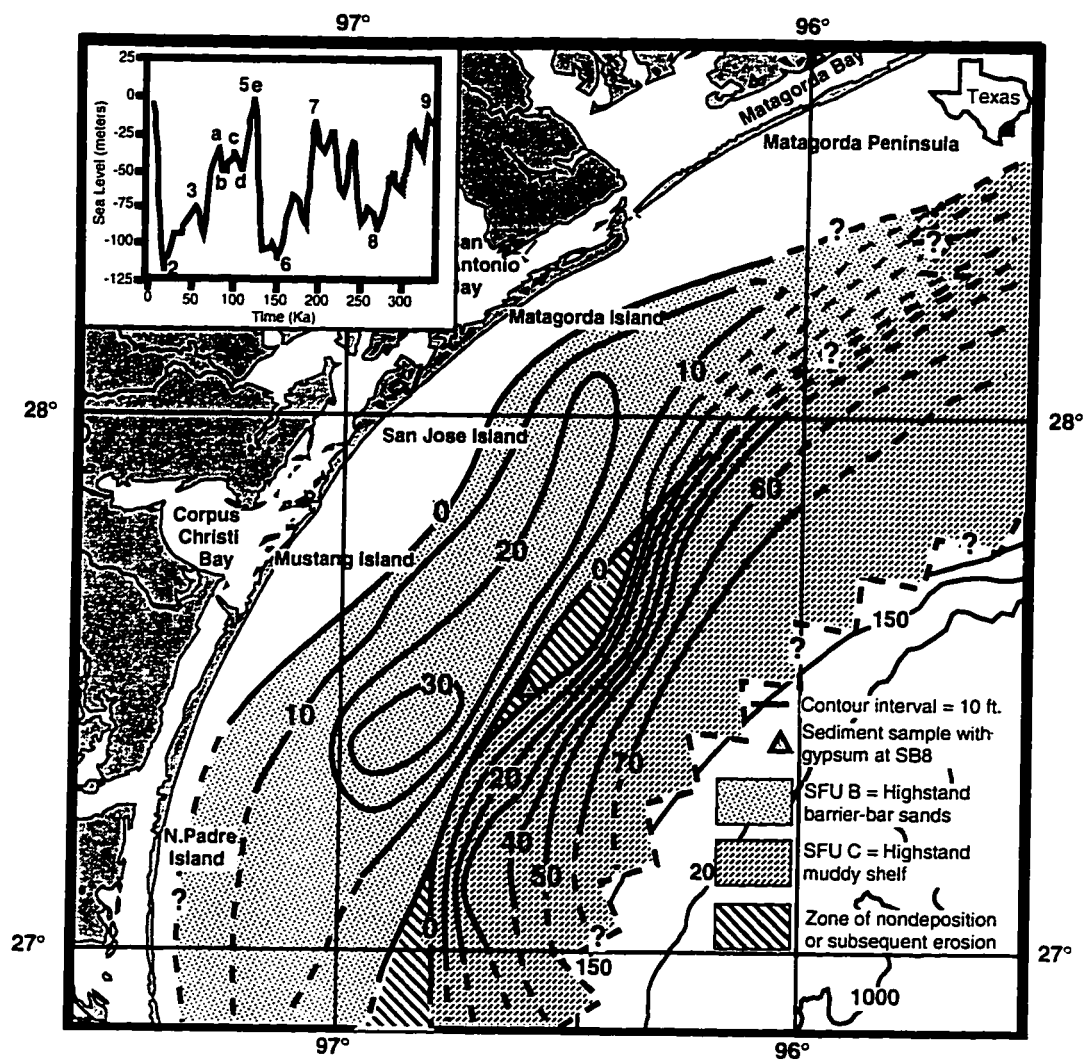


Figure 29. Areal distribution and isopach map of Stage 9 highstand depositional units.

muddy shelf. In areas where the two facies do not overlap, either the barrier-bar sands did not prograde out far enough to reach the muddy facies or erosion associated with SB8 has occurred. Another indication of erosion associated with SB8 is a few channels that incised through the Stage 9 deposits. Fine sand-sized, well-preserved gypsum crystals are observed at the Stage 8 sequence boundary in the B-92 platform boring. The gypsum crystals are interpreted as indicating a time of exposure and evaporation, that could have occurred in a back-barrier mud flat environment during a lowstand.

### **Stage 8 to 7 Transgressive Deposits**

Onlapping the Stage 8 sequence boundary and overlain by MFS7, the Stage 7 maximum flooding surface, is a unit composed of SFU A (Plates 1-5). SFU A is interpreted as transgressive muds. Oxygen isotopic analyses provide tentative chronologic control for this unit, and indicate that it was probably deposited during the sea level rise between approximately 250,000 and 200,000 yr BP (Fig. 28). The transgressive muds exist throughout the entire study area and have a maximum thickness of greater than 47 meters (150 ft) (Fig. 30).

Since the transgressive muds extend landward of the study area, their coastal onlap is not observed in this seismic dataset. Therefore, although

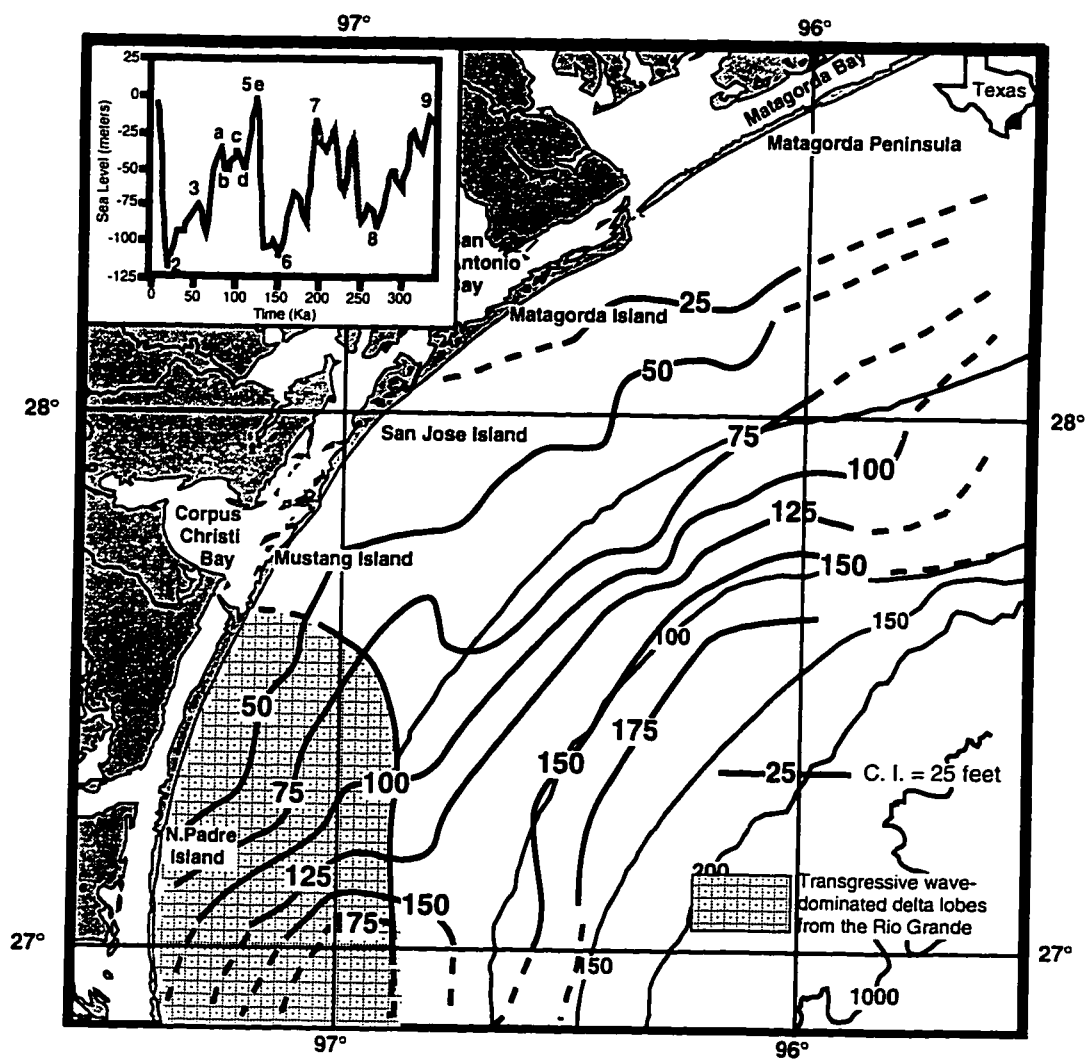


Figure 30. Isopach map of Stage 8 to 7 transgressive muds.

the maximum extent of the Stage 8 to 7 transgression in this area is not known, it extended farther landward than the -20 meter isobath of present-day water depth. The maximum thickness of this transgressive unit occurs in the southern region of the study area where seismic data indicates the existence of three backstepping lens-shaped deposits. The lens-shaped deposits originate to the south of the study area and pinch out in the central part of the study area. Their areal extent is shown on Figure 30. These deposits are interpreted as transgressive wave-dominated lobes of the Rio Grande delta. They are similar to strata observed just south of the study area by Banfield et al. (1996) that were deposited during the recent Stage 2 to 1 transgression.

### **Stage 7 Highstand Deposits**

Downlapping the Stage 7 maximum flooding surface (MFS7) and bounded above by the Stage 6 sequence boundary (SB6) is a unit composed of SFU B and SFU C (Plates 1-5). This unit has been tentatively identified as a Stage 7 highstand deposit by oxygen isotopic analyses and, therefore, is assigned a depositional period from approximately 210,000 to 160,000 yr BP (Fig. 28). As with the Stage 9 highstand deposits, SFU B and SFU C are interpreted as aggradational and progradational barrier-bar sands on the inner to middle shelf and coeval prograding muds on the outer shelf

(Fig. 31). The maximum thickness of SFU B is greater than 10 meters (32 ft), while the maximum thickness of SFU C is greater than 30 meters (100 ft) in places on the outer shelf.

The Stage 7 barrier-bar deposits (SFU B) narrow and nearly pinch out in the southern portion of the study area (Fig. 31). The thinning is potentially due to a lack of accommodation space, resulting from the bathymetric high created by the Stage 8 to 7 transgressive deposits in this area (Fig. 30). An alternate explanation would be that the Colorado delta was the main source of sands during this time period, resulting in a thinning of the barrier-bar system towards the Rio Grande area.

### **Stage 6 to 5 Transgressive Deposits**

A unit interpreted as transgressive muds (SFU A) onlaps the Stage 6 sequence boundary, SB6, and is capped by the Stage 5 flooding surface, MFS5 (Plates 1-5). Correlation with oxygen isotopic analyses and seismic data ties with previous works on the East Texas shelf (Abdulah, 1995) indicate that this unit was probably deposited between approximately 140,000 and 120,000 yr BP (Fig. 28). The transgressive muds range in thickness from 0 to over 39 meters (125 ft) (Fig. 32).

The Stage 6 to 5 transgressive deposits extend across the entire shelf in the northeastern portion of the study area, but they are absent from the



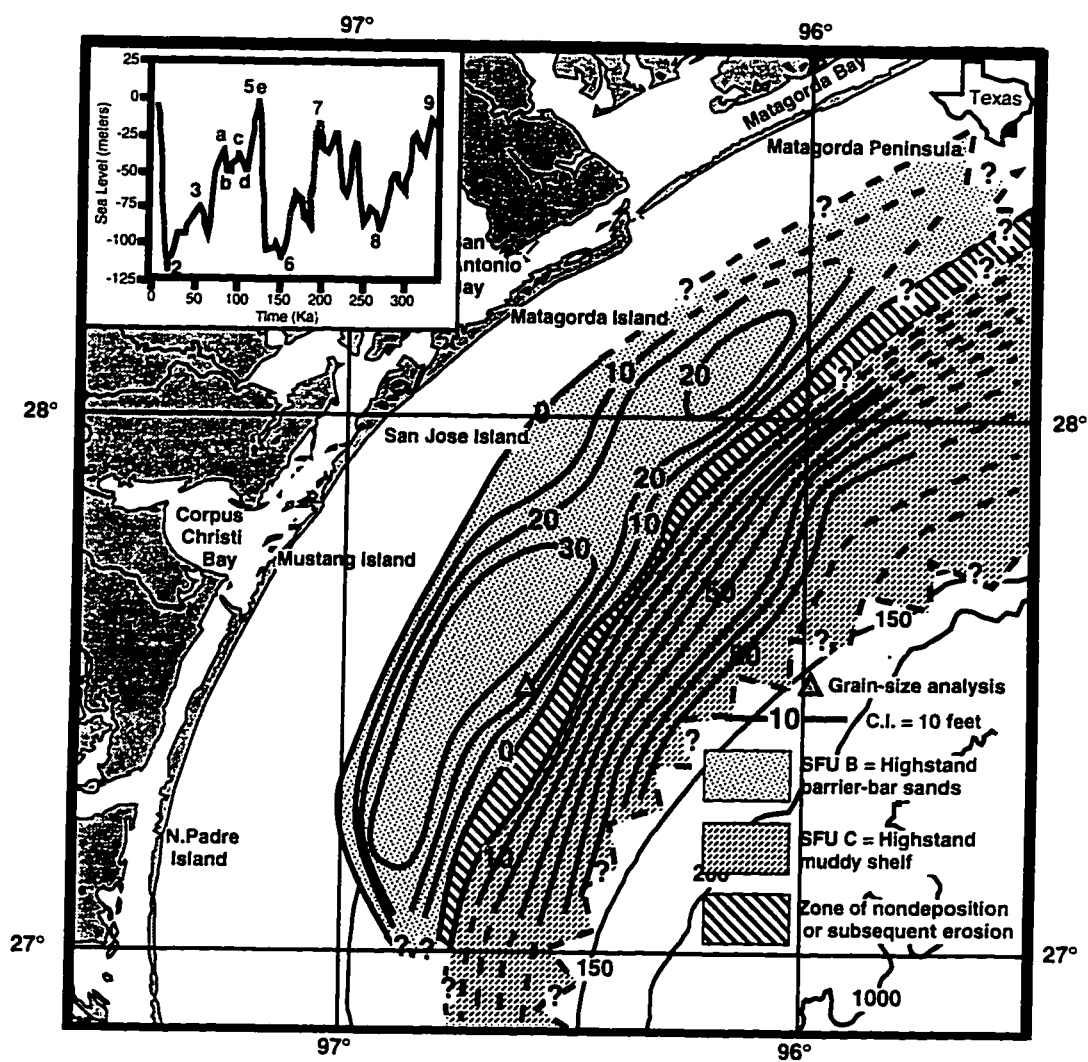


Figure 31. Distribution and isopach map of Stage 7 highstand barrier-bar sands and prograding shelf muds.

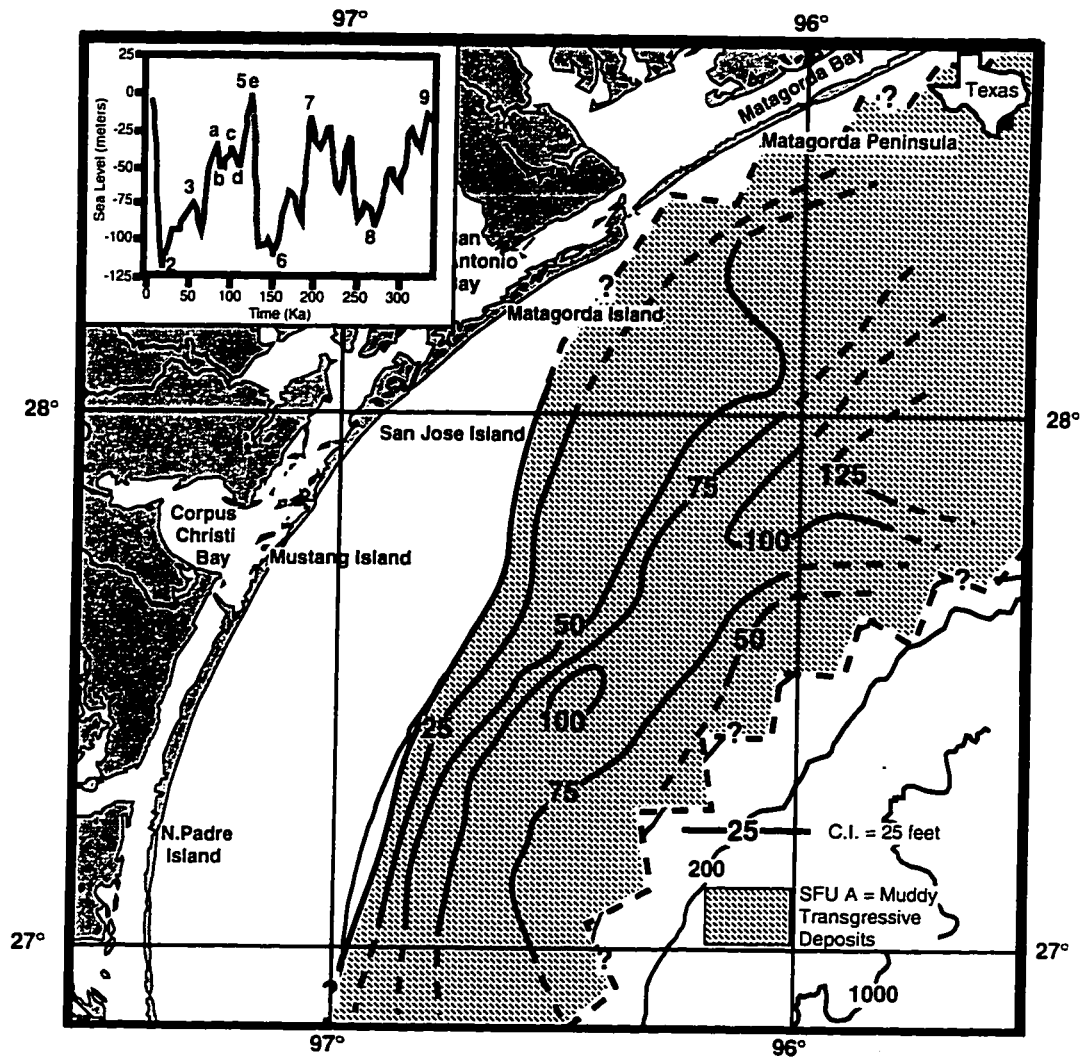


Figure 32. Distribution and isopach map of Stage 6 to 5 transgressive muds.

inner shelf in the southwest (Fig. 32). This mid-shelf pinchout is potentially due to the presence of the Stage 8 to 7 transgressive Rio Grande delta lobes (Fig. 30), which acted as a physiographic high during the transgression.

### **Stage 5 Highstand Deposits**

The Stage 5 highstand deposits observed in this study area (Fig. 33) were deposited during the 5c and 5a higher order fluctuations of sea level (Fig. 9). Missing are the Stage 5e deposits, which were deposited farther updip. The remnants of Stage 5e barrier-bars and strandplains are part of the Ingleside trend (Winker, 1979) and are observed just landward of the present-day coastline (Figs. 13 and 33). The location of these highstand deposits indicates that the Stage 5e maximum transgression was approximately 5 meters above modern sea-level. The Stage 5 deposits downlap the Stage 5e flooding surface, MFS5, and are bounded above by the Stage 4 sequence boundary, SB4 (Plates 1-5). Oxygen isotopic analyses and ties with previous works on the East Texas shelf (Abdulah, 1995) indicate that this unit was deposited between 115,000 and 80,000 yr BP (Fig. 28). The stacked Stage 5c and 5a highstand deposits are composed of SFU B, barrier-bar sands, and the coexisting SFU C, prograding muddy shelf (Fig. 33).

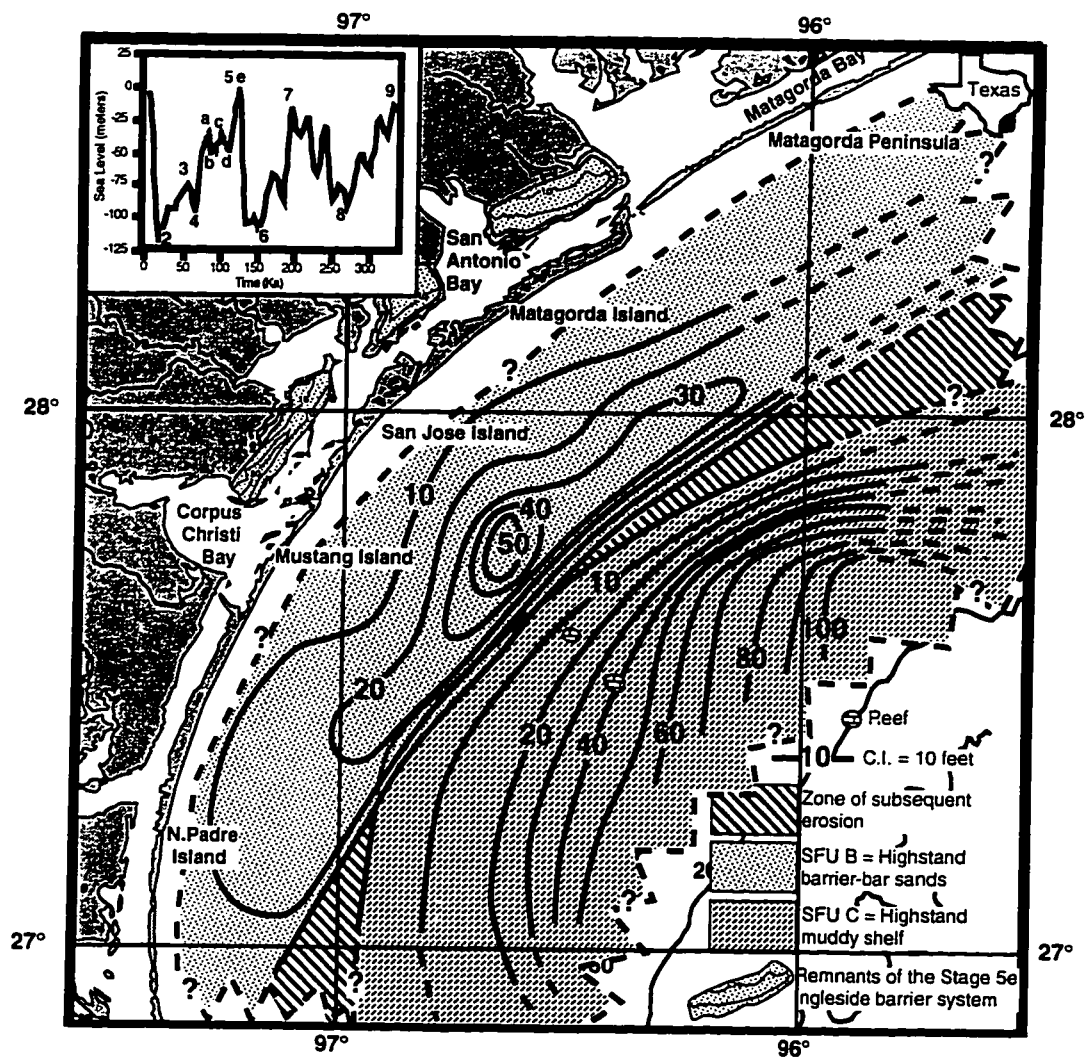


Figure 33. Distribution and isopach map of Stage 5 highstand barrier-bar sands, prograding shelf muds, and associated reefs.

The isopach map indicates that the thickness of the stacked barrier-bar sands is greater than 16 meters (50 ft) and that the muddy shelf thickens to greater than 30 meters (100 ft) in the northeast. The barrier-bar sands narrow and thin to the southwest (Fig. 33), probably indicating that their primary sand source is the Colorado delta to the northeast rather than the Rio Grande delta to the southwest. Two small reefs of SFU D are observed in the seismic data (Fig. 26) and appear to have developed on the MFS5 surface, probably during a higher order sea-level fall. Growth was halted either by drowning during a subsequent sea-level rise or by increased turbidity, and the reefs were later buried by highstand muddy shelf deposits.

### **Stage 3 Highstand Deposits**

Following the Stage 4 sea level fall, either no transgressive unit was deposited in this area or it was eroded by transgressive ravinement, producing an amalgamation of SB4 and the Stage 3 flooding surface, MFS3. Due to this amalgamation, the Stage 3 highstand deposit lies directly above the Stage 5 highstand deposits (Plates 1-5). The Stage 3 deposits downlap the MFS3 and have the Stage 2 sequence boundary, SB2, as an upper boundary (Plates 1-5). Oxygen isotopic analyses, radiocarbon

dating, and ties with Abdullah's (1995) work on the East Texas shelf indicate that this unit was deposited between 60,000 and 30,000 yr BP (Fig. 28). Similar to other highstand deposits, this unit consists of coastal barrier-bar sands (SFU B) and muddy shelf deposits (SFU C). The distribution of these facies is shown on Figure 34, with isopachs showing that the sands can be greater than 10 meters (32 ft) thick and that the muddy shelf deposits increase to greater than 38 meters (120 ft) thick.

The Stage 3 barrier-bar sands narrow and thin to the southwest, as did the Stage 5 deposits (Fig. 33). Again, this probably indicates that the primary source of sand at this time is the Colorado delta and that the Rio Grande delta is not a major contributor of sediment. It is not possible to determine the maximum sea-level at Stage 3 due to the previously noted lack of transgressive deposits. A range of potential values can be inferred by examining the location of Stage 3 barrier-bar deposits. Assuming that the initial aggrading bar sands were deposited at the coastline, the Stage 3 sea-level maximum would have been between 25 and 35 meters below present in this area.

## **Stage 2 to 1 Transgressive Deposits**

Onlapping SB2 is a unit consisting of transgressive muds, SFU A, bounded above by the modern seafloor (Plates 1-5). Oxygen isotopic

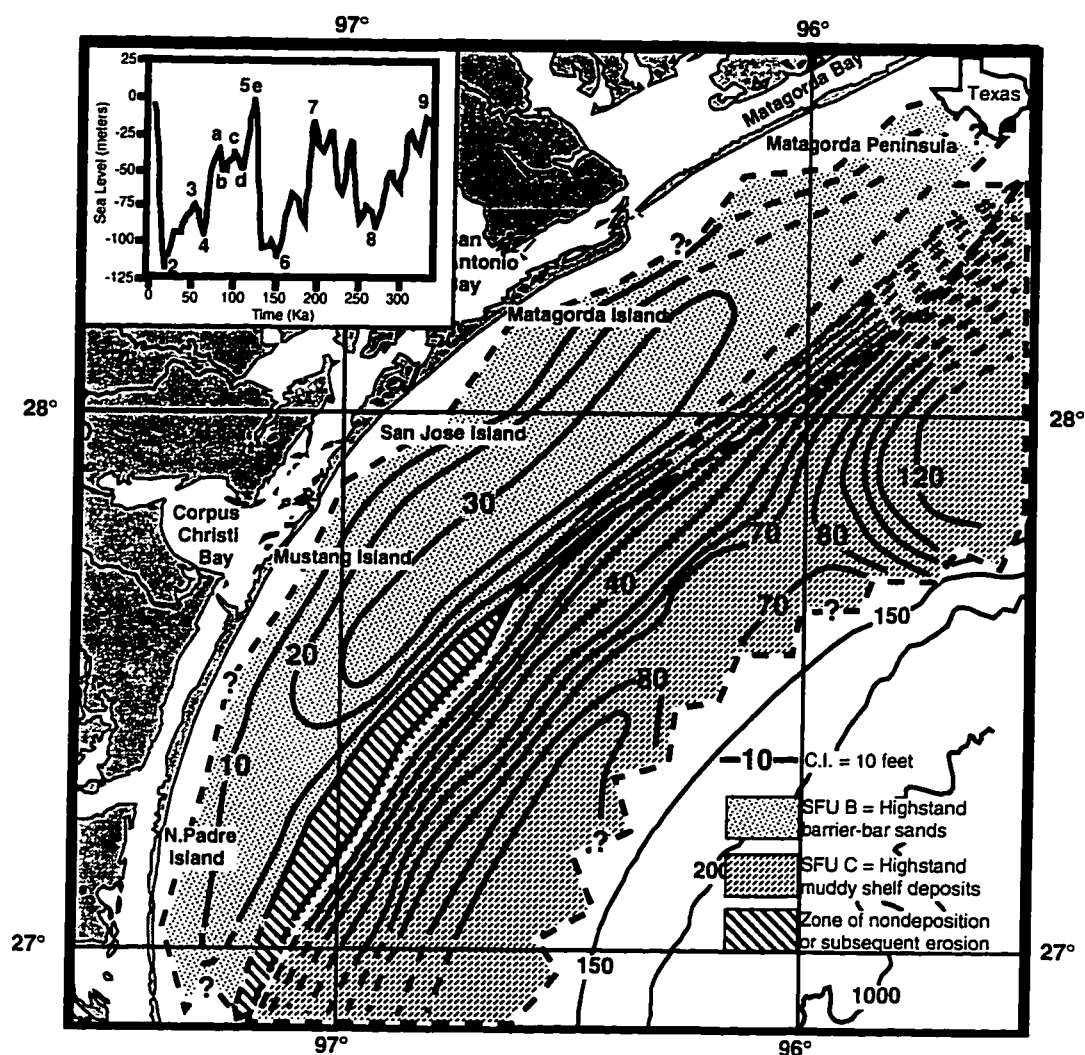


Figure 34. Distribution and isopach map of Stage 3 highstand barrier-bar sands and shelf muds.

analyses, radiocarbon dates, and seismic ties with previous works on the East Texas shelf (Abdulah, 1995) place these deposits into the recent transgression, indicating deposition commenced approximately 18,000 yr BP and continues today (Fig. 28). An isopach map (Fig. 35) shows these muds to be greater than 39 meters (125 ft) thick over part of the middle shelf, and thinning landward and basinward.

A series of small reefs, SFU D, appear to have developed on SB2 (Figs. 26 and 35) between the 65 and 80 meter modern-day isobaths. Only three reefs are observed in this dataset, but previous works (Berryhill, 1986; Bright and Rezak, 1976) show several others in the same region (Fig. 15). Reef growth ceased either from drowning in a rapid sea-level rise during the transgression, or from the influx of turbid waters (Shideler, 1981). The Stage 2 to 1 transgressive muds are burying these reefs, but many still protrude up to 15 meters above the sea floor.

## **DEPOSITIONAL MODELS**

An important aspect of this study is that during the approximately 350,000 years that the units were being deposited, three complete glacial-eustatic cycles occurred. It is significant that a repetition of depositional



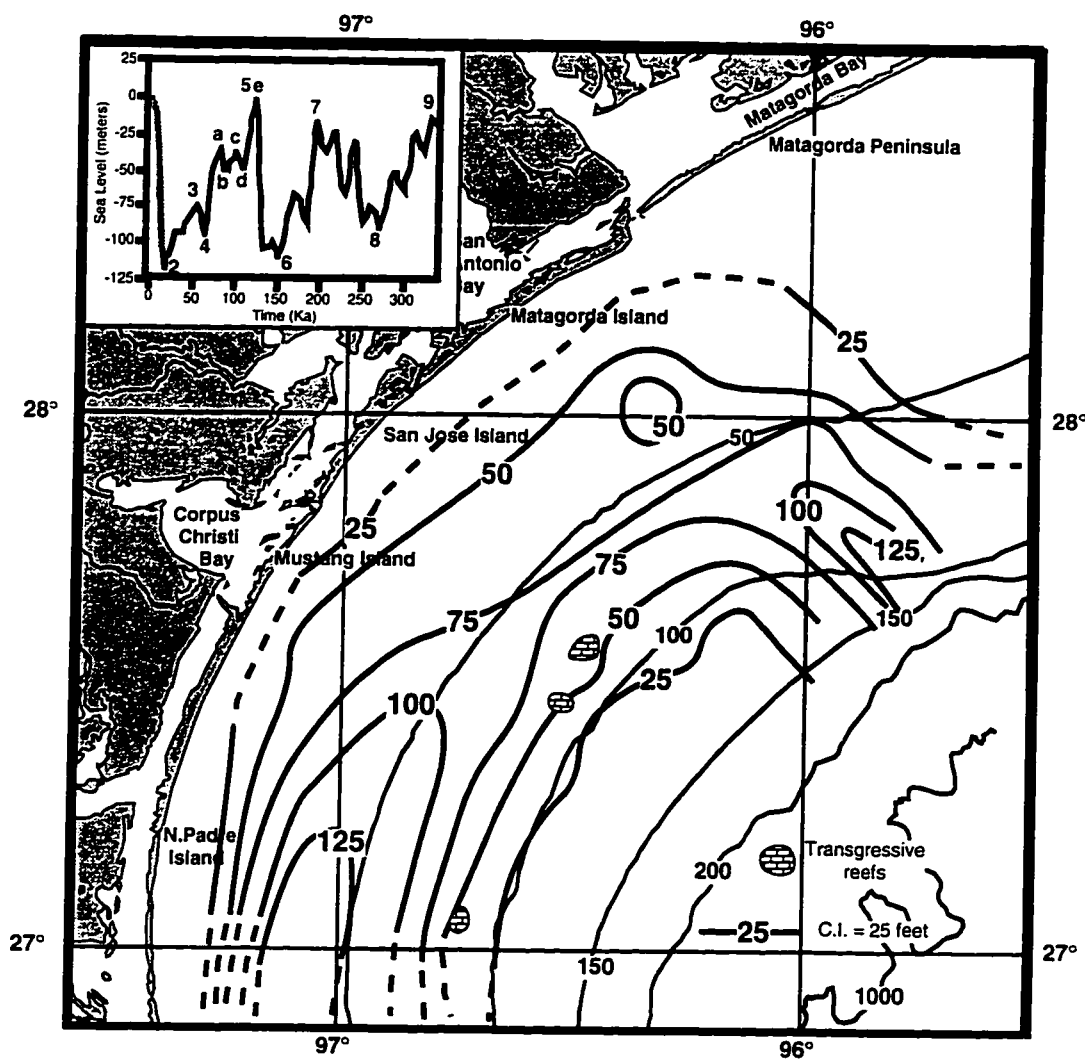


Figure 35. Isopach of Stage 2 to 1 transgressive muds and locations of associated reefs.

environments is observed during each cycle (see Plates 1-5 for a seismic example of the repetition). This repetition implies a consistent, and therefore, predictable pattern of deposition, allowing for the development of models that can be applied to ancient deposits in the exploration for hydrocarbons.

Two main stages of deposition are observed in each glacial-eustatic cycle. The first stage consists of highstand deposition, aggrading and prograding barrier-bar sands and a coeval prograding muddy shelf. As the rate of sea-level rise decreases and highstand deposition begins (as defined by Van Wagoner et al., 1988), barrier-bar sands (SFU B) accumulate (Fig. 36a). The sands aggrade until the available accommodation space is filled and then they prograde into shallow water (Fig. 36b). Occurring synchronously with barrier-bar deposition, hemipelagic muds settle out of suspension on the outer shelf, resulting in deposition of the highstand prograding muddy shelf, SFU C (Fig. 36). Once the rate of sea-level fall increases, the barrier-bar deposits are stranded and exposed. During the maximum sea-level fall some erosion occurs, but without significant fluvial input into the region, the amount of erosion is not great enough to remove the entire highstand deposit (Fig. 36c).

As the rate of sea-level rise increases after the maximum sea-level fall, accommodation space is created for transgressive deposits on the shelf.

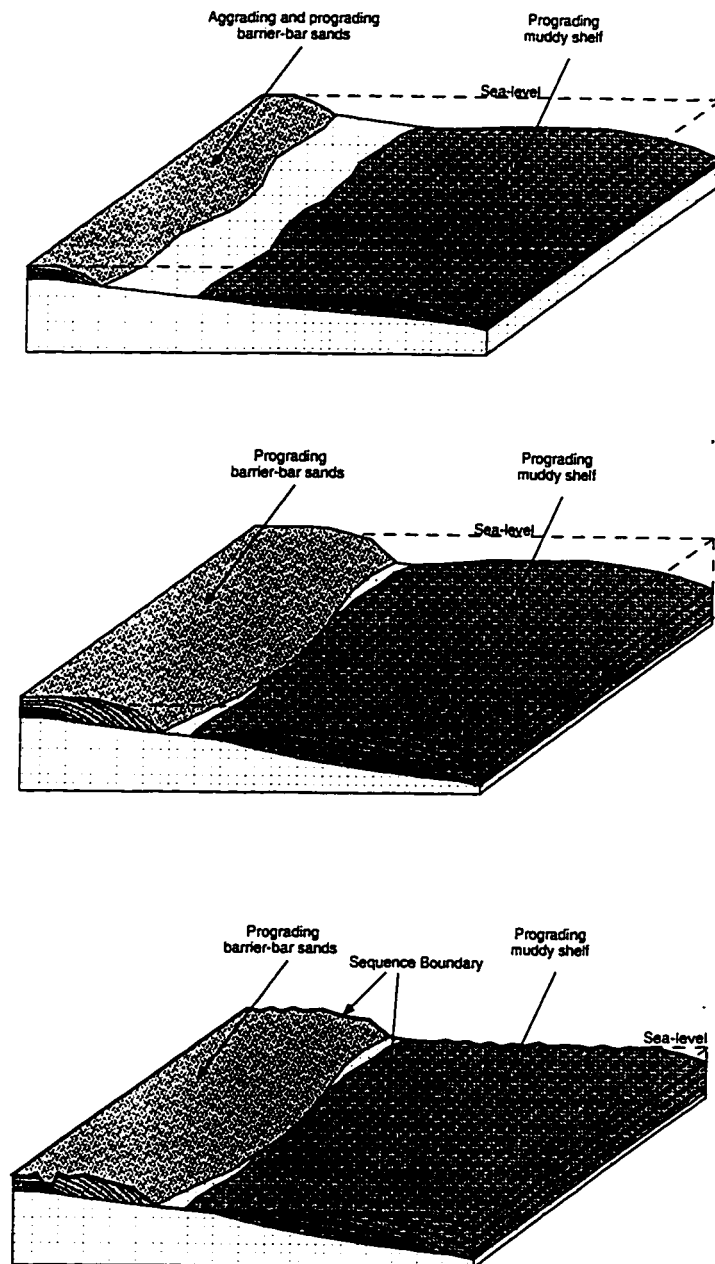


Figure 36. Model for highstand deposition on the central Texas shelf.

- a) Early highstand deposition consists of barrier-bar aggradation and progradation of shelf muds.
- b) Late highstand deposition consists of barrier-bar and shelf progradation.
- c) Maximum sea-level fall results in mild erosion of highstand deposits.

The deposits consist of hemipelagic muds onlapping the sequence boundary. During transgression, time periods of no or low sea-level rise may occur. These stillstands may result in the formation of barrier-bars at the coastline (Fig. 37a), but as the rate of sea-level rise increases, the barrier-bar deposits are likely to be reworked by ravinement and transported landward to a new coastline (Fig. 37b).

Once maximum transgression has occurred, highstand deposition begins again, resulting in a repetition of depositional environments. The same depositional environments are repeated during each glacial-eustatic cycle (Fig. 38). The major strength of the model developed in this study is that it agrees well with previous works on Early Tertiary barrier-bar formations of the central Texas coast (Boyd and Dyer, 1964; Fisher and McGowen, 1967; Galloway, 1982; Meckle and Galloway, 1996), and provides an understanding of cyclic deposition of potential hydrocarbon reservoirs in interdeltaic areas.

## **DISCUSSION**

The central Texas shelf is an interdeltaic region with little fluvial influence and relatively high subsidence rates ( $\sim 1$  mm/yr), creating an ideal

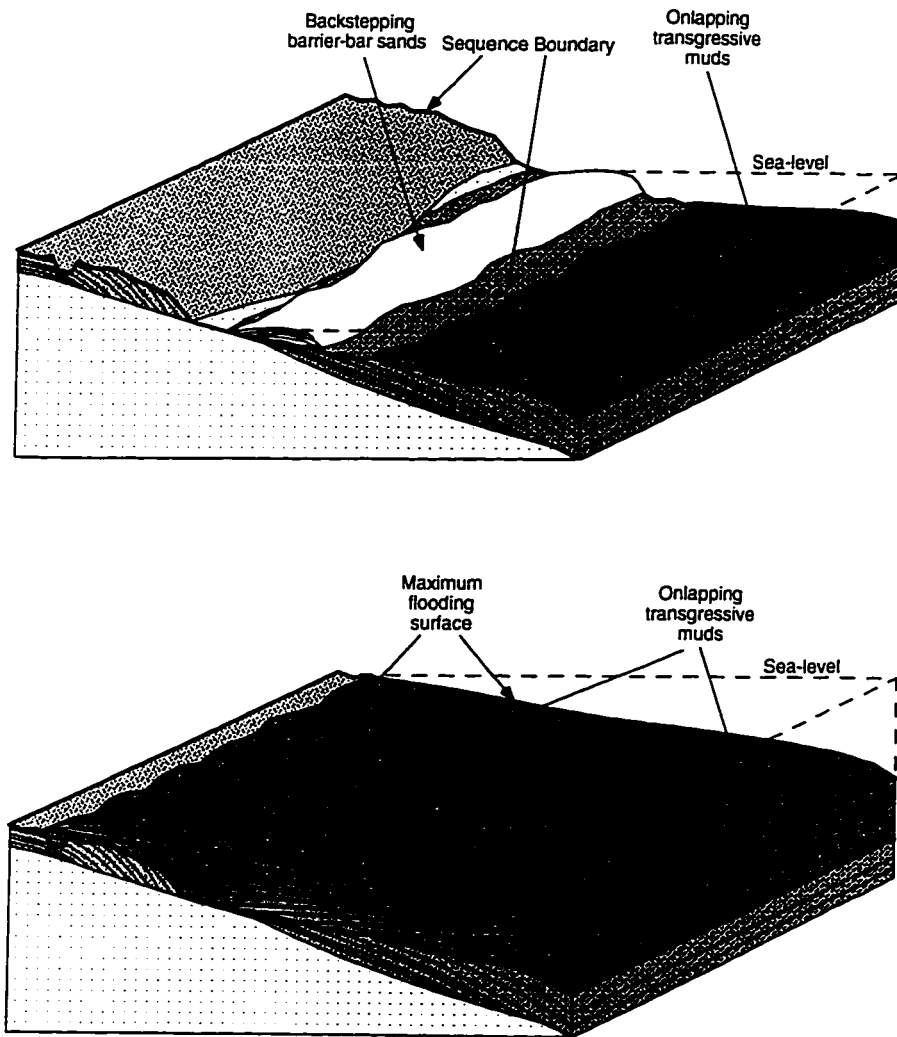


Figure 37. Model for transgressive deposition on the central Texas shelf. a) Early transgression followed by a sea-level stillstand results in onlapping transgressive muds and initial accumulation of shoreline sand into a barrier-bar system. b) Continuation of sea-level rise causes ravinement of bar sands and further deposition of onlapping muds.

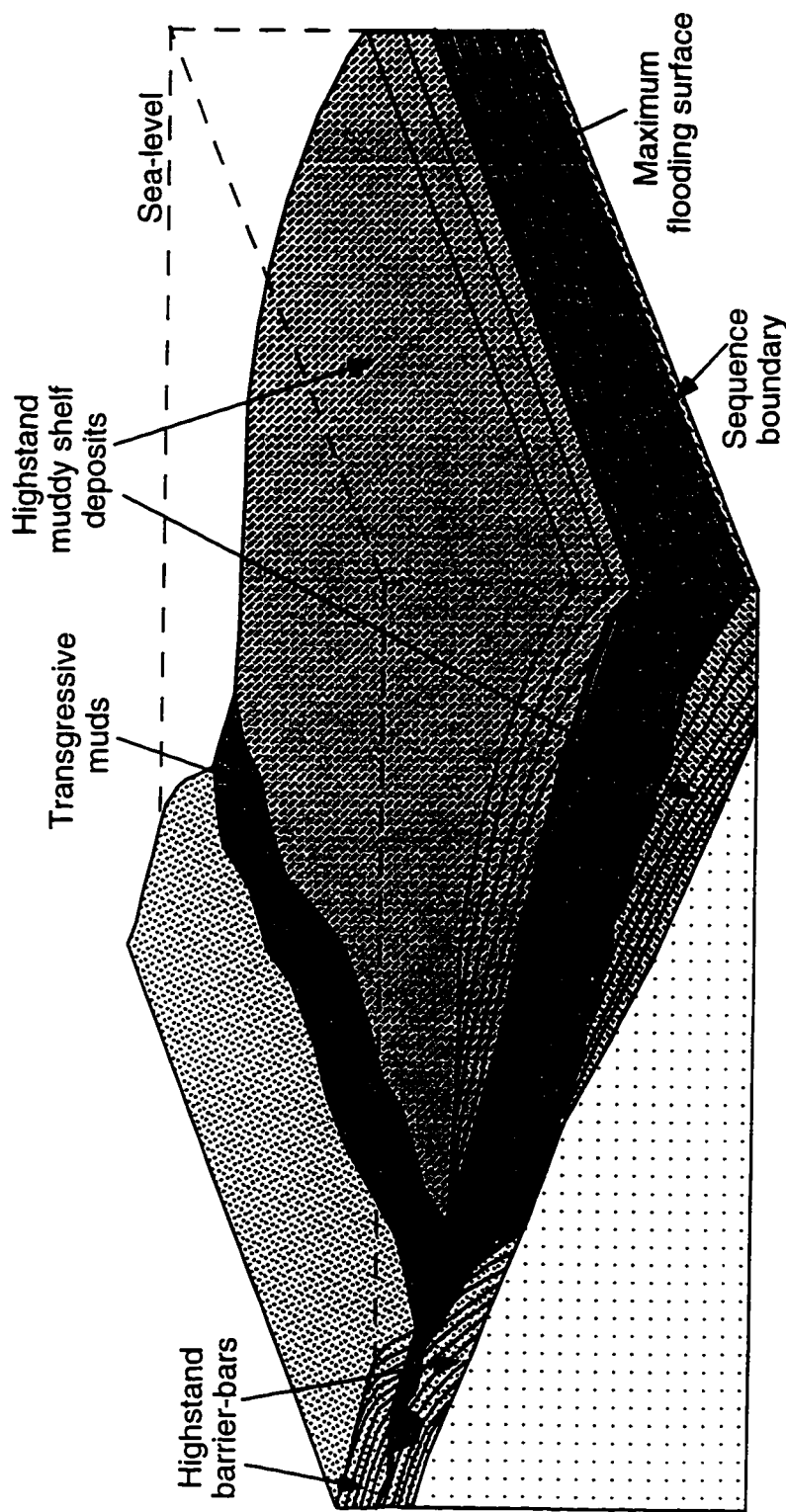


Figure 38. Model for cyclic deposition on the central Texas shelf. Highstand deposition of barrier-bar sands and prograding shelf muds is followed by a maximum sea-level fall, resulting in erosion associated with the sequence boundary (see Figure 36). Transgressive muds are deposited during the subsequent sea-level rise, with the maximum rise indicated by the maximum flooding surface (see Figure 37). Highstand deposition resumes, completing the cycle.

situation for deconvolving autocyclic and glacio-eustatic influences on deposition. As evidenced by the cyclic nature of the facies deposited (Fig. 38) and the strong correlation of these units with a glacio-eustatic sea level curve (Fig. 28), fourth order (100,000 yr) cycles are the primary mechanism controlling deposition in this area. Autocyclic factors such as sediment supply influence the morphology and size of the observed deposits, but not the distribution of depositional systems. These fourth order glacio-eustatic sea-level cycles are demonstrated independently by seismic cyclostratigraphy and by oxygen isotope analyses performed on platform boring B-92 (Fig. 27). These separate data agree well with each other and with the depth-converted SPECMAP curve (Fig. 28).

Unlike fluvio-deltaic regions, where lowstand deposition often dominates the stratigraphic record (Miall, 1991; Sarzalejo, 1993; Abdulah, 1995), the central Texas shelf is dominated by highstand and transgressive deposits as seen on the seismic data and depositional maps (Figs. 19, 21, 23, and 29-35; Plates 1-5). Lowstand deposits are missing from the shelf in this area, but are predicted to occur on the slope. Highstand and transgressive deposits are better preserved on the central Texas shelf than they may be in other areas due to the combination of high subsidence and lack of major rivers. Subsidence aids in lowering the deposits below the level of shoreface ravinement, and without much fluvial influence, erosion

during the maximum sea-level fall is minor, preventing the deposits from being removed by erosion. The central Texas shelf also differs from the east and south Texas shelf regions in that glacial-eustasy dominates systems tract development and autocyclic effects (i.e. delta lobe shifting) are minimal.

Previously termed the “Texas Mud Blanket” (Shideler, 1981), the study area of the central Texas shelf was thought to be blanketed in a hemipelagic mud drape, but platform boring descriptions and isopach maps exhibit extensive strike-oriented highstand barrier-bar sand bodies on the inner shelf. These sand bodies are typically greater than 10 meters (32 ft) thick (Figs. 22, 29, 31, 33, and 35). The sands were transported into the study area via longshore currents that converge on the central Texas shelf (Lohse, 1995; Curray, 1960, Rezak et al., 1985). The fact that longshore currents are primarily responsible for the movement for such a large volume of sand over such a short period of time (tens of thousands of years) is a significant outcome of this study. Longshore currents have not typically been considered to play such a major role in the development of depositional systems. The sand is thought to be eroded by these currents from transgressive and highstand deltas of the Colorado river to the north and the Rio Grande to the south, transported into the study area, and deposited along shore by converging longshore currents and nearshore



wind-driven currents. Ongoing studies by Rodriguez (pers. comm.) and Snow (pers. comm.) reveal fewer and smaller transgressive sand bodies near the mouths of the Brazos and Colorado rivers than predicted, further indicating a longshore source for the central Texas shelf sands.

High-resolution seismic investigations such as this one (Thomas, 1990; Sarzalejo, 1993; Sydow and Roberts, 1994; Abdulah, 1995) demonstrate a strong correlation between seismic facies and lithofacies. In this study, sandy lithofacies are typically portrayed as low-amplitude, chaotic seismic facies (Figs 21 and 22). Muds and clays are generally represented by sub-parallel, continuous reflection patterns (Figs. 19, 20, 23, and 24). Carbonate reef lithofacies are depicted as a low-amplitude, chaotic seismic facies - like the sands - but within pinnacles of small areal extent (Figs. 25 and 26). These correlations enable lithofacies to be extrapolated and predicted in regions of the study area where platform boring data is not available.

Other Late Quaternary seismic studies in the Gulf of Mexico have typically investigated deposition over only the most recent glacial cycle, approximately the past 125,000 years (Sydow, 1992; Sarzalejo, 1993; Abdulah, 1995). Due to thinner depositional packages on the central Texas shelf, older units were imaged by the seismic data resulting in the analysis of deposits up to 350,000 years old, covering three complete glacio-eustatic

cycles. By observing deposition over several glacio-eustatic cycles, a repetition of depositional environments with each cycle was discovered. These same depositional environments are observed to occur in the Wilcox, Yegua, and Frio formations of the Early Tertiary on the central Texas shelf (Boyd and Dyer, 1964; Fisher and McGowen, 1967; Galloway, 1982; Meckle and Galloway, 1996). This repetition indicates that the controlling factors on deposition have remained essentially the same since the Early Tertiary. It also enables the development of depositional models based on data from this study (Figs. 36, 37, and 38) that can be directly applied to Tertiary formations in the exploration for hydrocarbons.

## CONCLUSIONS

- 1) The distribution of facies on the central Texas shelf is dominantly controlled by fourth-order (100,000 year) eustatic cycles.
- 2) The volume, type, and location of fluvial discharge and sediment load from the Colorado and Rio Grande rivers (autocyclic controls) can affect the morphology of barrier-bar deposits in central Texas.

- 3) Seven stages of evolution over the past 350,000 years are observed on the central Texas shelf.
- 4) In the interdeltic region studied, sand is found only in the highstand deposits and is deposited as a coastal barrier-bar complex that forms parallel to the shoreline. These sands were transported into the area by longshore and near-shore wind-driven currents. These currents have the capacity to transport large volumes of sand into the study area and deposit it along shore within tens of thousands of years. The products of this near-shore sand transport are widespread (thousands of square kilometers) and thick (> 10 meters) sand bodies on the shelf.
- 5) A strong correlation exists between seismic facies and lithofacies, therefore enabling the prediction of lithofacies where core control is not available. The following correlations have been observed:
  - a) Discontinuous, low-amplitude, chaotic seismic character and a sandy lithofacies.
  - b) Sub-parallel, continuous reflection patterns of low to moderate amplitude and muddy lithofacies.

- c) Low-amplitude, discontinuous, chaotic reflection patterns within a pinnacle geometry that obliterate data directly beneath them and carbonate reef lithofacies.
- 6) Sediments are deposited and preserved in a repetitive manner during each glacial-eustatic cycle. The repetition of depositional environments through time allows for the development of depositional models.
- a) Highstand = coastal barrier-bar sands and shelf muds
  - b) Lowstand = minor erosion and no deposition, even at the shelf break.
  - c) Transgression = transgressive shelf muds
- 7) The oxygen isotope Stage 3 highstand is estimated to have been 25-35 meters (80-112 ft) below today's sea level.

## REFERENCES

- Abdulah, K. C., and J. B. Anderson, 1991, Eustatic Controls on the Evolution of the Pleistocene Brazos-Colorado Deltas, Texas: GCSSEPM Foundation Twelfth Annual Research Conference, p. 1-7.
- Abdulah, K. C., and J. B. Anderson, 1994, Contrasting Styles of Deltaic Deposition and the Role of Eustasy - Example from the Quaternary Deltas of the Texas Continental Shelf: AAPG Hedberg Research Conference: Application of Sequence Stratigraphy to Oil Field Development, p. 1-11.
- Abdulah, K. C., 1995, The Evolution of the Brazos and Colorado Fluvial/Deltaic Systems During the Late Quaternary: An Integrated Study, Offshore Texas: doctoral thesis, Rice University, Houston, 284 p.
- Anderson, J. B., K. C. Abdulah, F. P. Siringan, and S. Sarzalejo, 1994, Application of High-Resolution Seismic Reflection Data in Assessing the Size, Shape, and Lithology of Near-Surface Sand Bodies: Offshore Technology Conference, p. 21-30.
- Banfield, L. A., J. B. Anderson, and P. R. Vail, 1996, Sequence Stratigraphic Model of the Rio Grande Delta, South West Texas: Potential Analog for the Niger Delta: American Association of Petroleum Geologists, p. A9-A10.
- Bebout, D. G., R. G. Loucks, and A. R. Gregory, 1978, Frio sandstone reservoirs in the deep subsurface along the Texas Gulf Coast, Austin, Texas, The University of Texas at Austin Bureau of Economic Geology.
- Berryhill, H. L., J. R. Suter, and N. S. Hardin, 1986, Late Quaternary Facies and Structure, Northern Gulf of Mexico: Interpretations from Seismic Data: AAPG Studies in Geology, v. 23: Tulsa, OK, The American Association of Petroleum Geologists, 289 p.
- Boyd, D. R., and B. F. Dyer, 1964, Frio Barrier Bar System of South Texas: Gulf Coast Association of Geological Societies Transactions, v. 14, p. 309-322.

- Bradshaw, B. E., and J. S. Watkins, 1994, Growth-fault evolution in offshore Texas: Gulf Coast Association of Geological Societies Transactions, p. 103-110.
- Bright, T. J., and R. Rezak, 1976, A biological and geological reconnaissance of selected topographical features of the Texas continental shelf, College Station, Texas, Texas A&M Research Foundation and Department of Oceanography.
- Curry, J. R., 1960, Sediments and history of Holocene transgression, continental shelf, northwest Gulf of Mexico, in F. P. Shepard, F. B. Phleger, and T. H. v. Andel, eds., Recent Sediments, Northwest Gulf of Mexico, Tulsa, Oklahoma, The American Association of Petroleum Geologists, p. 221-266.
- Fisher, W. L., and J. L. McGowen, 1967, Depositional systems in the Wilcox Group of Texas and their relationship to occurrence of oil and gas: Gulf Coast Association of Geological Societies Transactions, v. 17, p. 105-125.
- Fisk, H. N., 1944, Geology of Avoyelles and Rapin Parishes, Louisiana: Louisiana Department of Conservation Geology Bulletin, v. 18, p. 3-240.
- Galloway, W. E., D. K. Holiday, and K. Magara, 1982, Frio Formation of the Texas Gulf coast basin: Depositional systems, structural framework, and hydrocarbon origin, migration, distribution, and exploration potential, Austin, Texas, University of Texas Bureau of Economic Geology.
- Imbrie, J., J. D. Hays, D. G. Martinson, A. McIntyre, A. C. Mix, J. J. Morley, N. G. Pisias, W. L. Prell, and N. J. Shackleton, 1984, The orbital theory of Pleistocene climate: support from a revised chronology of the marine  $\delta^{18}\text{O}$  record, in A. L. B. e. al., ed., Milankovitch and Climate, D. Reidel Publishing Company, p. 269-305.
- LeBlanc, R. J., and W. D. Hodgson, 1959, Origin and Development of the Texas Shoreline, p. 197-219.

- Lohse, E. A., 1956, Dynamic geology of the modern coastal region, northwest Gulf of Mexico, in J. L. Hough, and H. W. Menard, eds., *Finding Ancient Shorelines*, Tulsa, OK, Society of Economic Paleontologists and Mineralogists, p. 99-105.
- Meckle, L. D., and W. E. Galloway, 1996, Formation of high-frequency sequences and their bounding surfaces: case study of the Eocene Yegua Formation, Texas Gulf Coast, USA: *Sedimentary Geology*, v. 102, p. 155-186.
- Miall, A. D., 1991, Stratigraphic sequences and their chronostratigraphic correlation: *Journal of Sedimentary Petrology*, v. 61, p. 497-505.
- Rezak, R., T. J. Bright, and D. W. McGrail, 1985, *Reefs and Banks of the Northwestern Gulf of Mexico*: College Station, TX, John Wiley & Sons.
- Salvador, A., 1991, Origin and Development of the Gulf of Mexico Basin, in A. Salvador, ed., *The Geology of North America: The Gulf of Mexico Basin*, Boulder, The Geological Society of America, p. 389-443.
- Sarzalejo, S., 1993, Later Quaternary Stratigraphic Evolution of East Texas Mid-Outer Shelf and Upper Slope: Master's thesis, Rice University, Houston, 175 p.
- Sawyer, D. S., R. T. Buffler, and J. Rex H. Pilger, 1991, The Crust Under the Gulf of Mexico Basin, in A. Salvador, ed., *The Geology of North America: The Gulf of Mexico Basin*, Boulder, The Geological Society of America, p. 53-72.
- Shackleton, N. J., and N. D. Opdyke, 1973, Oxygen isotope and paleomagnetic stratigraphy of equatorial Pacific core V28-238: Oxygen isotope temperatures and ice volumes on a 10<sup>5</sup> and 10<sup>6</sup> year scale: *Quaternary Research*, v. 3, p. 39-55.
- Shideler, G. L., 1981, Development of the Benthic Nepheloid Layer on the South Texas Continental Shelf, Western Gulf of Mexico: *Marine Geology*, v. 41, p. 37-61.

- Siringan, F. P., and J. B. Anderson, 1993, Seismic Facies, Architecture, and Evolution of the Bolivar Roads Tidal Inlet/Delta Complex, East Texas Gulf Coast: *Journal of Sedimentary Petrology*, v. 63, p. 794-808.
- Sydow, J. C., 1992, The Stratigraphic Framework of a Shelf Edge Delta, Northeast Gulf of Mexico: Master's thesis, Louisiana State University, Baton Rouge, 131 p.
- Sydow, J., and H. H. Roberts, 1994, Stratigraphic Framework of a Late Pleistocene Shelf-Edge Delta, Northeast Gulf of Mexico: The American Association of Petroleum Geologists Bulletin, v. 78, p. 1276-1312.
- Thomas, M. A., 1990, The Impact of Long-term and Short-term Sea Level Changes on the Evolution of the Wisconsinian-Holocene Trinity/Sabine Incised Valley System: Ph.D. thesis, Rice University, Houston, TX, 247 p.
- Thomas, M. A., and J. B. Anderson, 1991, Late Pleistocene Sequence Stratigraphy of the Texas continental Shelf: Relationship to  $\delta^{18}O$  curves: GCSSEPM.
- Vail, P. R., R. M. Mitchum Jr., R. G. Todd, J. M. Widmier, I. S. Thompson, J. B. Sangree, J. N. Bub, and W. G. Hatlelid, 1977, Seismic Stratigraphy and Global Changes of Sea Level, in C. E. Payton, ed., *Seismic Stratigraphy - applications to hydrocarbon exploration*, Tulsa, OK, The American Association of Petroleum Geologists, p. 49-212.
- Van Wagoner, J. C., H. W. Posamentier, R. M. Mitchum, P. R. Vail, J. F. Sarg, T. S. Loutit, and J. Hardenbol, 1988, An Overview of the Fundamentals of Sequence Stratigraphy and Key Definitions, in C. K. Wilgus, B. S. Hastings, C. G. S. C. Kendall, H. W. Posamentier, C. A. Ross, and J. C. Van Wagoner, eds., *Sea-level changes: an integrated approach*, Tulsa, Oklahoma, Society of Economic Paleontologists and Mineralogists, p. 39-45.
- Walcott, R. I., 1972, Gravity, flexure, and the growth of sedimentary basins at a continental edge: *Geological Society of America Bulletin*, v. 83, p. 1845-1848.



- Winker, C. D., 1979, Late Pleistocene Fluvial-Deltaic Deposition: Texas Coastal Plain and Shelf: M.A. thesis, The University of Texas at Austin, Austin, TX, 187 p.
- Worrall, D. M., and S. Snelson, 1989, Evolution of the northern Gulf of Mexico with emphasis on Cenozoic growth faulting and the role of salt, in A. W. Bally, and A. R. Palmer, eds., The Geology of North America -- an overview: The Geology of North America, Boulder, CO, GSA, Inc., p. 97-137.

**Appendix 1.**

List of data for samples from  
platform boring B-92.

### Platform Boring B-92 Isotope Analyses

Sample #	Depth (ft)	# rubers picked	CAAdjPDB	OAdjPDB
1	1	27	0.7	-0.76
2	1.5	9	1.65	-1.66
3	2	18	1.28	-1.57
4	4	18	1.33	-1.18
5	4.5	17	0.96	-1.03
6	5	10	1.28	-1.97
7	7	9	1.36	-1.96
8	7.5	27	1.56	-0.86
9	8	17	1.01	-1.8
10	SAMPLE NEVER RECEIVED			
11	10.5	20	1.24	-2.3
12	13	17	0.89	-1.14
13	13.5	10	1.22	-1.95
14	14	23	1.09	-1.83
15	16	14	1.33	-1.63
16	16.5	27	1.26	-1.41
17	17	26	1.07	-1.12
18	19	8	0.79	-0.96
19	19.5	0 - NO SLIDE		
20	21.5	17	1.45	-1.25
21	SAMPLE NEVER RECEIVED			
22	22.5	11	1.38	-1.72
23	25	19	0.95	-1.21
24	25.5	15	1.13	-1.53
25	26	23	0.99	-1.59
26	27.5	11	0.68	-1.53
27	28	21	0.95	-1.56
28	30.5	12	1.01	-1.54
29	34	13	1.12	-1.91
30	34.5	0 - NO SLIDE		
31	37	6	1.12	-2.02
32	37.5	14	1.37	-1.52
33	38	22	0.76	-1.92
34	SAMPLE NEVER RECEIVED			
35	40	29	0.95	-1.58
36	40.5	13	0.95	-1.67
37	43	6 - UNABLE TO RUN ISOTOPES		
38	43.5	28	0.85	-0.75
39	45.5	27	1.39	-1.47
40	46.5	32	1.29	-1.18
41	49	10	1.58	-2.26

### Platform Boring B-92 Isotope Analyses

Sample #	Depth (ft)	# rubers picked	CAAdjPDB	OAdjPDB
42	49.5	27	1.01	-1.93
43	50	13	1.3	-1.48
44	52	7	0.67	-1.37
45	52.5	24	1.24	-1.72
46	53	12	0.89	-1.33
47	55	18	1.05	-1.41
48	55.5	6	0.84	-1.56
49	56	2	1.41	-2.14
50	58	17	1.02	-1
51	58.5	10	1.29	-1.73
52	59	16	0.84	-1.2
53	61	11	0.7	-1.26
54	61.5	4 - UNABLE TO RUN ISOTOPES		
55	62	26	1.05	-1.25
56	63.5	6	1.32	-1.68
57	64	20	0.94	-1.56
58	SAMPLE NEVER RECEIVED			
59	67.5	22	0.93	-1.33
60	68	12	0.98	-1.58
61	SAMPLE NEVER RECEIVED			
62	70.5	31 (2 slides)	0.69	-1.45
63	71	22 (2 slides)	0.79	-2.41
64	73	19	0.5	-2.17
65	73.5	20	0.68	-1.42
66	75.5	7	0.19	-1.68
67	76	8	0.49	-2.5
68	78.5	11	0.18	-2.23
69	SAMPLE NEVER RECEIVED			
70	79.5	11	0.41	-1.9
71	SAMPLE NEVER RECEIVED			
72	82.5	15	0.26	-1.4
73	83	8 - UNABLE TO RUN ISOTOPES		
74	84.5	6	0.58	-1.75
75	88	27	0.66	-2.07
76	88.5	8	0.27	-2.23
77	89	10	0.43	-1.75
78	SAMPLE NEVER RECEIVED			
79	91.5	11	0.46	-2.69
80	92	3 - UNABLE TO RUN ISOTOPES		
81	93.5	4	-0.34	-2.75
82	94	6	0.08	-2.12

### Platform Boring B-92 Isotope Analyses

Sample #	Depth (ft)	# rubers picked	CAdjPDB	OAdjPDB
83	97	8	0.22	-2.65
84	97.5	10 (2 slides)	0	-2.06
85	98	0 - NO SLIDE		
86	SAMPLE NEVER RECEIVED			
87	100.5	29	0.32	-2.06
88	101	14	0.15	-1.35
89	104	11	0.68	-2.29
90	104.5	10	-0.01	-1.88
91	105	13	-0.22	-2.32
92	SAMPLE NEVER RECEIVED			
93	SAMPLE NEVER RECEIVED			
94	SAMPLE NEVER RECEIVED			
95	124.5	25	0.35	-2.64
96	SAMPLE NEVER RECEIVED			
97	125	21	0.62	-1.92
98	SAMPLE NEVER RECEIVED			
99	SAMPLE NEVER RECEIVED			
100	135	30	0.78	-1.13
101	SAMPLE NEVER RECEIVED			
102	145.5	10	0.1	-1.94
103	146	0 - NO SLIDE		
104	155	22	1.45	-0.65
105	155.5	13	1.12	-2.26
106	156	12	0.86	-2.05
107	165	8	0.53	-1.65
108	165	25	0.53	-2.34
109	166	12	0.44	-1.63
110	176	20	0.83	-1.95
111	176.5	27	0.92	-1.82
112	177	7	-0.36	-1.35
113	185.5	0 - NO SLIDE		
114	195.5	0 - NO SLIDE		
115	205.5	0 - NO SLIDE		
116	216	4	1.25	-1.83
117	216.5	9	0.35	-1.46
118	217	4	0.2	-1.73
119	226	5	0.04	-1.16
120	226.5	7	0.08	-1.81
121	227	1	0.16	-2.14
122	236	10	0.75	-1.33
123	236.5	6	0.65	-2.25

### Platform Boring B-92 Isotope Analyses

Sample #	Depth (ft)	# rubers picked	CAdjPDB	OAdjPDB
124	237	6	0.23	-1.7
125	246	20	0.71	-1.07
126	246.5	25	1.25	-1.72
127	247	16	0.35	-0.97
128	256	8	1.52	-1.32
129	256.5	4	0.77	-1.31
130	257	14	0.22	-1.51
131	267	13	1.37	-1.48
132	267.5	6	0.66	-0.57
133	268	2 - UNABLE TO RUN ISOTOPES		
134	277	30	1.05	-1.86
135	277.5	9	1.15	-1.52
136	278	10	0.82	-0.94
137	287	32	1.26	-1.19
138	287.5	5	1.14	-1.14
139	288	30	0.74	-1.5
140	297	18	0.66	-0.92
141	297.5	23	1.06	-1.23
142	298	19	0.84	-0.98
143	307	30	1.06	-1.37
144	307.5	12	0.79	-1.46
145	308	10	1.03	-0.44
146	317	17	0.91	-1.34
147	317.5	18	0.71	-1.4
148	318	12	0.82	-1.12
149	328	27	0.77	-0.99
150	328.5	20	1.03	-1.01
151	329	27	1.1	-1.47
152	338	8	0.55	-2.53
153	338.5	4	0.47	-2.93
154	339	4	0.43	-1.97
155	349.5	1	0.77	-4.05
156	SAMPLE NEVER RECEIVED			
157	359	28	0.98	-2.52
158	359.5	27	1.36	-2.68
159	360	15	0.93	-2.49
160	369	11	0.64	-1.19
161	369.5	12	0.85	-2.23
162	370	10	0.93	-1.73
163	379	6	0.98	-1.33
164	379.5	15	1.43	-2.17

### Platform Boring B-92 Isotope Analyses

Sample #	Depth (ft)	# rubers picked	CAAdjPDB	OAdjPDB
165	380	5	1.51	-2.04
166	390	11	0.21	-2.71
167	390.5	17	0.6	-3.8
168	391	15	0.33	-3.58
169	400	27	0.35	-3.72
170	400.5	29	0.47	-1.78
171	401	16	0.43	-2.07

**Appendix 2.**

Grain size analyses results for samples  
from platform boring B-92.



## Platform Boring B-92 Grain Size Analysis

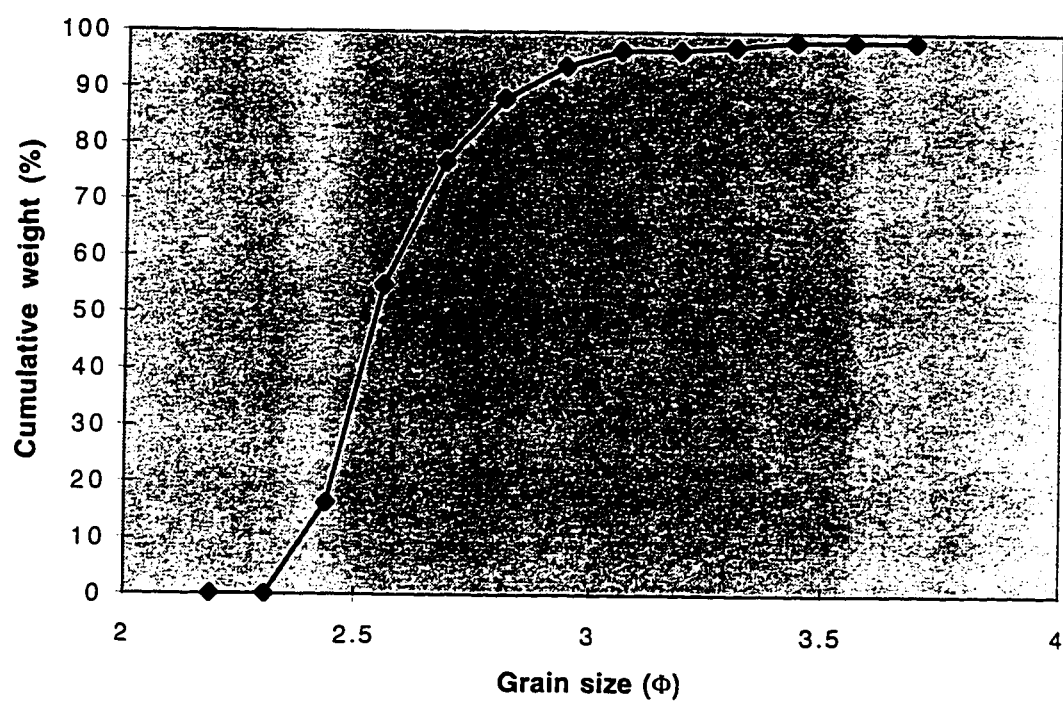
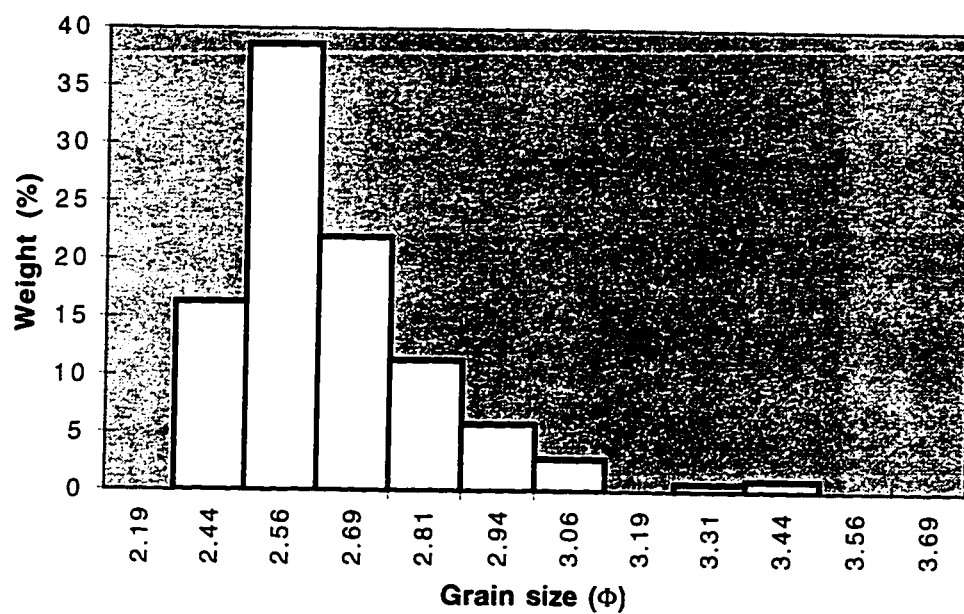
---

Sample #: 113      Depth: 185.5 feet

Grain size ( $\Phi$ )	Individual Weight (%)	Cumulative Weight (%)
2.13-2.25	0	0
2.25-2.38	0	0
2.38-2.5	16.3	16.3
2.5-2.63	38.6	54.9
2.63-2.75	21.9	76.8
2.75-2.88	11.3	88.1
2.88-3	5.8	93.9
3-3.13	2.8	96.7
3.13-3.25	0	96.7
3.25-3.38	0.7	97.4
3.38-3.5	1	98.4
3.5-3.63	0	98.4
3.63-3.75	0	98.4

Sample #: 113

Depth: 185.5 feet



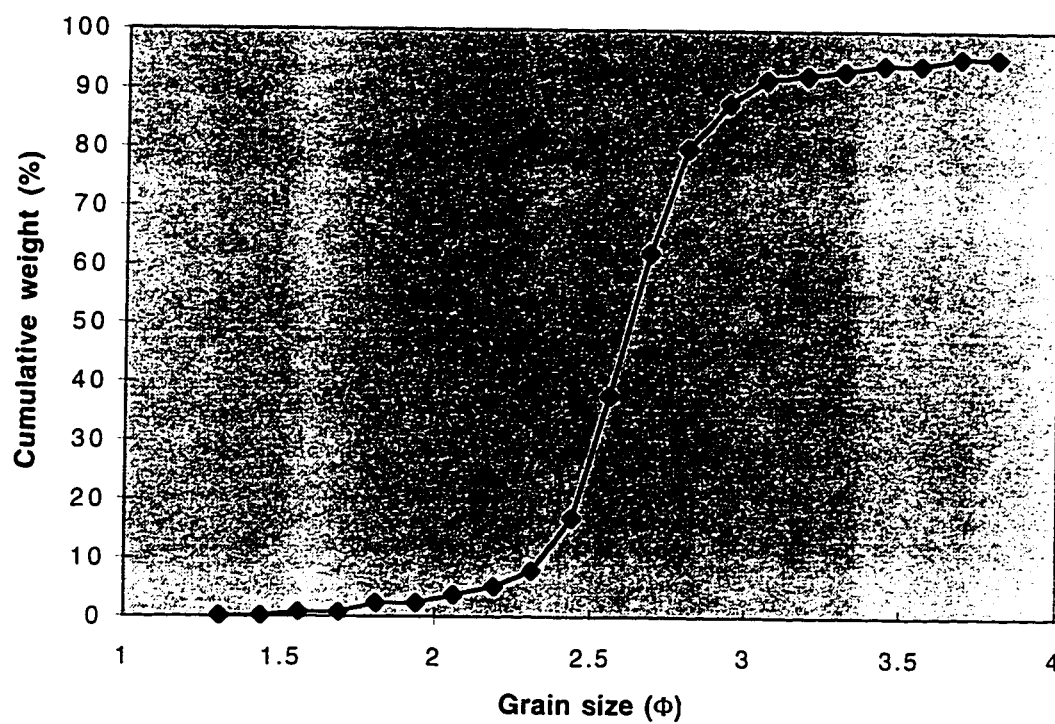
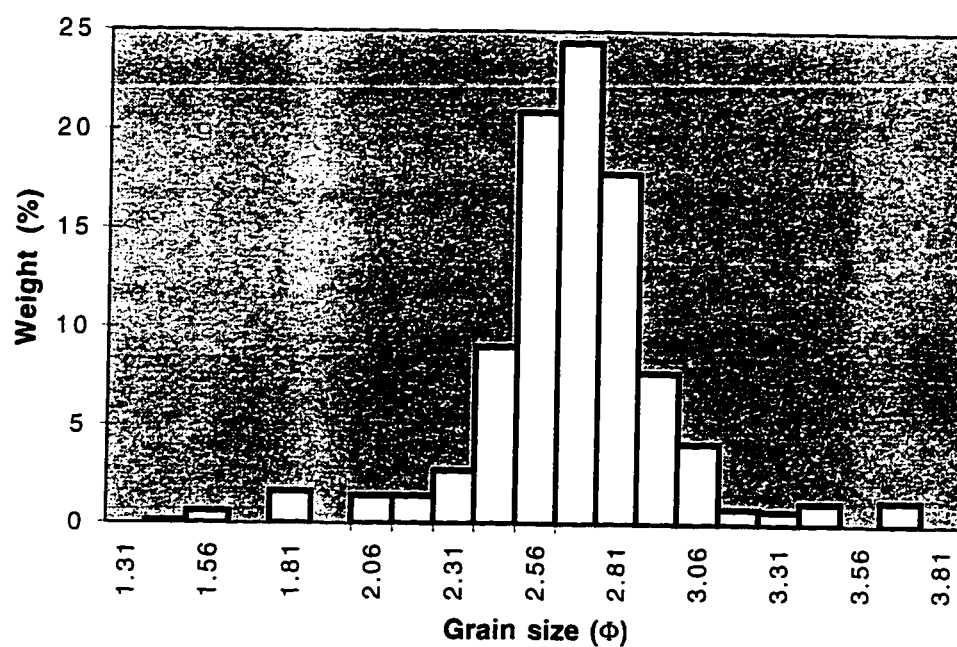
## Platform Boring B-92 Grain Size Analysis

---

Sample #:                      114 Depth:            195.5 feet

Grain size ( $\Phi$ )	Individual Weight (%)	Cumulative Weight (%)
1.25-1.38	0	0
1.38-1.5	0.1	0.1
1.5-1.63	0.6	0.7
1.63-1.75	0	0.7
1.75-1.88	1.6	2.3
1.88-2	0	2.3
2-2.13	1.4	3.7
2.13-2.25	1.4	5.1
2.25-2.38	2.7	7.8
2.38-2.5	9	16.8
2.5-2.63	20.9	37.7
2.63-2.75	24.4	62.1
2.75-2.88	17.8	79.9
2.88-3	7.7	87.6
3-3.13	4.1	91.7
3.13-3.25	0.8	92.5
3.25-3.38	0.7	93.2
3.38-3.5	1.1	94.3
3.5-3.63	0	94.3
3.63-3.75	1.2	95.5
3.75-3.88	0	95.5

Sample #: 114 Depth: 195.5 feet



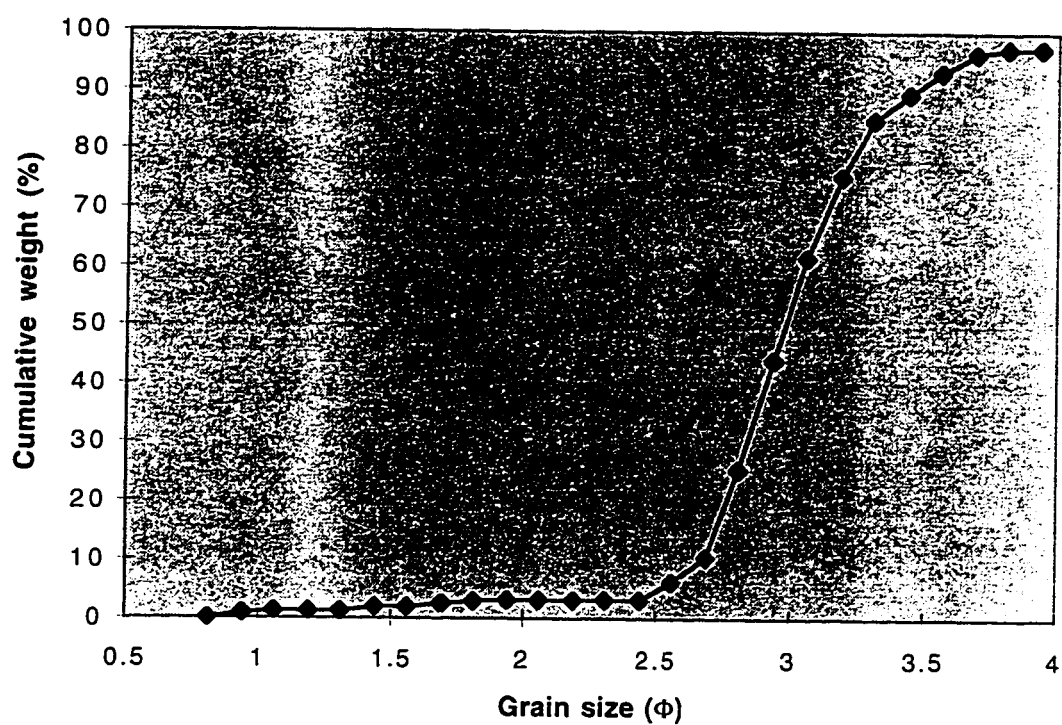
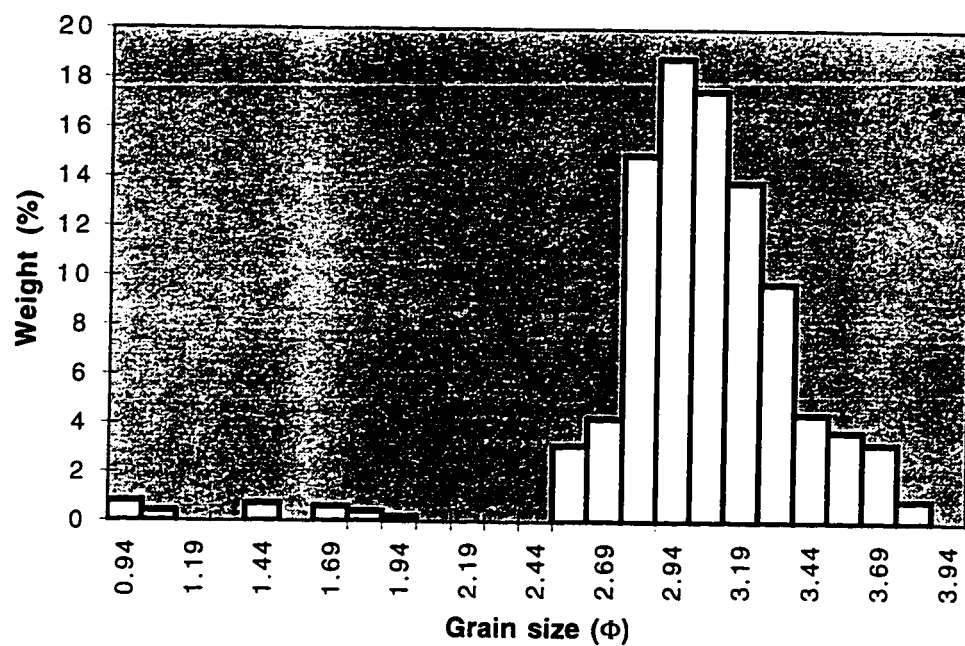
## Platform Boring B-92 Grain Size Analysis

---

Sample #:                      115 Depth:            205.5 feet

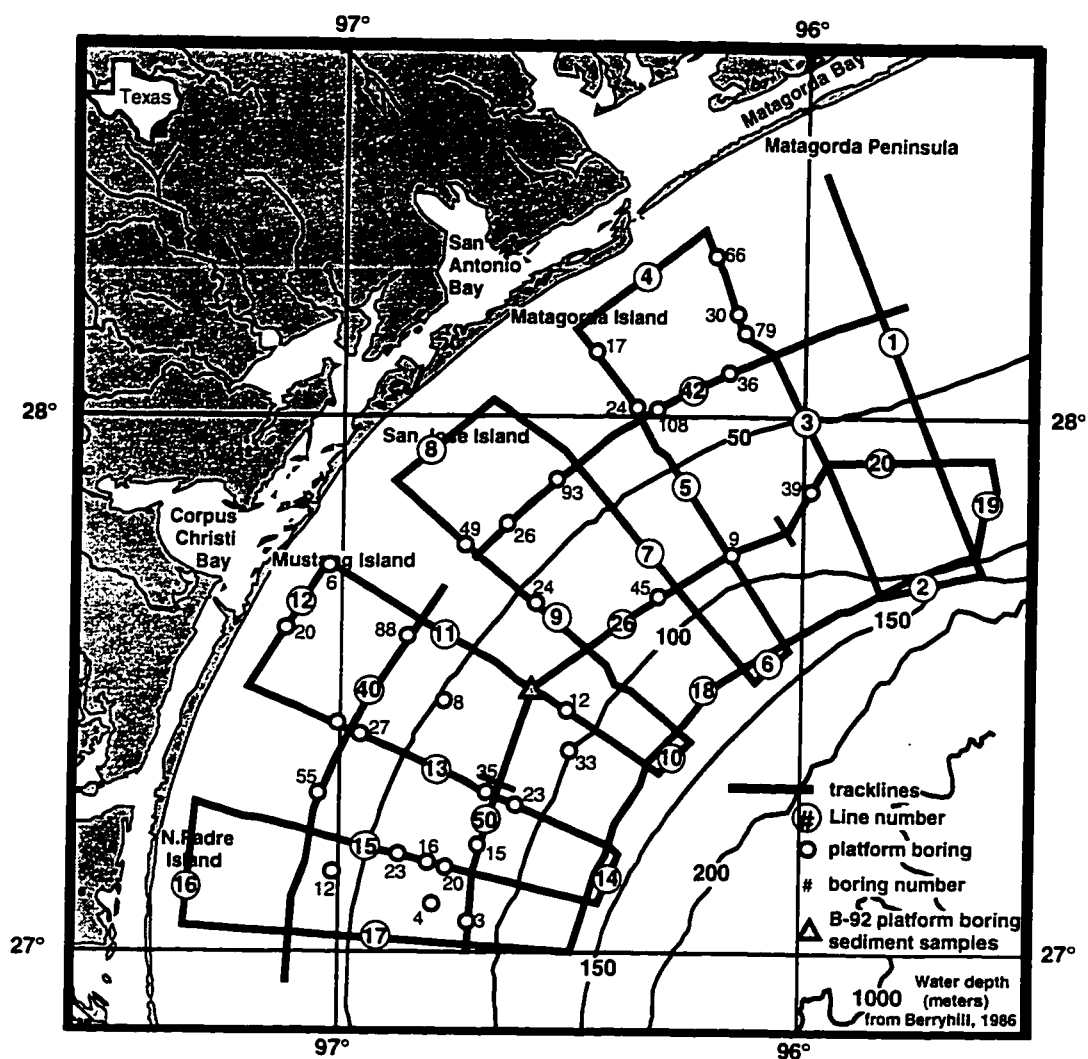
Grain size ( $\Phi$ )	Individual Weight (%)	Cumulative Weight (%)
0.75-0.88	0	0
0.88-1.00	0.8	0.8
1.00-1.13	0.4	1.2
1.13-1.25	0	1.2
1.25-1.38	0	1.2
1.38-1.5	0.7	1.9
1.5-1.63	0	1.9
1.63-1.75	0.6	2.5
1.75-1.88	0.4	2.9
1.88-2	0.2	3.1
2-2.13	0	3.1
2.13-2.25	0	3.1
2.25-2.38	0	3.1
2.38-2.5	0	3.1
2.5-2.63	3.1	6.2
2.63-2.75	4.2	10.4
2.75-2.88	14.9	25.3
2.88-3	18.8	44.1
3-3.13	17.5	61.6
3.13-3.25	13.8	75.4
3.25-3.38	9.7	85.1
3.38-3.5	4.4	89.5
3.5-3.63	3.7	93.2
3.63-3.75	3.2	96.4
3.75-3.88	0.9	97.3
3.88-4.00	0	97.3

Sample #: 115 Depth: 205.5 feet



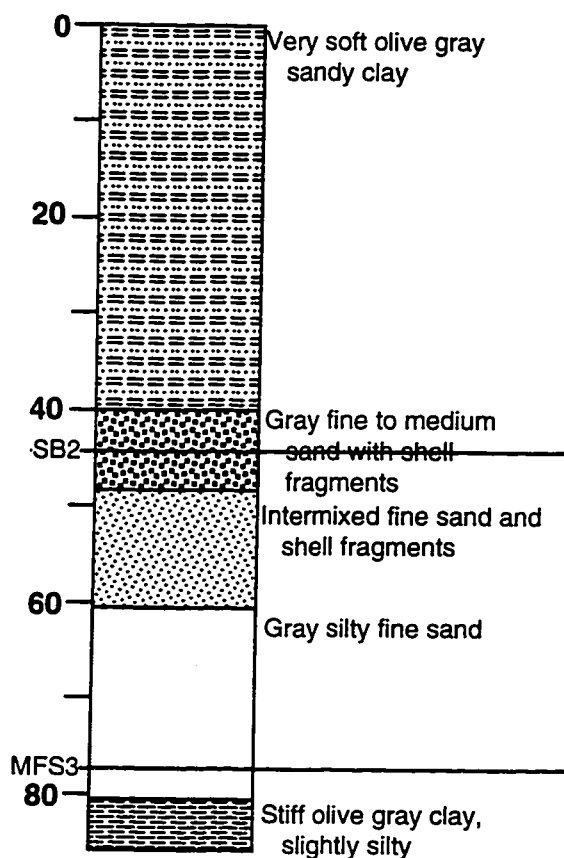
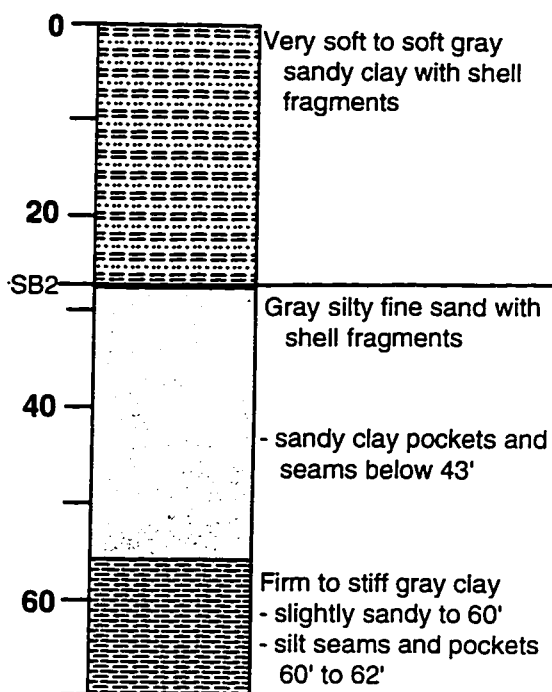
**Appendix 3.**

Condensed platform boring  
descriptions and location map.

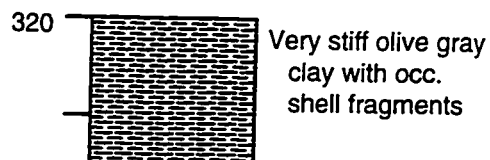
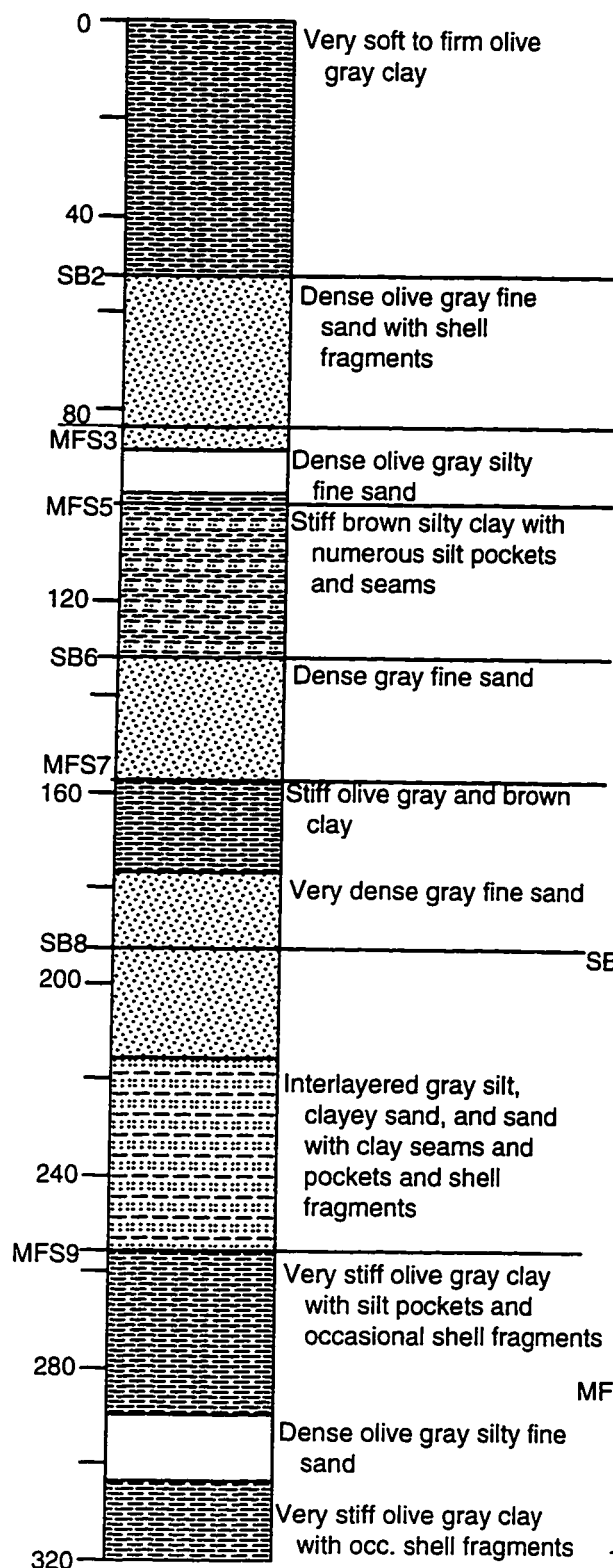


Dataset map showing locations of condensed platform boring descriptions.

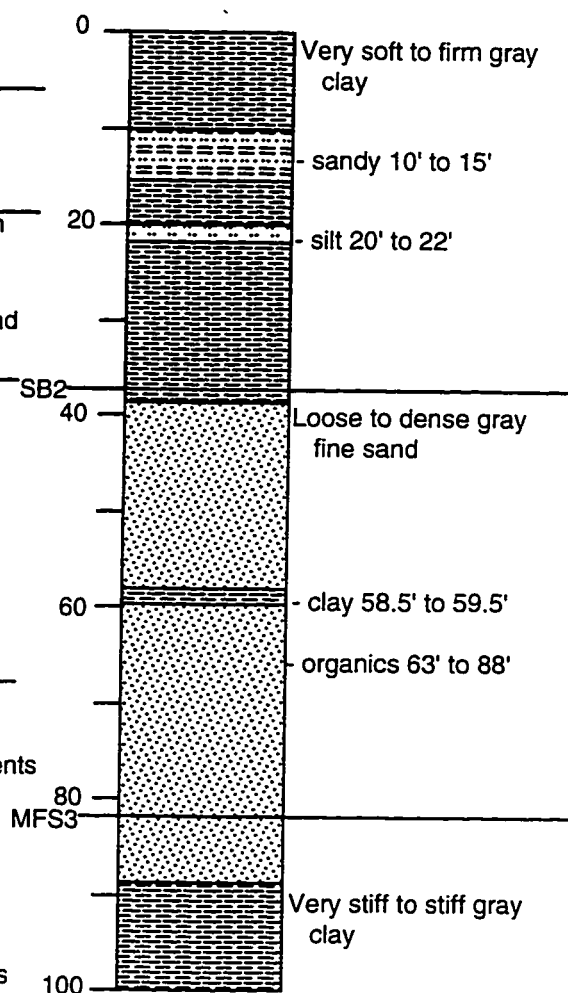


**Matagorda Island  
Block 634 B-17****Matagorda Island  
Block 605 B-30**

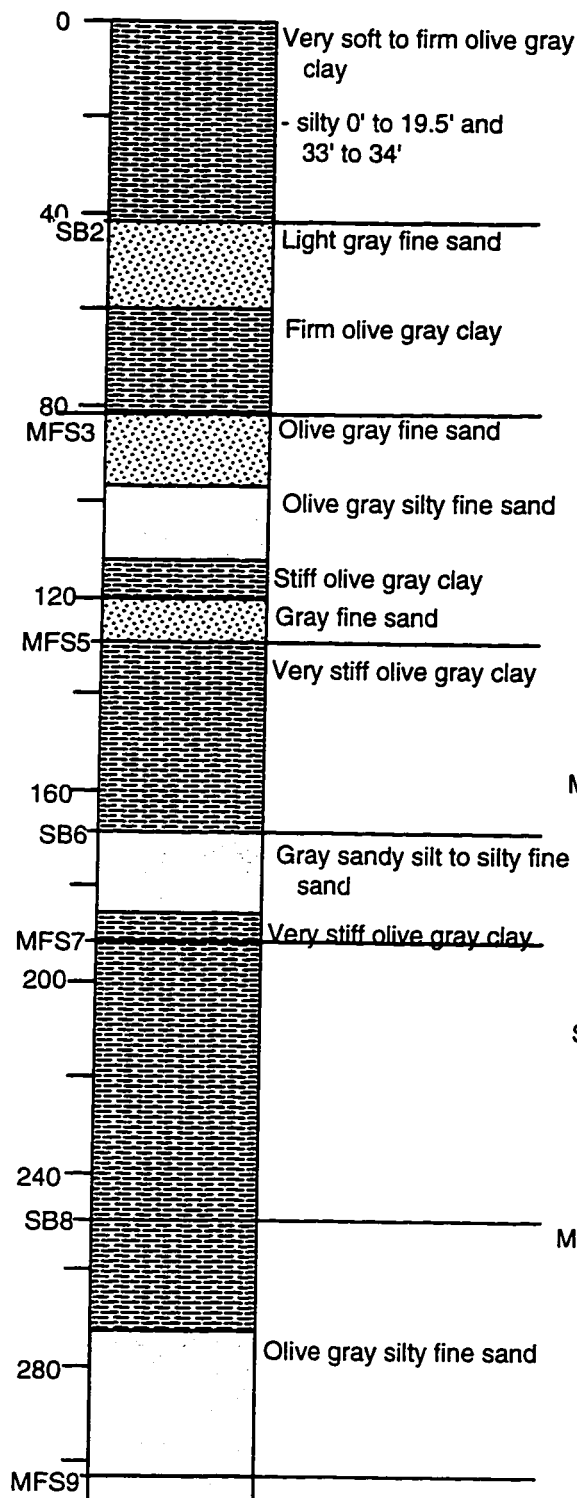
**Matagorda Island  
Block 681 B-24**



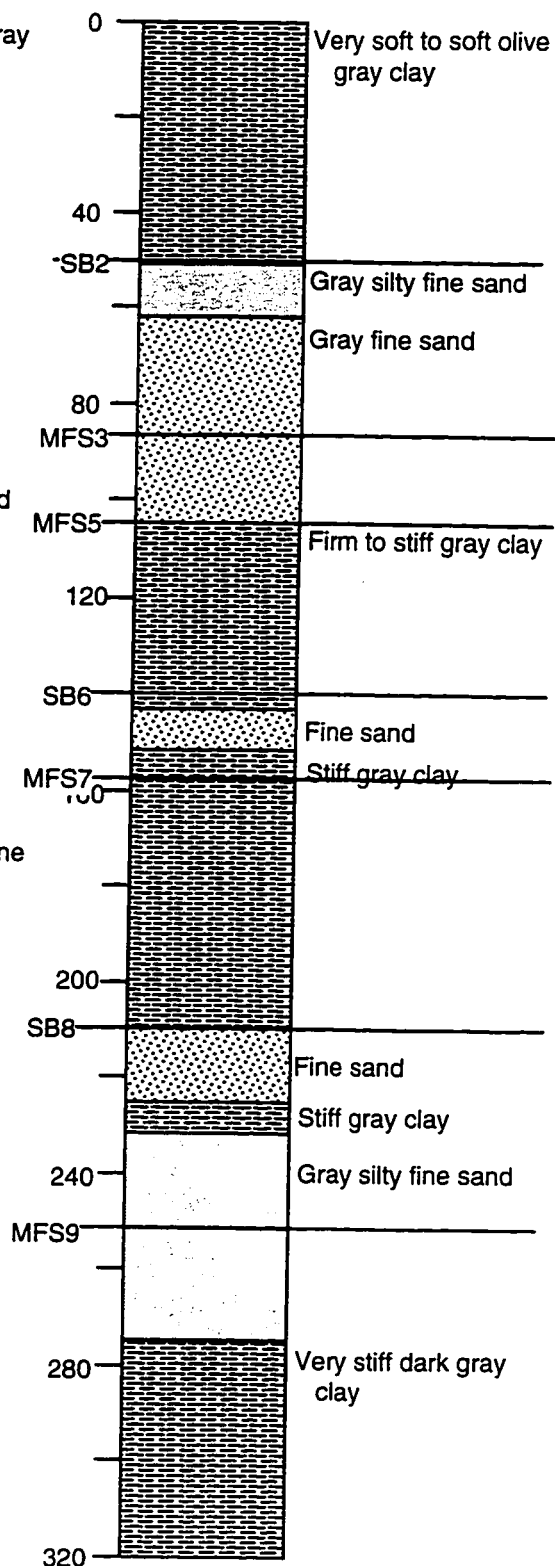
**Matagorda Island  
Block 566 B-66**

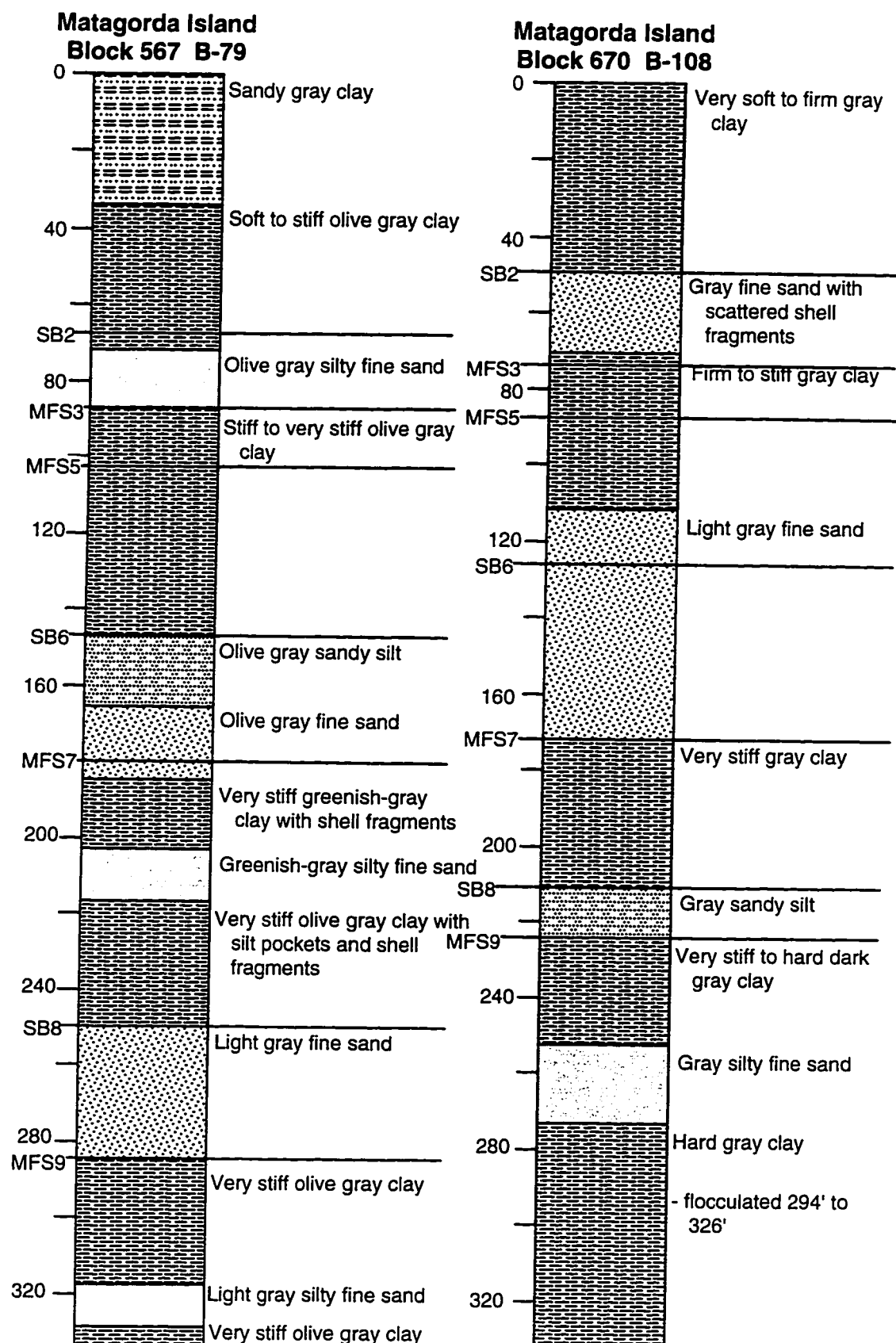


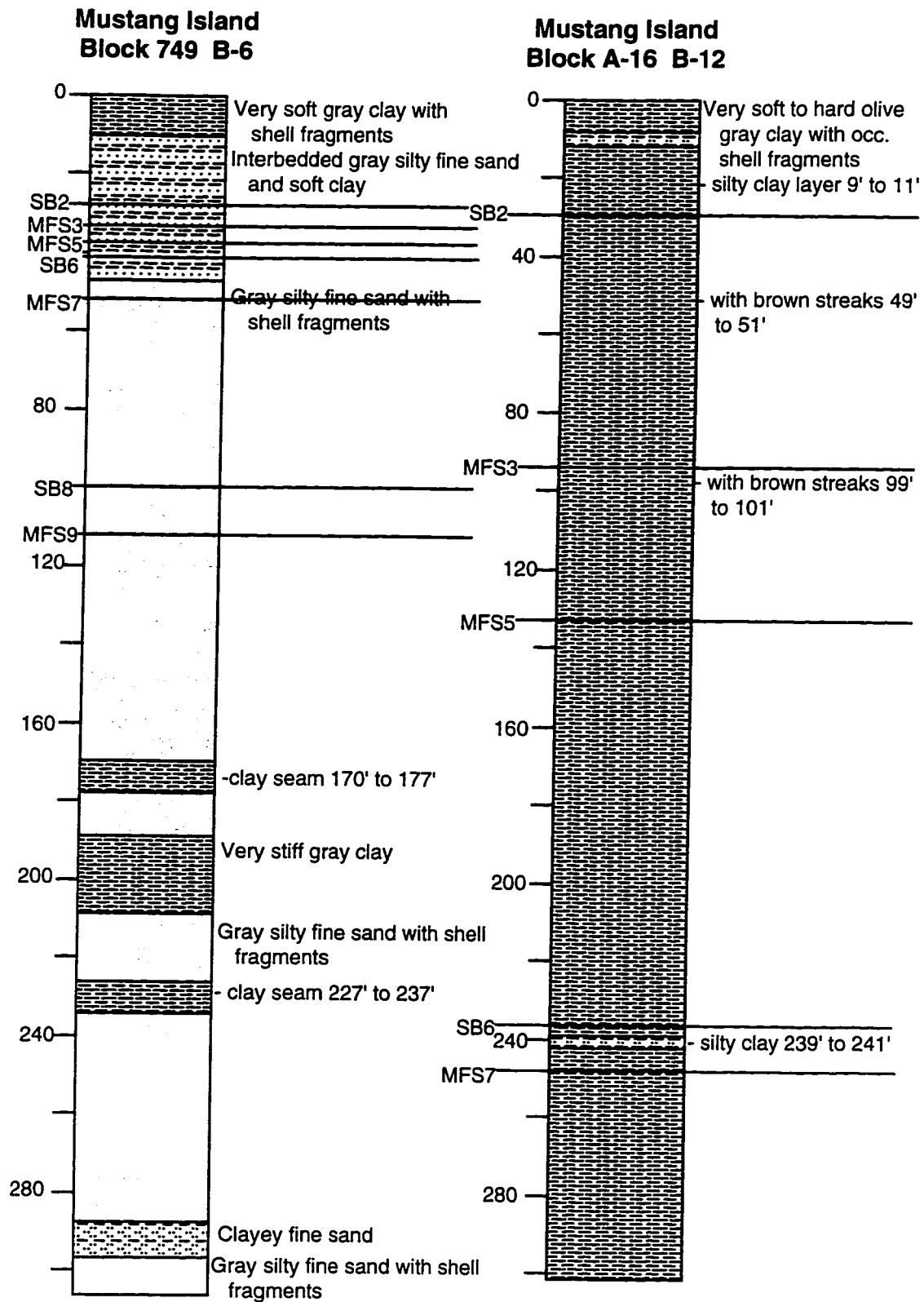
**Matagorda Island  
Block 639 B-36**

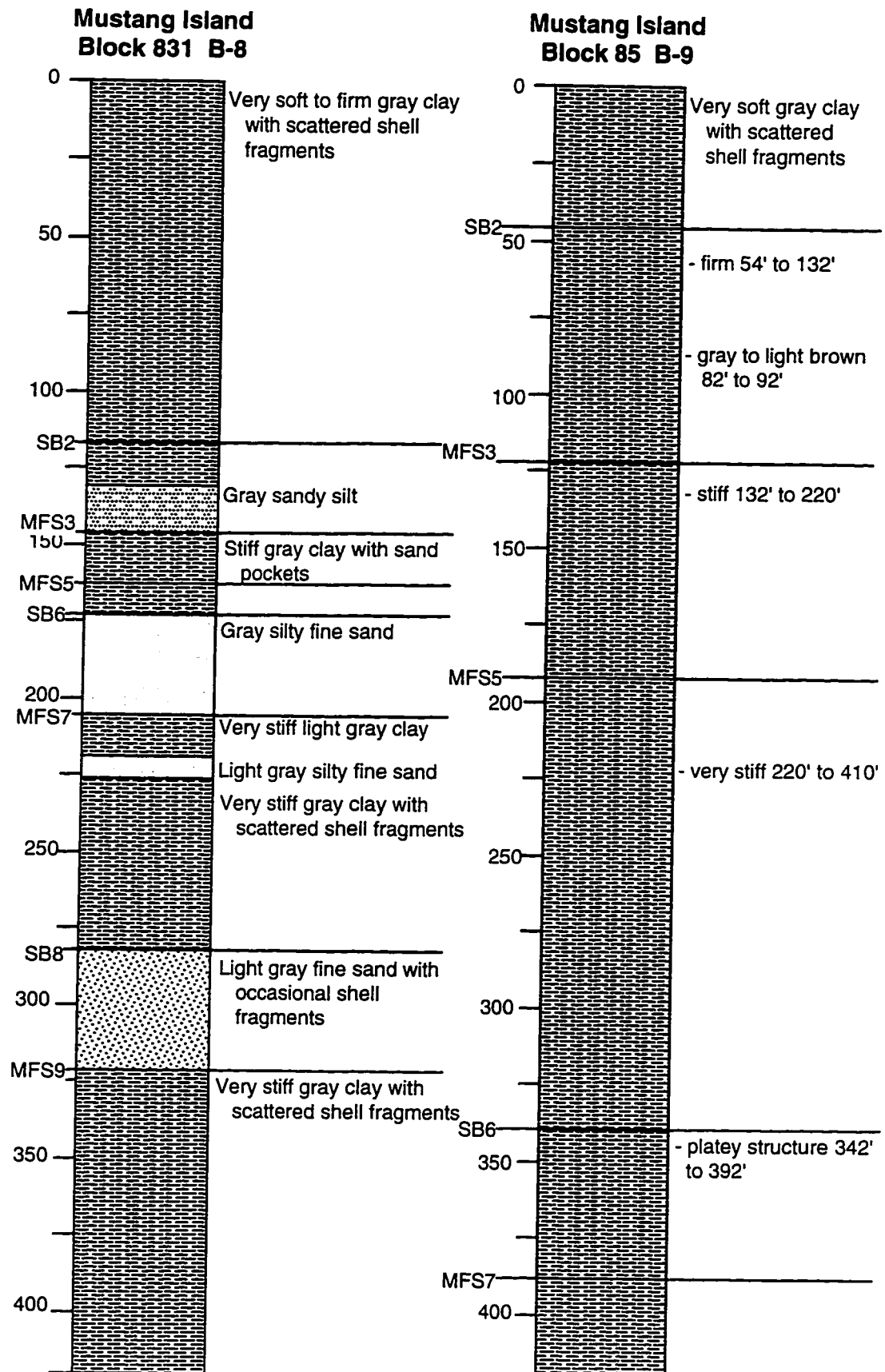


**Matagorda Island  
Block 712 B-93**

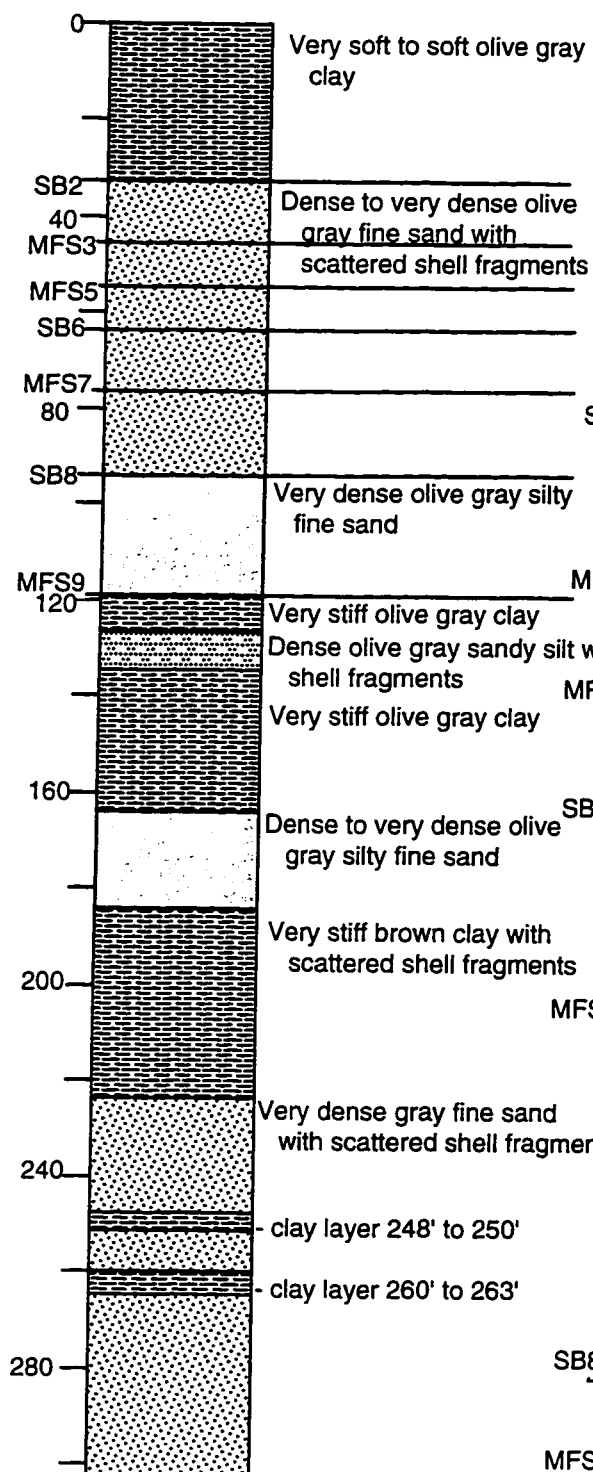




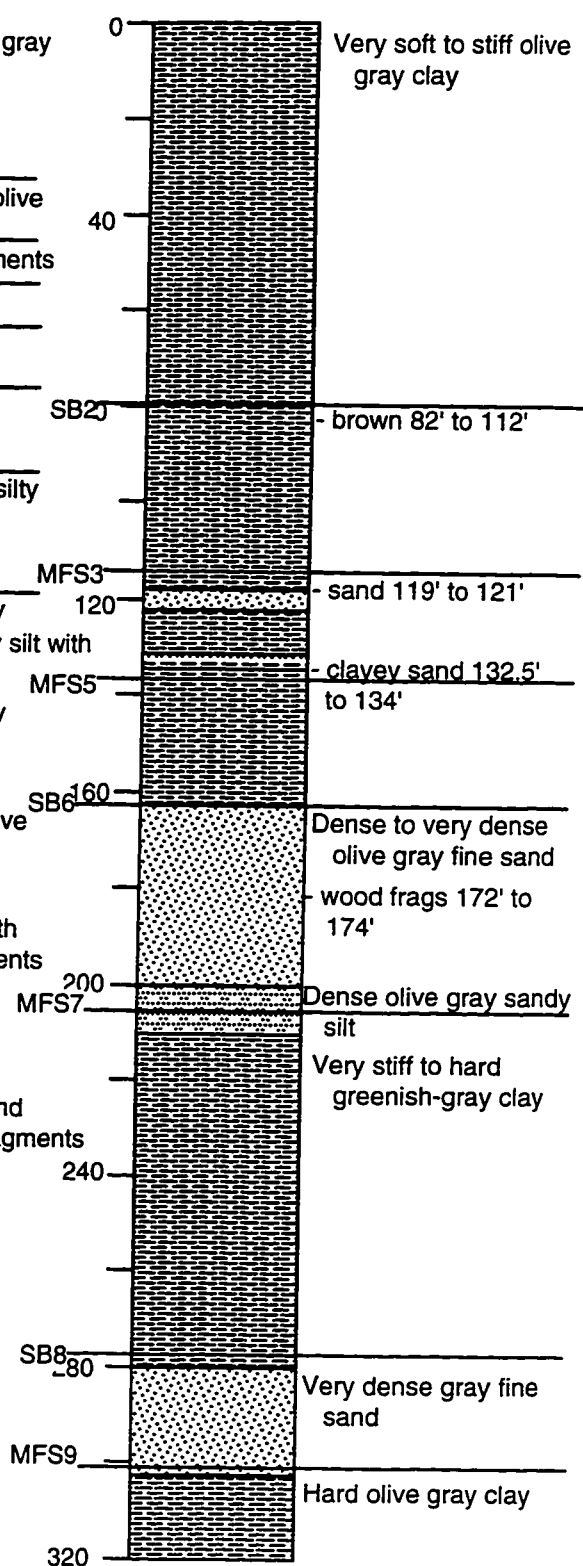




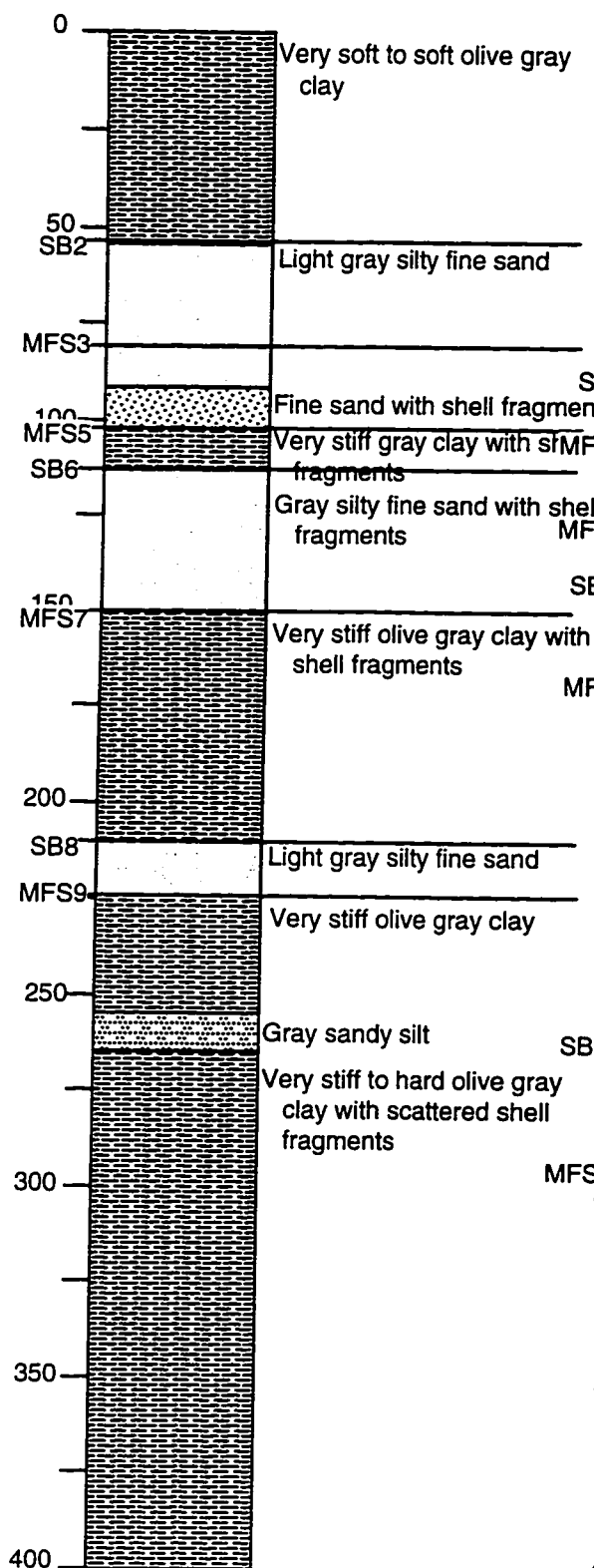
**Mustang Island  
Block 797L B-20**



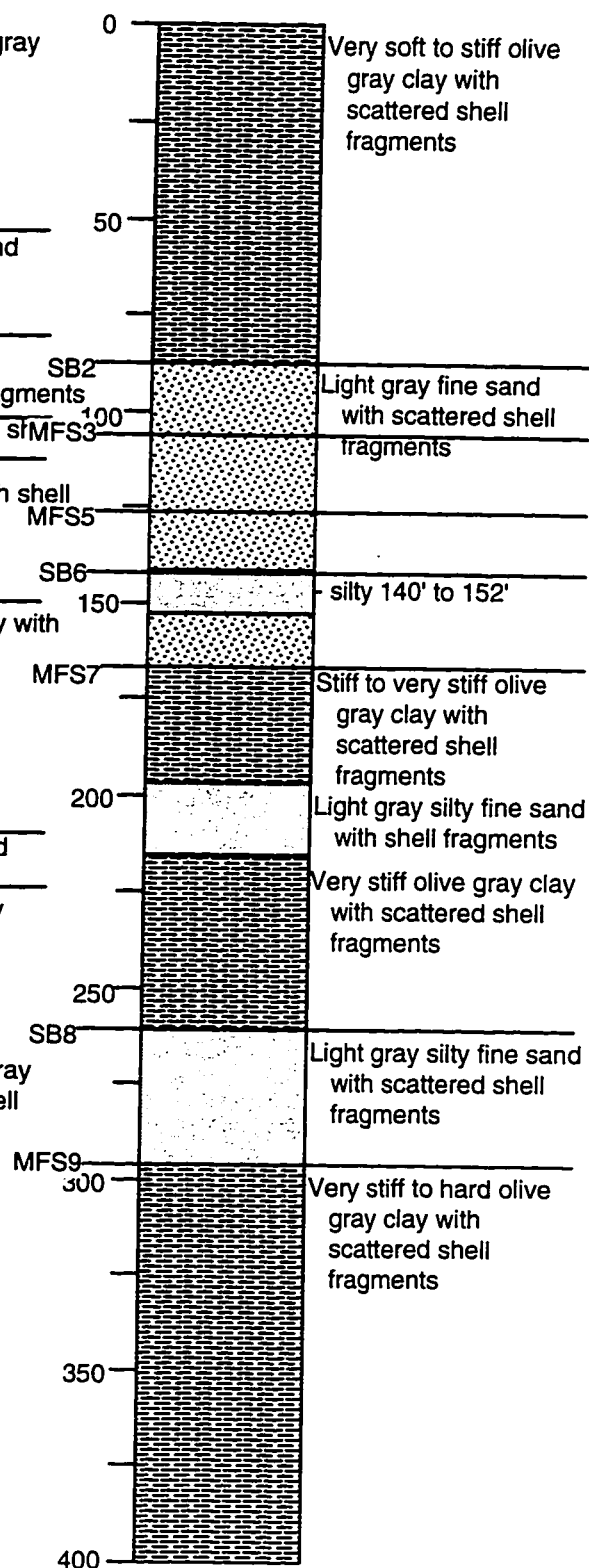
**Mustang Island  
Block 784 B-24**



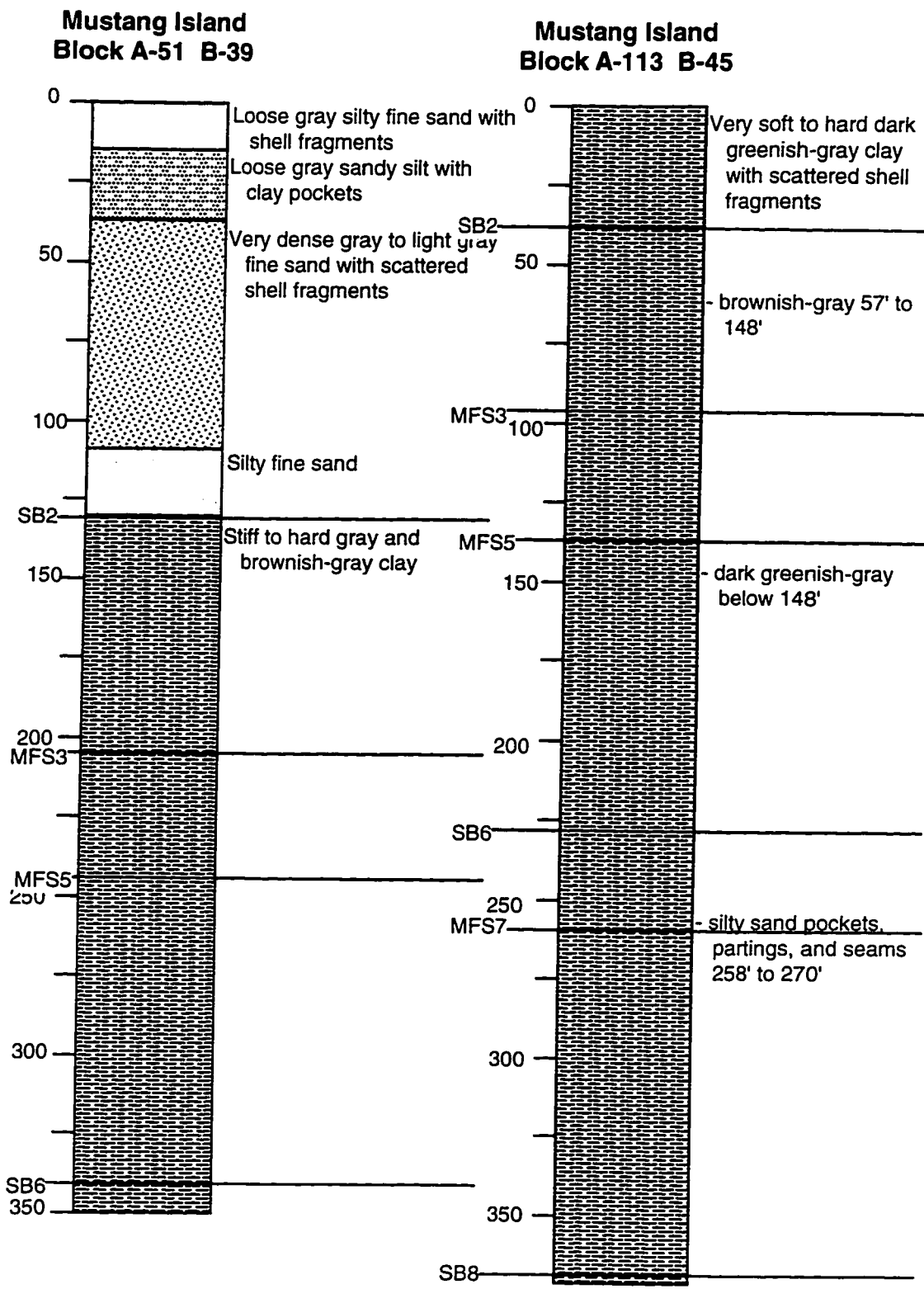
**Mustang Island  
Block 739 B-26**

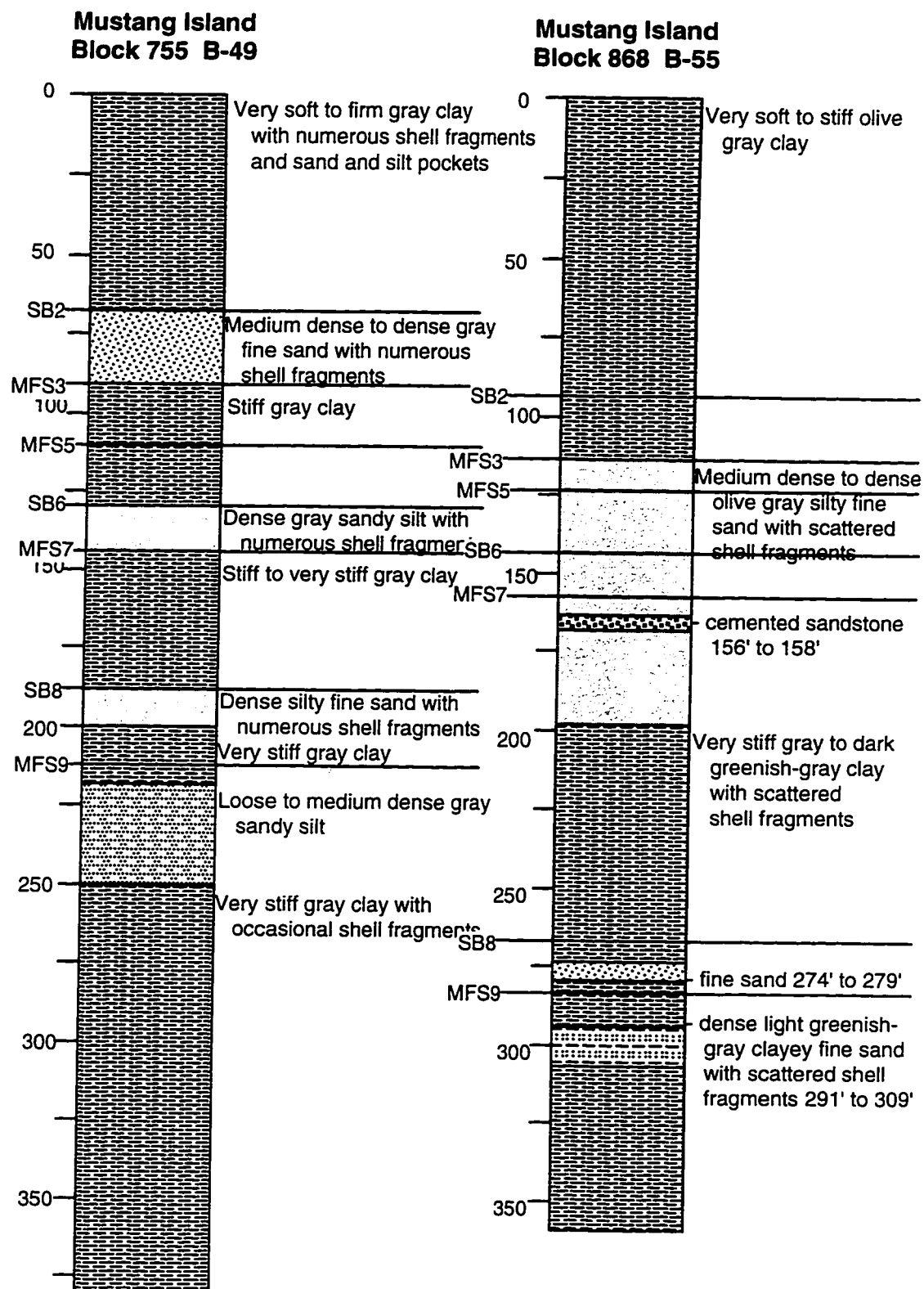


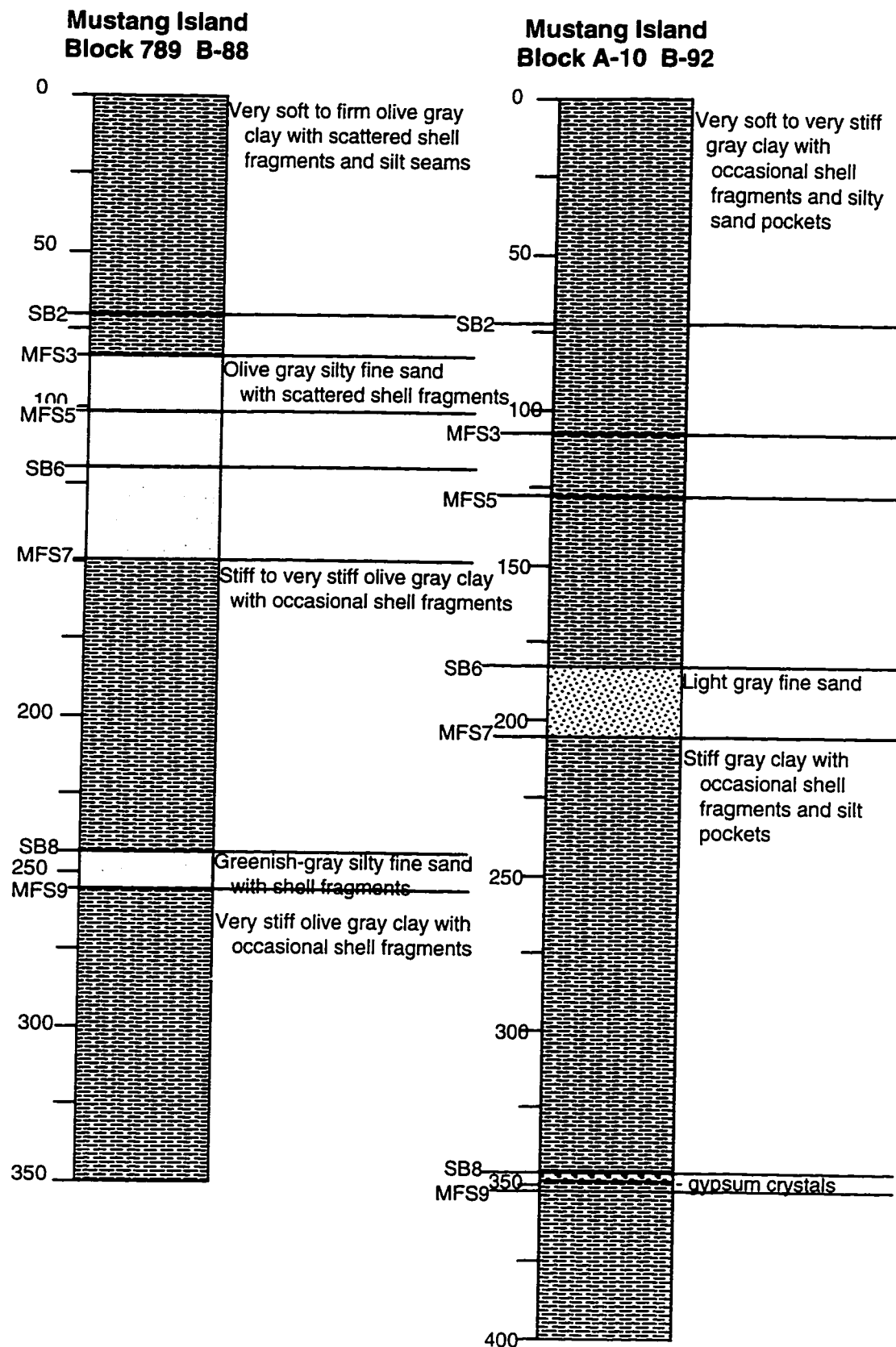
**Mustang Island  
Block 847 B-27**

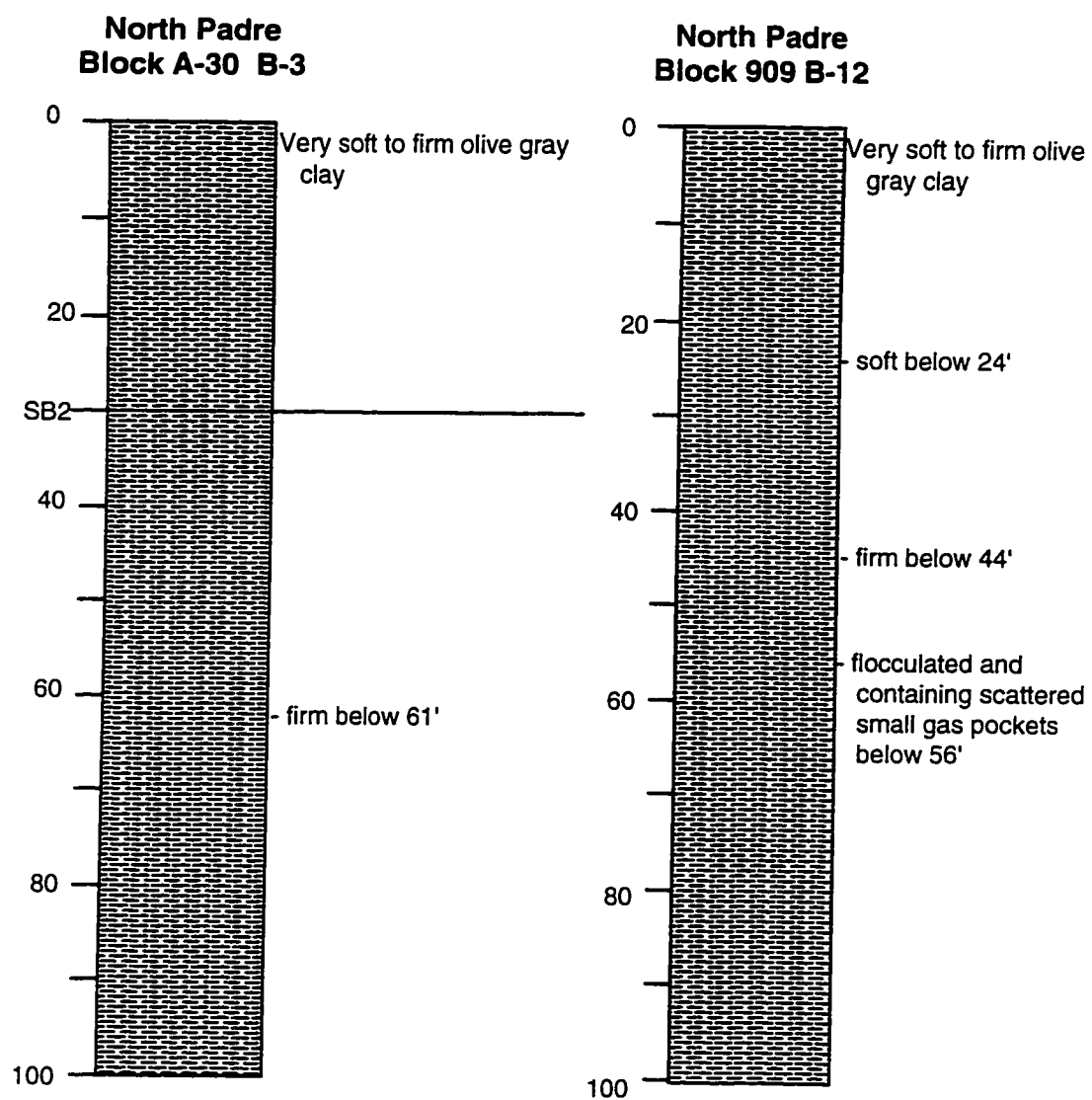


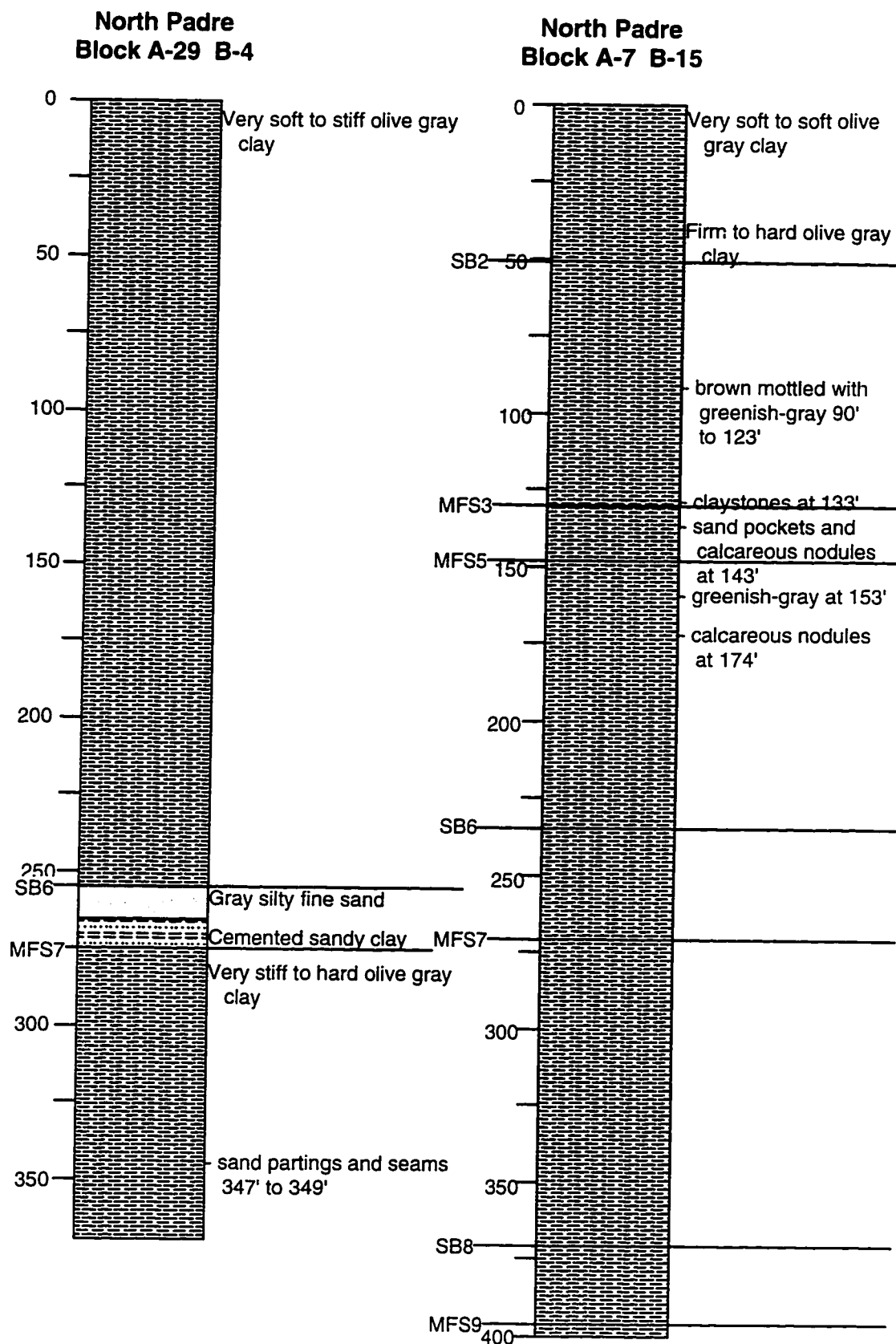


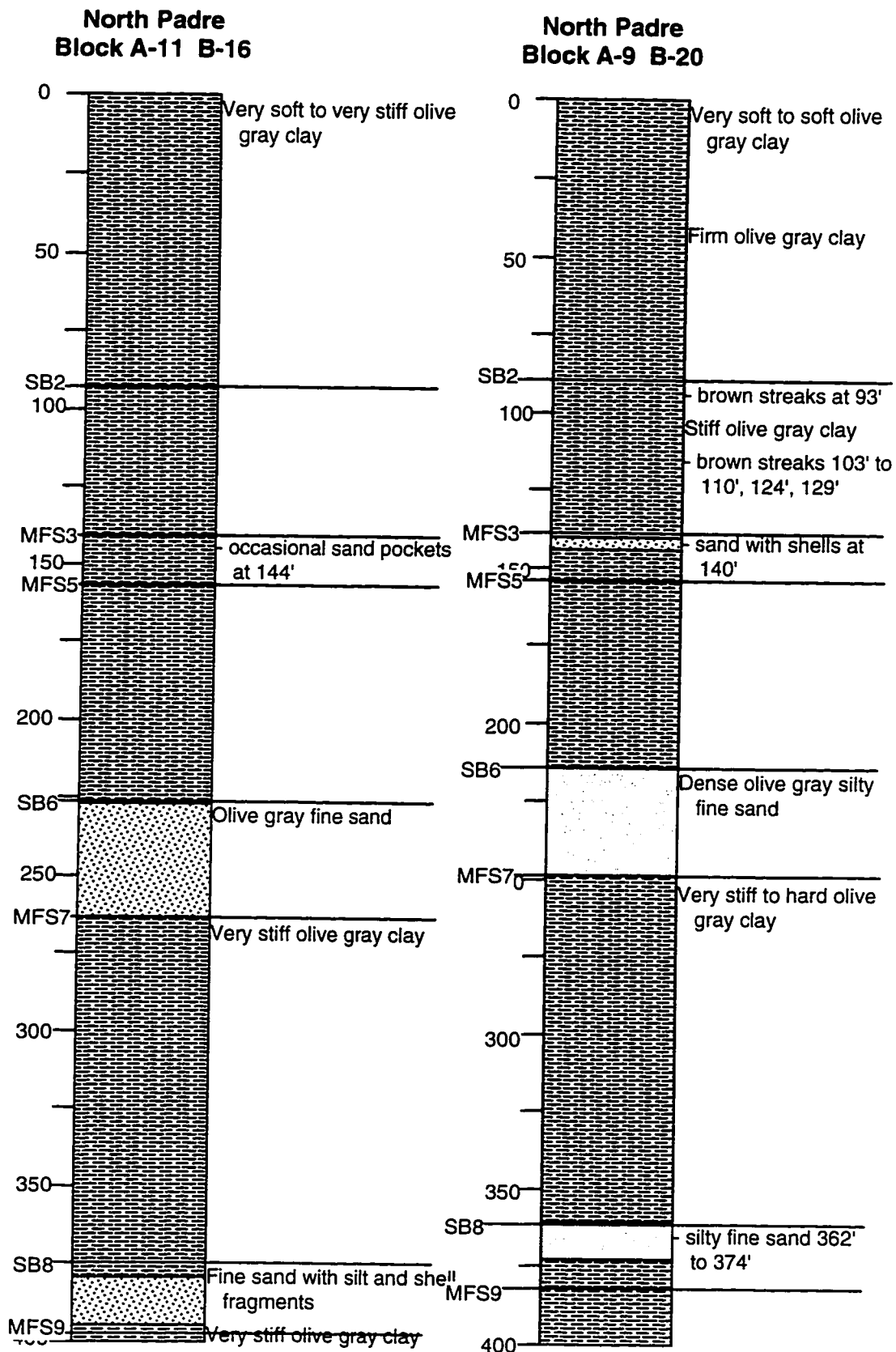


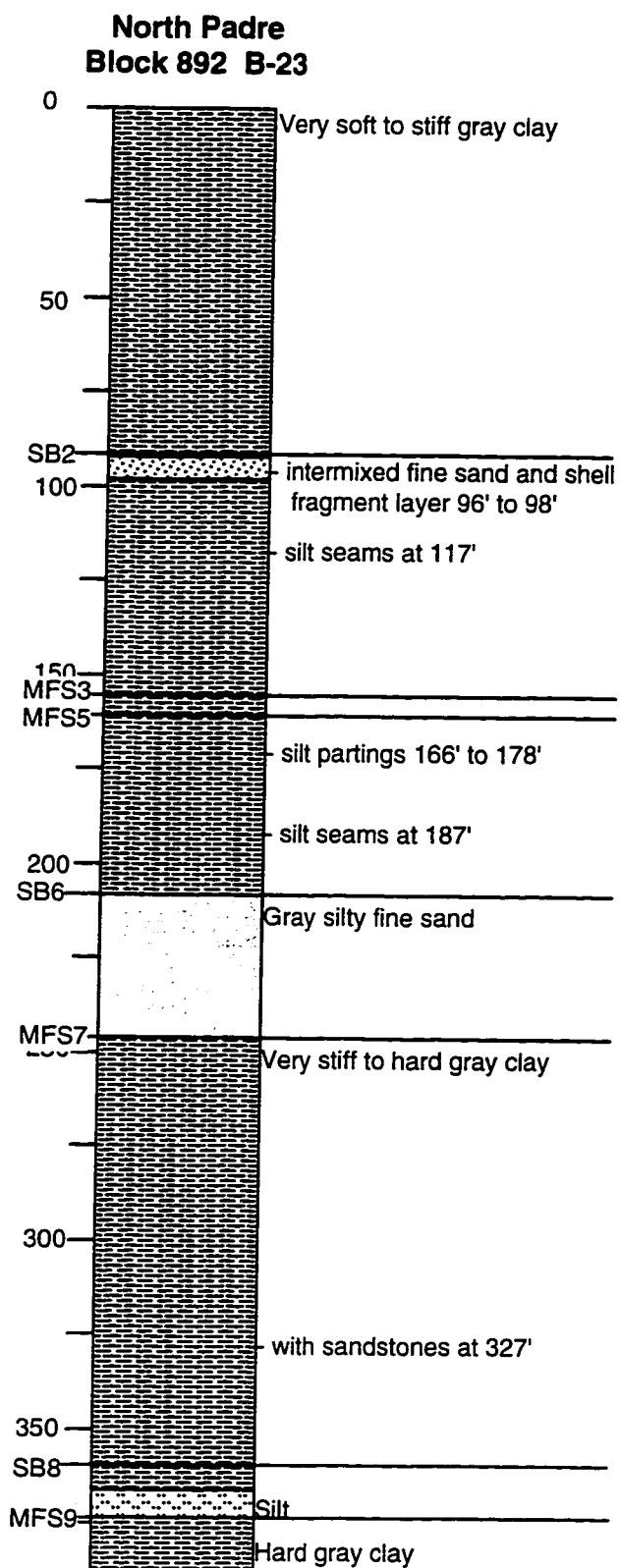












**PLEASE NOTE:**

Oversize maps and charts are filmed in sections in the following manner:

**LEFT TO RIGHT, TOP TO BOTTOM, WITH SMALL OVERLAPS**

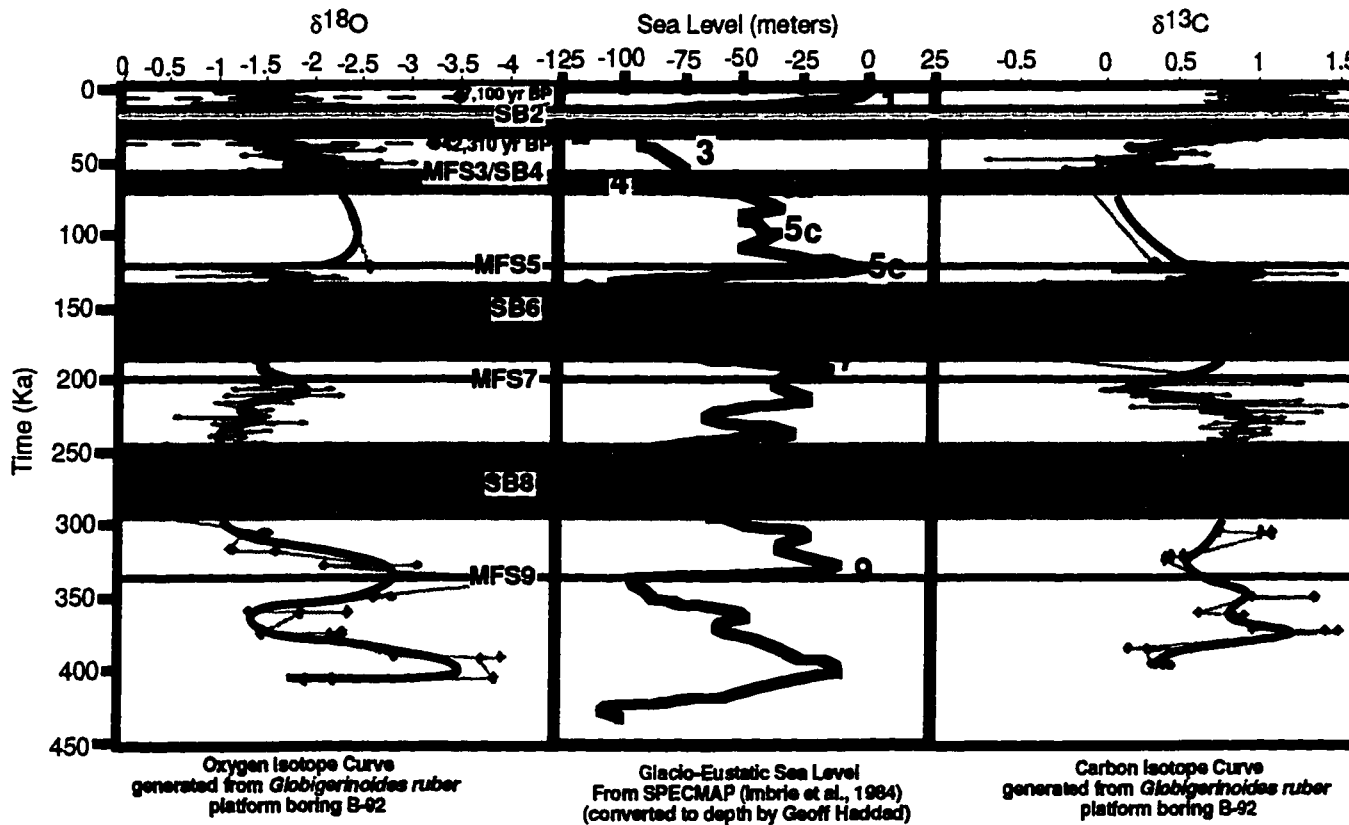
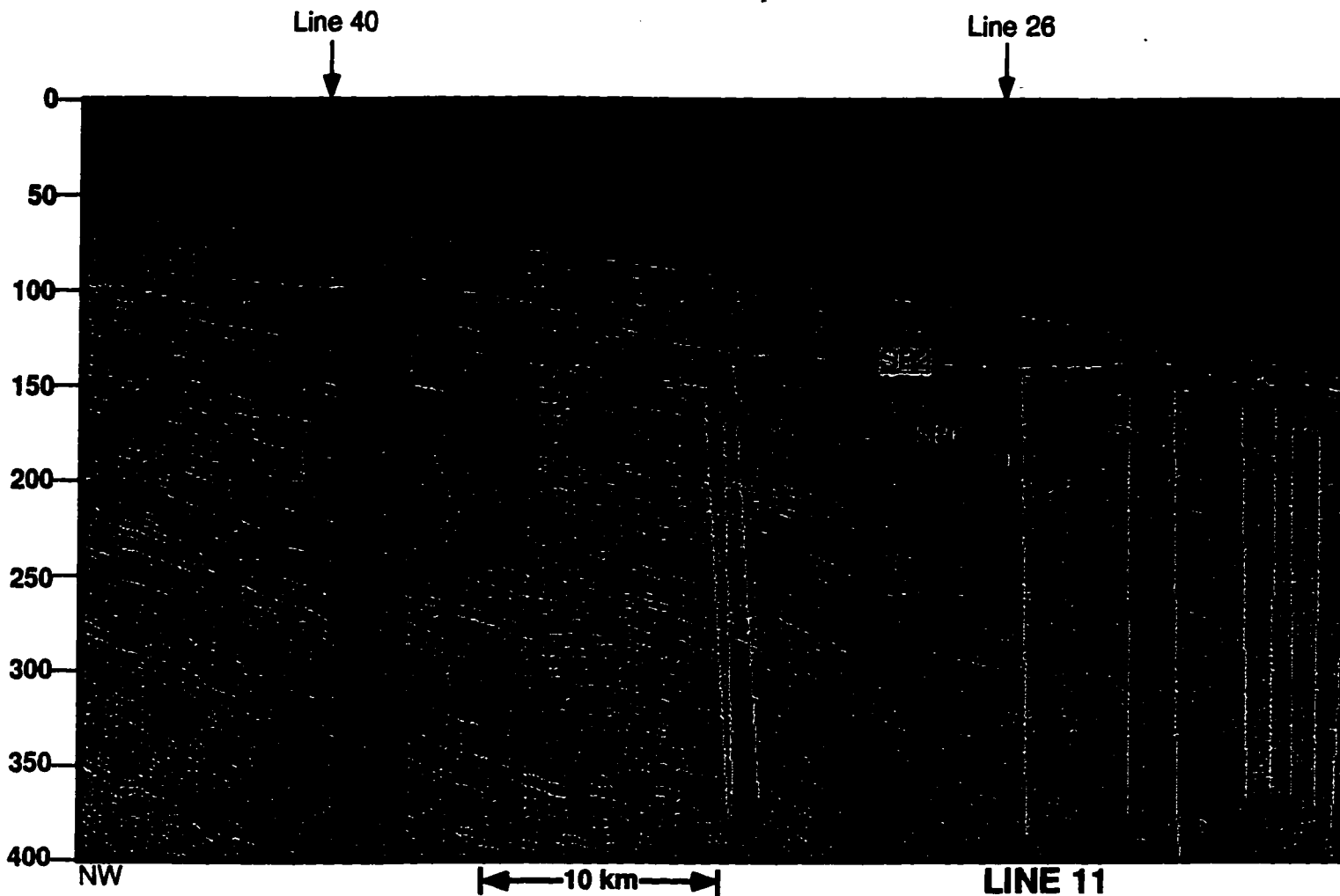
The following map or chart has been refilmed in its entirety at the end of this dissertation (not available on microfiche). A xerographic reproduction has been provided for paper copies and is inserted into the inside of the back cover.

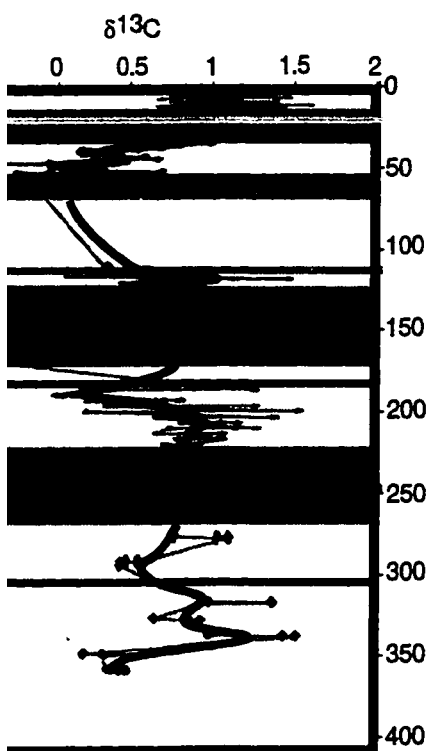
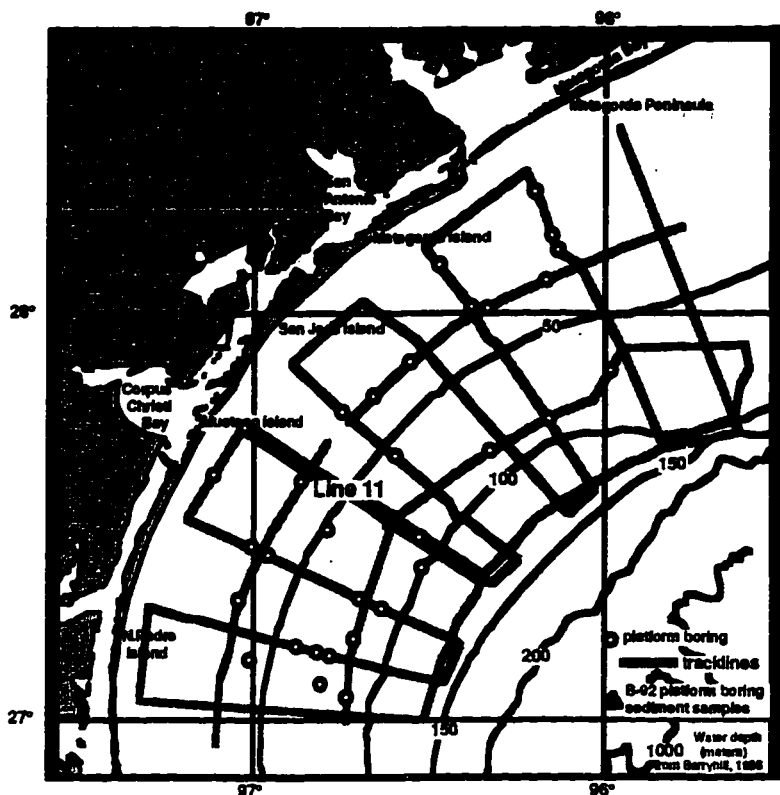
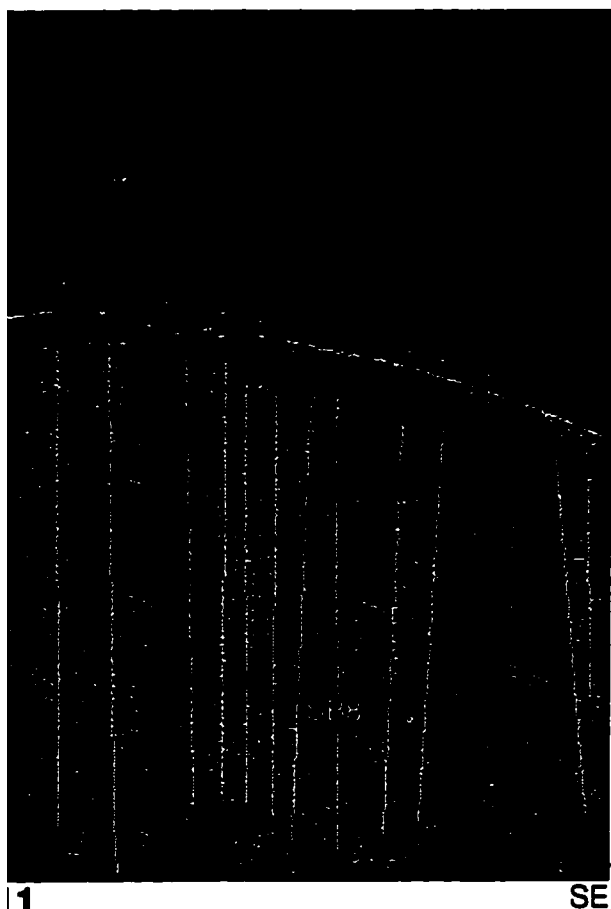
Black and white photographic prints (17" x 23") are available for an additional charge.

**UMI**









Carbon isotope Curve  
 ated from *Globigerinoides ruber*  
 platform boring B-92

Plate 1. Seismic line 11 illustrates stratigraphic surfaces, seismic facies, and corresponding platform boring B-92 lithofacies. Chronostratigraphic framework demonstrates correlation between seismic stratigraphic surfaces and oxygen isotope curve. Map shows location of seismic line 11 and platform boring B-92.

**PLEASE NOTE:**

Oversize maps and charts are filmed in sections in the following manner:

**LEFT TO RIGHT, TOP TO BOTTOM, WITH SMALL OVERLAPS**

The following map or chart has been refilmed in its entirety at the end of this dissertation (not available on microfiche). A xerographic reproduction has been provided for paper copies and is inserted into the inside of the back cover.

Black and white photographic prints (17" x 23") are available for an additional charge.

**UMI**





# **strating strategic surfaces**

---



**cess and facies.**

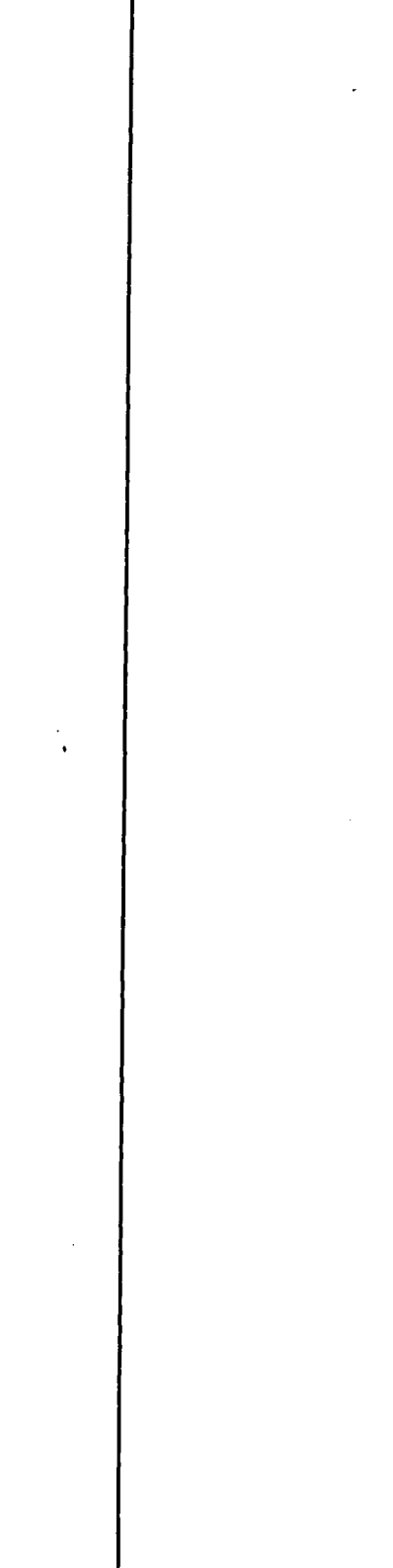
---



**kill**



•





**PLEASE NOTE:**

Oversize maps and charts are filmed in sections in the following manner:

**LEFT TO RIGHT, TOP TO BOTTOM, WITH SMALL OVERLAPS**

The following map or chart has been refilmed in its entirety at the end of this dissertation (not available on microfiche). A xerographic reproduction has been provided for paper copies and is inserted into the inside of the back cover.

Black and white photographic prints (17" x 23") are available for an additional charge.

**UMI**

